

AFML-TR-79-4075

LEVEL

2

AD A 077168

AN EVALUATION OF FOUR CURRENT MODELS TO PREDICT
THE CREEP-FATIGUE INTERACTION IN RENE 95

Henry L. Bernstein
Systems Research Laboratories, Inc.
2800 Indian Ripple Rd.
Dayton, OH 45440

DDC
NOV 23 1979
E

June 1979

TECHNICAL REPORT AFML-TR-79-4075

Approved for public release; distribution unlimited

DDC FILE COPY

AIR FORCE MATERIALS LABORATORY
AIR FORCE WRIGHT AERONAUTICAL LABORATORIES
Air Force Systems Command
Wright-Patterson Air Force Base, OH 45433

70 11 01 079

NOTICE

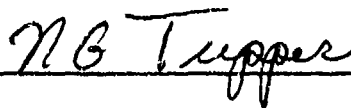
When Government drawings, specifications, or other data are used for any purpose other than in connection with a definitely related Government procurement operation, the United States Government thereby incurs no responsibility nor any obligation whatsoever; and the fact that the government may have formulated, furnished, or in any way supplied the said drawings, specifications, or other data, is not to be regarded by implication or otherwise as in any manner licensing the holder or any other person or corporation, or conveying any rights or permission to manufacture, use, or sell any patented invention that may in any way be related thereto.

This report has been reviewed by the Information Office (OI) and is releasable to the National Technical Information Service (NTIS). At NTIS, it will be available to the general public, including foreign nations.

This technical report has been reviewed and is approved for publication.



DR. T. NICHOLAS
Metals Behavior Branch
Metals and Ceramics Division



NATHAN G. TUPPER, Chief
Metals Behavior Branch
Metals and Ceramics Division

"If your address has changed, if you wish to be removed from our mailing list, or if the addressee is no longer employed by your organization please notify AIRL/LLN, W-PAFB, OK 45433 to help us maintain a current mailing list".

Copies of this report should not be returned unless return is required by security considerations, contractual obligations, or notice on a specific document.

19 REPORT DOCUMENTATION PAGE		READ INSTRUCTIONS BEFORE COMPLETING FORM
1. REPORT NUMBER AFML-TR-79-4075	2. GOVT ACCESSION NO.	3. RECIPIENT'S CATALOG NUMBER
4. TITLE (and Subtitle) AN EVALUATION OF FOUR CURRENT MODELS TO PREDICT THE CREEP-FATIGUE INTERACTION IN RENÉ 95	5. AUTHOR(s) Henry L. Bernstein	6. PERFORMING ORG. REPORT NUMBER 6909 Tech. Report
7. AUTHOR(s) Henry L. Bernstein	8. CONTRACT OR GRANT NUMBER(s) F33615-76-C-5191	9. TYPE OF REPORT & PERIOD COVERED Technical Report, Jan 77-Aug 78
9. PERFORMING ORGANIZATION NAME AND ADDRESS Systems Research Laboratories, Inc. 2800 Indian Ripple Road Dayton, OH 45440	10. PROGRAM ELEMENT, PROJECT, TASK AREA & WORK UNIT NUMBERS Prog. Element 62102F, Proj. 7351, Task Area 735106, Work Unit 73510690	11. CONTROLLING OFFICE NAME AND ADDRESS Air Force Materials Laboratory AFML/LLN Wright-Patterson AFB, OH 45433
14. MONITORING AGENCY NAME & ADDRESS (if different from Controlling Office) 111	15. SECURITY CLASS. (of this report) Unclassified	12. REPORT DATE June 1979
16. DISTRIBUTION STATEMENT (of this Report) Approved for public release; distribution unlimited.	13. NUMBER OF PAGES 110	14. SECURITY CLASS. (of this report) Unclassified
17. DISTRIBUTION STATEMENT (of the abstract entered in Block 20, if different from Report) 576-6907-TR	15. DECLASSIFICATION/DOWNGRADING SCHEDULE	
18. SUPPLEMENTARY NOTES		
19. KEY WORDS (Continue on reverse side if necessary and identify by block number) René 95 Creep-Fatigue Interaction High Temperature Fatigue Time-Dependent Fatigue Nickel-base Superalloys Strainrange Partitioning Frequency Separation Ostergren Model Damage Rate Model		
20. ABSTRACT (Continue on reverse side if necessary and identify by block number) Four current models for the creep-fatigue interaction were evaluated for their ability to predict fatigue behavior at 1200°F (650°C) of thermomechanically processed René 95—an advanced nickel-base superalloy used for turbine disks. These models are the Strainrange-Partitioning Model, the Frequency-Separation Model, the Ostergren Model, and the Damage-Rate Model. A series of strain-controlled fatigue tests was conducted to evaluate these models. These tests consisted of continuously cycling tests at two different frequencies, various types of strain-hold tests, and dual-rate continuously cycling tests. These		

340 400

Handwritten signature/initials

UNCLASSIFIED

SECURITY CLASSIFICATION OF THIS PAGE(When Data Entered)

20. Abstract Continued

fatigue tests were divided into two groups--baseline tests and verification tests. The baseline tests were used to determine the constants in the models and the correlation ability of the models. The verification tests were used to determine the predictive ability of the models. The best correlation of the baseline tests was to within a scatter band of ± 3.6 and was achieved by the Frequency-Separation Model and the Ostergren Model. The other two models had scatter bands greater than ± 5 . The best prediction of the verification tests was to within a factor of ± 5.2 and was achieved by the Ostergren Model. The other models predicted the verification tests from factors of ± 6.1 to ± 18 . Each of the models consistently overpredicted or underpredicted the lives of certain types of tests that form the data base. Based upon the results of this study, it was concluded that these models in their present form could not adequately predict the fatigue life of René 95 at 1200°F (650°C).

UNCLASSIFIED

SECURITY CLASSIFICATION OF THIS PAGE(When Data Entered)

FOREWORD

This report was prepared by the Research Applications Division, Systems Research Laboratories, Inc., Dayton, OH, under Contract No. F33615-76-C-5191, "Mechanical Property Testing and Materials Evaluation." The contract was initiated under Project No. 7351, Task No. 735106, and was administered under the direction of the Air Force Materials Laboratory, Metals Behavior Branch (AFML/LLN), by Dr. Theodore Nicholas, Project Manager. The research reported here was conducted by H. L. Bernstein and was performed during the period January 1977 to August 1978.

The high-temperature strain-control testing was performed by Mar-Test, Inc., under Air Force Contract F33615-76-C-5245. The author gratefully acknowledges the valuable discussions with Messrs. Stentz, Conway, and Berling of Mar-Test, Inc. The results of the research of Dr. M. N. Menon while at the Air Force Materials Laboratory contributed to this work. The author also wishes to thank his colleagues, especially Dr. W. H. Reimann, Dr. T. Nicholas, and Capt. Jack M. Hyzak of the Air Force Materials Laboratory, and Dr. N. Ashbaugh of Systems Research Laboratories, Inc., for their assistance. The research reported here was performed under Air Force Contract F33615-76-C-5191.

Accession For	
MLL	GA&I
L. C. EYB	
Unannounced	<input checked="" type="checkbox"/>
Justification	<input type="checkbox"/>
By	
Distribution/	
Availability Codes	
Dist	Avail and/or special
A	

TABLE OF CONTENTS

Section	Page
I INTRODUCTION	1
II EVALUATION PROCEDURE	3
EXPERIMENTAL PROGRAM	3
Material	3
Fatigue Tests	7
PARAMETERS USED FOR EVALUATION OF THE MODELS	19
III EXPERIMENTAL RESULTS	21
IV MODELS	38
STRAINRANGE PARTITIONING MODEL	38
FREQUENCY-SEPARATION MODEL	69
OSTERGREN MODEL	75
DAMAGE RATE MODEL	86
V COMPARISON OF THE MODELS	95
VI CONCLUSIONS	100
REFERENCES	101

LIST OF ILLUSTRATIONS

Figure		Page
1	Microstructure of René 95	4
2	Stress-Strain Curve for René 95 at 1200°F (650°C)	6
3	Hysteresis Loops at Four Different Frequencies. $\Delta\epsilon_t = 1.4\%$	8
4	Hourglass Fatigue Specimens	10
5	Waveforms and Hysteresis Loops of Baseline Tests	13
6	Waveforms and Hysteresis Loops of Verification Tests	16
7	Stress Range as Function of Total Strainrange for 20-cpm and 0.05-cpm Continuously Cycling Tests	26
8	Mean Stress as Function of Total Strainrange	27
9	Typical Stress-Relaxation Behavior	29
10	Hysteresis Loops of 20-1/2-0.05 cpm, 1-1/2-20 cpm, and 0-05-1/2-20 cpm Tests Indicating Type of Strain-Recovery Process	30
11	Hysteresis Loops of 20-0.05 cpm and 0.05-20 cpm Tests With Their Companion Specimens Indicating Stress Relaxation	31
12	Elastic and Inelastic Strain as Function of Life for 20-cpm Tests	33
13	Total Strainrange as Function of Cycles to Failure	34
14	Inelastic Strainrange as Function of Cycles to Failure	36
15	Typical High-Temperature Hysteresis Loop to Explain Strainrange Partitioning	39
16	Inelastic Strain and Force Strip Charts and Hysteresis Loop for a cp Test	45
17a	Inelastic Strainrange as Function of N_{pp}	47
17b	Inelastic Strainrange as Function of N_{cp}	48
17c	Inelastic Strainrange as Function of N_{pc}	49

LIST OF ILLUSTRATIONS (Continued)

Figure		Page
17d	Inelastic Strainrange as Function of N_{cc}	50
17e	Strainrange-Partitioning Lines	51
18a	Life Predictions of Baseline Tests by the Strainrange-Partitioning Model	59
18b	Life Predictions of Baseline Tests by the Frequency-Separation Model	60
18c	Life Predictions of Baseline Tests by the Ostergren Model	61
18d	Life Predictions of Baseline Tests by the Damage-Rate Model	62
19a	Life Predictions of Verification Tests by Strainrange-Partitioning Model	63
19b	Life Predictions of Verification Tests by the Frequency-Separation Model	64
19c	Life Predictions of Verification Tests by the Ostergren Model	65
19d	Life Predictions of Verification Tests by the Damage-Rate Model	66
20	Illustration of Tension-Going and Compression-Going Time	71
21	Inelastic Strainrange as Function of Cycles to Failure for 1/1, 10/0, 10/1, and 1/10 Tests	76
22	$\Delta\epsilon_{inel} \times \sigma_t$ for 10/0, 0/10, 0.05-20 cpm, 0.05-1/2-20 cpm, 20-0.05 cpm, and 20-1/2-0.05 cpm Tests	84
23	$\Delta\epsilon_{inel} \times \sigma_t$ as Function of N_f	85
24	Illustration of Inelastic Strain Used in the Damage-Rate Model for a cp Test	92

LIST OF TABLES

Table		Page
I	TENSILE PROPERTIES OF RENE 95 AT 1200°F (650°C)	5
II	CREEP TESTS AT 1200°F (650°C)	9
III	BASELINE TESTS	14
IV	VERIFICATION TESTS	18
V	BASELINE DATA	22
VI	VERIFICATION DATA	25
VII	PARTITIONED STRAINRANGES	52
VIII	LIFE PREDICTIONS OF BASELINE TESTS	56
IX	LIFE PREDICTIONS OF VERIFICATION TESTS	67
X	VALUES OF THE FREQUENCY TERMS USED IN THE FREQUENCY- SEPARATION MODEL	73
XI	FORMULATIONS OF THE OSTERGREN MODEL	80
XII	VALUES OF THE FREQUENCY TERMS USED IN THE OSTERGREN MODEL	81
XIII	CONSTANTS, SCATTER BANDS, AND STANDARD DEVIATIONS FOR THE VARIOUS FORMULATIONS OF THE OSTERGREN MODEL	82
XIV	OVERALL ABILITY OF THE MODELS TO FIT THE DATA	96
XV	SEGREGATION OF THE DATA BY THE MODELS	97

Section I
INTRODUCTION

A major thrust in the development and use of military jet engines is cost reduction through better life-cycle management. Turbine disks represent an expensive engine component and are currently being replaced before their actual life has been reached. One of the reasons for this premature replacement is the inability to accurately predict the crack-initiation life of the disks. Even under simple loading conditions, this life cannot be predicted accurately. A major difficulty in predicting the crack-initiation life is accounting for the high-temperature effects of creep and environmental attack. The relative importance of these effects and how to incorporate them into a life-prediction scheme are not well understood at the present time.

Many models have been proposed for predicting crack initiation at elevated temperature. Of these models the following four have been applied to other materials with promising results and are the subject of study of the present report:

- Strainrange-Partitioning Model (SRP)^{1,2,3}
- Frequency-Separation Model (FS)^{4,5}
- Ostergren Model^{6,7}
- Damage-Rate Model (DRM)^{8,9,10}

These models were developed mainly for low-strength, high-ductility materials. The fatigue behavior of these materials in their range of application is characterized by large inelastic strain, few cycles to failure (< 1000), and long cyclic periods. The materials used for turbine disks are high-strength, low-ductility nickel-base superalloys. Their fatigue behavior at operating temperatures is almost exactly opposite that of the materials used in developing the above four models. The fatigue of disk materials is characterized by small, almost non-existent inelastic strains, fatigue lives of 10,000 - 50,000 cycles, and cyclic periods of 1 - 2 hr.

The purpose of the study described in this report is to determine whether these four models in their present form can be used to predict the crack-initiation lives of nickel-base superalloys at operating temperatures. This is an attempt to determine whether the models can be extended from low-strength, high-ductility materials to high-strength, low-ductility materials. For making this determination a representative nickel-base superalloy, cast and wrought René 95, was chosen. A series of fatigue tests--both continuous cycling tests at different frequencies and strain-hold tests--was run at 1200°F (650°C), which is the operating temperature of René 95. Each of the models was evaluated independently for its ability to predict the crack initiation lives, and then the models were compared to each other.

This work is a continuation of previous studies. Menon¹¹ evaluated the SRP and Frequency-Modified¹² Models using a smaller data base than that of the present study. Bernstein¹³ made a preliminary evaluation of these four models using a somewhat larger data base. A detailed evaluation of the SRP Model was made by Hyzak and Bernstein¹⁴ using the same data base as in the present report with the exception of six tests.

Section II
EVALUATION PROCEDURE

EXPERIMENTAL PROGRAM

Material

The material used to evaluate the models was thermomechanically processed, cast and wrought René 95--an advanced nickel-base superalloy designed for jet-engine turbine disks which operate at 1200°F (650°C). René 95 has both high tensile strength and excellent creep resistance at this temperature.

The processing and heat-treatment procedures are given in Ref. 11 along with the chemical composition. The final product was a circular pancake, 15 in. (38 cm.) in diam. and 1.5 in. (3.8 cm.) thick.

The thermomechanical processing (TMP) which the material underwent produced a duplex microstructure^{15,16} as shown in Fig. 1. The large grains (labeled B) were surrounded by very small grains (labeled A) which recrystallized in the grain boundaries due to TMP. Further information concerning the microstructure can be found in Refs. 11 and 16.

The tensile properties of René 95 at 1200°F (650°C) are given in Table I, and the stress-strain curve is shown in Fig. 2. The 0.2% yield point was 175 ksi, and the ultimate strength was 210 ksi. The modulus of elasticity and the yield point were the same in compression as in tension. The cyclic stress-strain curve was similar to the monotonic curve up to 1.1% strain.* The material had a limited amount of ductility, with an elongation of 11%.

At 1200°F (650°C), René 95 appeared to be strain-rate insensitive. Tensile tests were run in an Instron machine at head rates ranging from 0.002 to 0.5 in./min. (0.00508 - 1.27 cm/min.). Similar

*The cyclic stress-strain curve was determined from the half-life values of the tensile stress and strain in the 20-cpm tests.

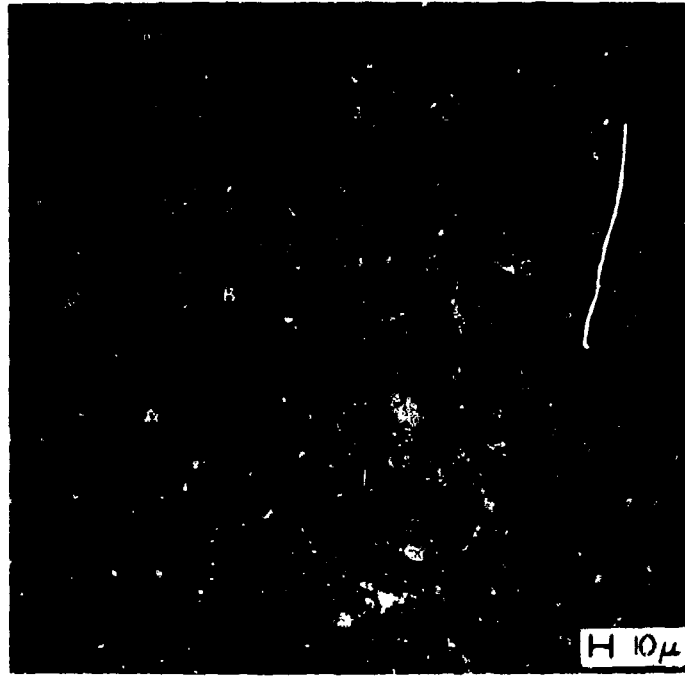


Figure 1 Microstructure of René 95

TABLE I
TENSILE PROPERTIES OF RENÉ 95 AT 1200°F (650°C)

0.2% Yield Stress:	175 ksi
Ultimate Stress:	210 ksi
Modulus of Elasticity:	25.4×10^3 ksi
% Reduction in Area:	12%
% Elongation:	11%

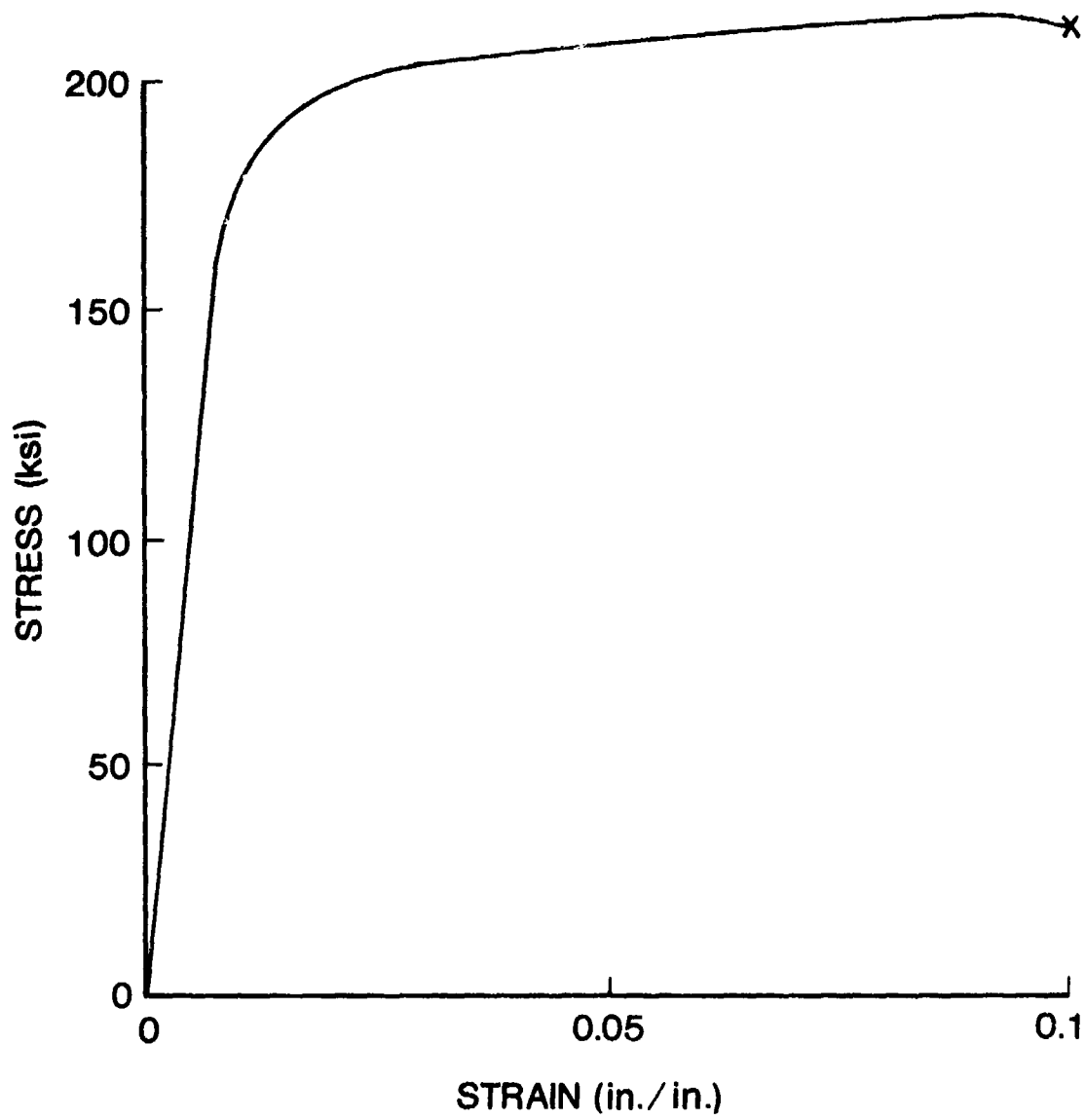


Figure 2 Stress-Strain Curve for René 95 at 1200°F (650°C)

stress-strain curves were obtained and no trend with respect to strain rate was evident.* A test was conducted in which a single specimen was cycled at rates of 20, 10, 2, 0.2 and 0.05 cpm, which is a range of over two decades. Stabilized hysteresis loops for each of these rates are shown in Fig. 3. There is little difference in stress-strain behavior between these rates.

The creep properties of René 95 are given in Table II. The creep properties have a large amount of scatter. This is thought to be due to attaching the extensometer to the shoulders of the specimen and to misalignment of the specimen caused by the threaded connections.

Fatigue Tests

The fatigue tests were performed using 1/4-in. (6.35-mm) diam. hourglass specimens. The diametral strain was measured and converted by an analog computer into equivalent axial strain. This axial strain was controlled during the test by a servo-hydraulic testing machine. The specimen was heated by an induction coil. A continuous strip-chart recording was made of the inelastic strain and force throughout the test. Hysteresis loops were recorded at the beginning of every test and during some, but not all, tests. A description of the test procedure can be found in Refs. 17 and 18.

The specimen geometry used is shown in Fig. 4. The hourglass section was longitudinally polished to 16 rms. Both burtonhead and threaded ends were used, with no effect upon the life due to these different ends being observed. The specimens were taken in the tangential direction of the pancake. The two pancakes used for the specimens in this study were cut from the same ingot. Specimens taken from the first pancake had identification numbers from 0 to 99 and those from the second pancake from 200 to 299. No difference in tensile, creep, or fatigue behavior was observed between the two pancakes.

*Within the experimental accuracy of the extensometry--and considering material scatter--the stress-strain curves were similar and showed no ordering with respect to strain rate.

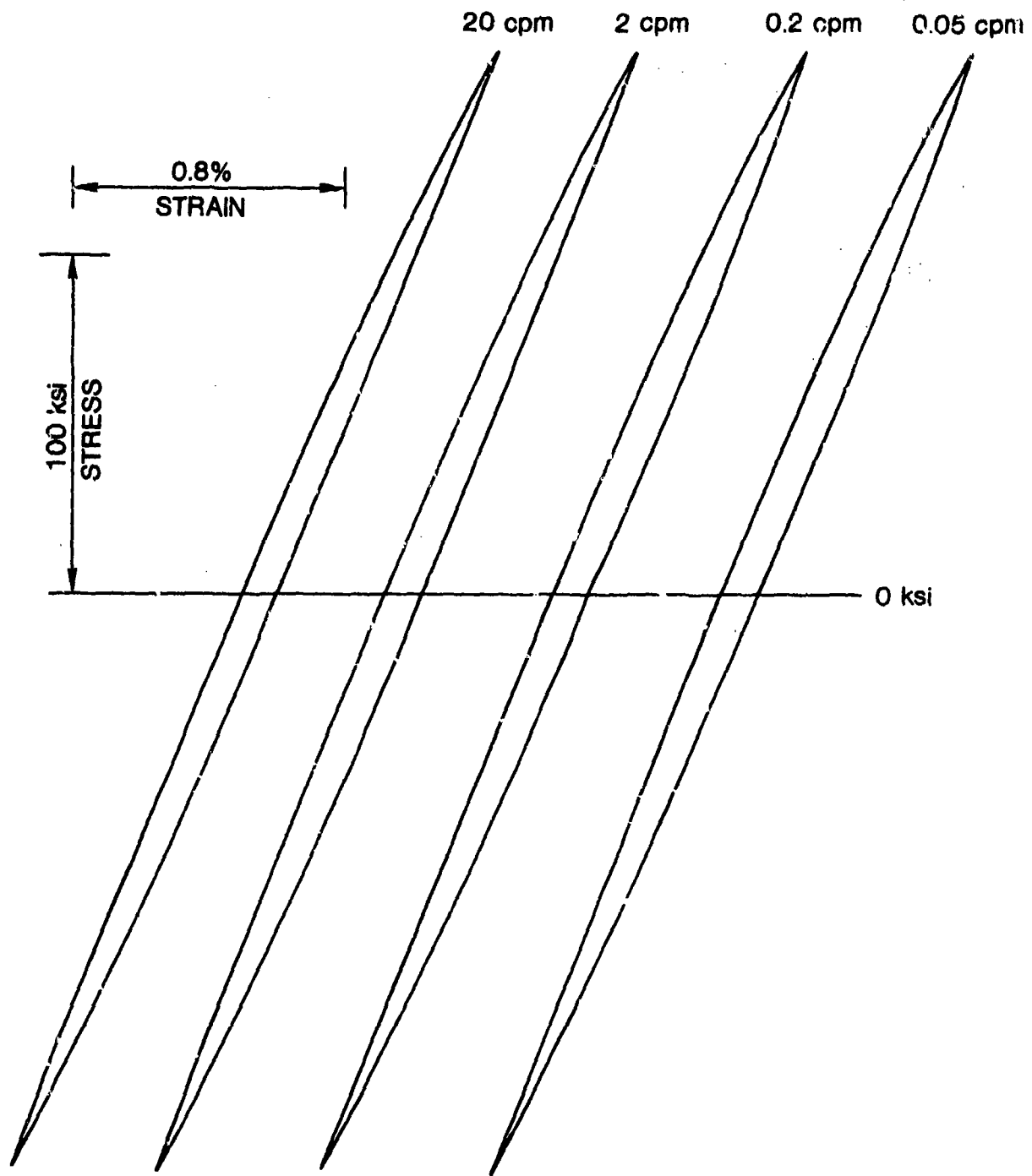


Figure 3 Hysteresis Loops at Four Different Frequencies. $\Delta\epsilon_t = 1.4\%$

TABLE II
 CREEP TESTS AT 1200°F (650°C)

Specimen	Stress* (ksi)	Secondary Creep Rate (in./in./min.)	Time to Failure (min.)
C-1-B	180	5.26×10^{-4}	94
C-2-B	171	4.85×10^{-5}	433
C-4	171	6.90×10^{-5}	430
219	160	4.00×10^{-5}	960
C-5	147	1.11×10^{-6}	4,147
47	147	1.87×10^{-6}	11,400
R-20-B	128	4.41×10^{-7}	30,255

*Stress = $\frac{\text{Load}}{\text{Area at 1200°F (650°C)}}$

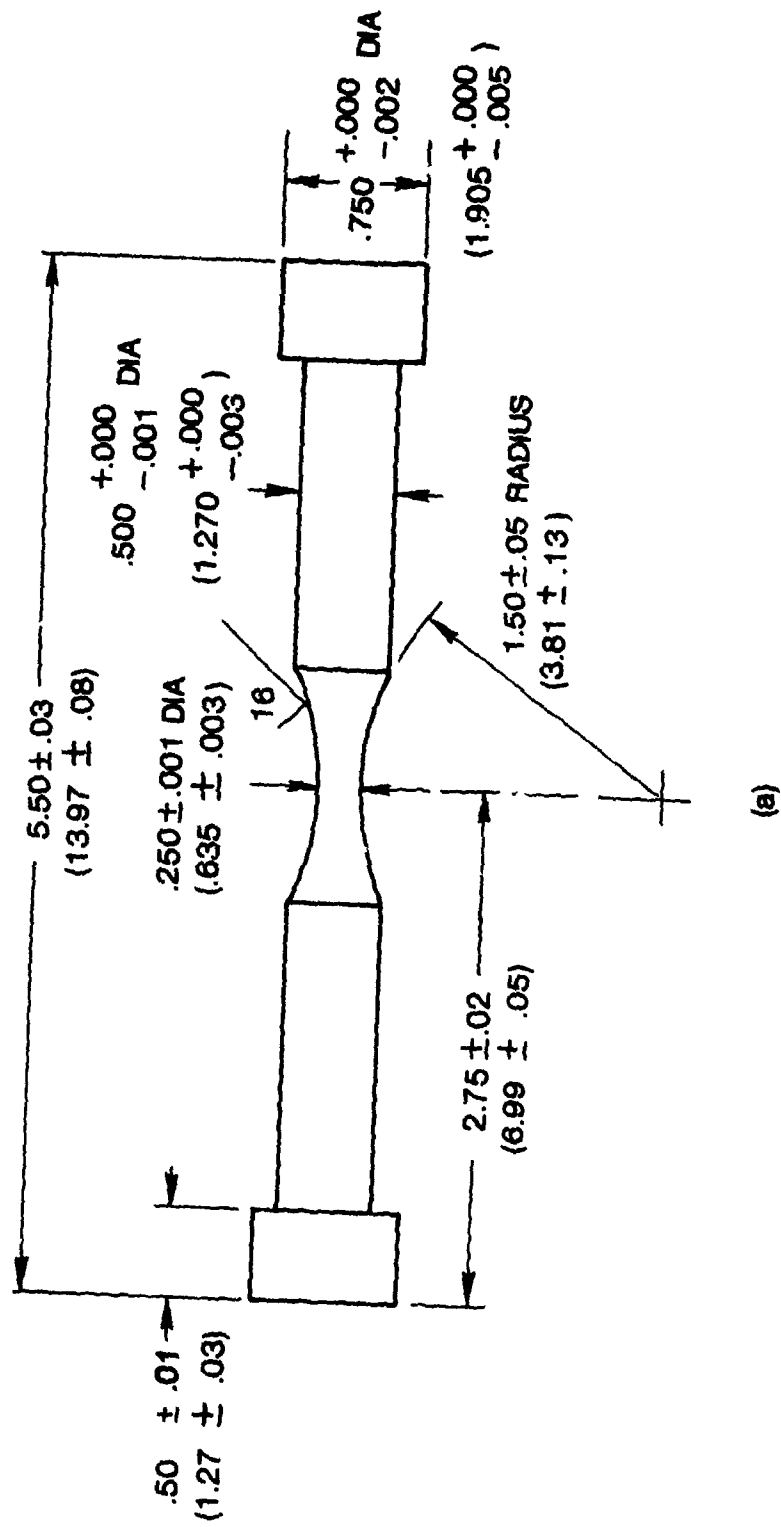


Figure 4 Hourglass Fatigue Specimens
 (Dimensions in Inches with Centimeter Equivalents in Parentheses)

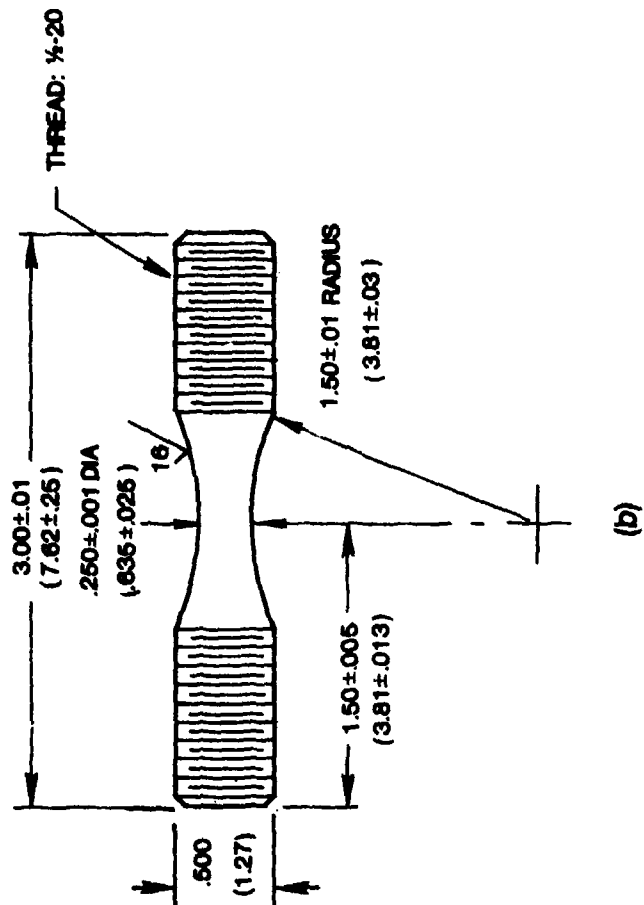


Figure 4 (Continued)

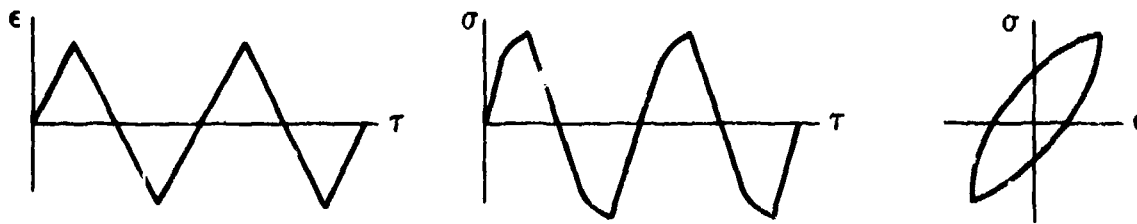
Completely reversed, push-pull, strain-controlled tests having a zero mean strain were performed at 1200°F (650°C). The testing program was divided into two parts--baseline tests and verification tests. The former were used to establish the constants in the models and the latter to determine whether the model could predict the lives of tests not used in establishing the constants of the model. The waveforms of the verification tests were different from those of the baseline tests.

In the baseline tests, continuous cycling and strain-hold waveforms were used. The continuous-cycling tests were run at two frequencies--20 and 0.05 cycles per minute (cpm). These continuous-cycling tests are identified as "20-cpm" or "0.05-cpm" tests. The strain-hold tests consisted of tensile strain holds (cp tests), compressive strain holds (pc tests), and both tensile and compressive strain holds (cc tests).* The strain was held constant for either 1 or 10 min. The waveforms used for the baseline tests are shown in Fig. 5 and summarized in Table III. The strain-hold tests are identified by a two-digit code x/y, where x is the amount of time spent in a tensile-strain hold and y the amount of time spent in a compressive strain hold. For example, a test having a 1-min. strain hold in tension and compression is called a 1/1 test, and a test having a 1-min. strain hold in tension only is called a 1/0 test.

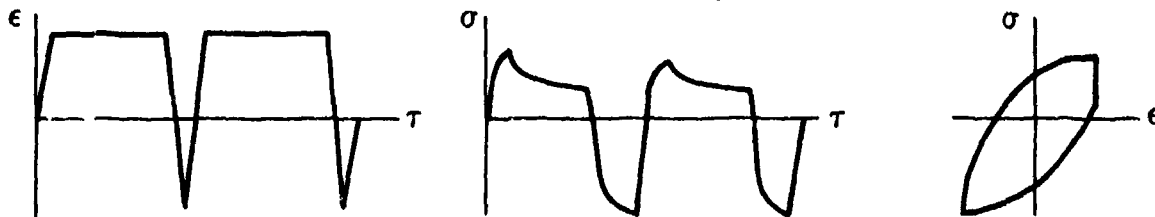
In all except the 0.05-cpm tests, the total axial strain was the controlled variable. All the 0.05-cpm tests except one were controlled by the axial inelastic strain. Neither the stress-strain behavior nor the life appeared to be influenced by controlling the inelastic strain instead of the total strain. The behavior of the one 0.05-cpm test (No. 34), where total strain was controlled, was similar to the 0.05-cpm tests where inelastic strain was controlled.

*The terms cp, pc, and cc tests originated from the Strainrange-Partitioning Model, and the rationale for their use is discussed in the section on this model.

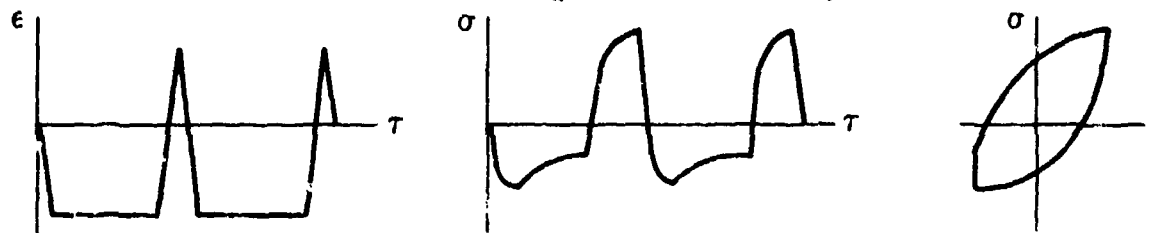
CONTINUOUS STRAIN CYCLING (20 cpm, .05 cpm)



TENSION STRAIN HOLD (cp - 1/0, 10/0)



COMPRESSION STRAIN HOLD (pc - 0/1, 0/10)



TENSION AND COMPRESSION STRAIN HOLD (cc - 1/1, 10/10)

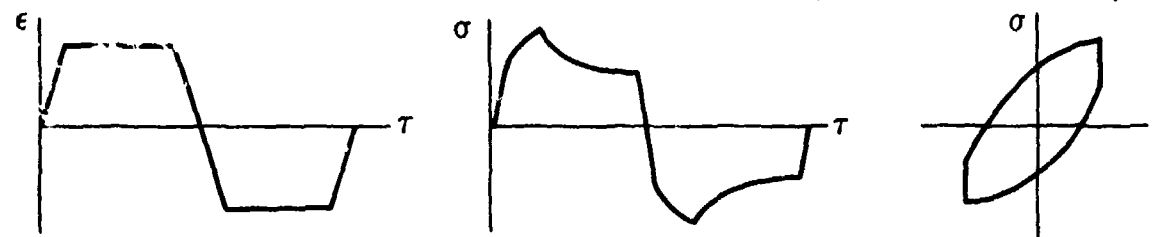


Figure 5 Waveforms and Hysteresis Loops of Baseline Tests

TABLE III
BASELINE TESTS*

Symbol	Description
20 cpm (or pp)	Continuous cycling at a frequency of 20 cycles/min. or 3 sec/cycle.
0.05 cpm	Continuous cycling at a frequency of 0.05 cycles/min. or 20 min./cycle. In all but one of these tests, the plastic strain was the controlled variable.
1-0 (or cp)	1-min. hold time at maximum strain in tension. 20-cpm ramps for the strain reversals.
10-0 (or cp)	As in 1-0, except 10-min. hold time instead of 1 min.
0-1 (or pc)	1-min hold time at maximum strain in compression. 20-cpm ramps for the strain reversals.
0-10 (or pc)	As in 0-1, except 10-min. hold time instead of 1 min.
1-1 (or cc)	1-min. hold time at maximum strain both in tension and compression. 20-cpm ramps for the strain reversals.
10-10 (or cc)	As in 1-1, except 10-min. hold instead of 1 min.

*These tests were conducted at 1200°F (650°C), with an A ratio on total strain of infinity. All of the specimens tested were of the hourglass configuration.

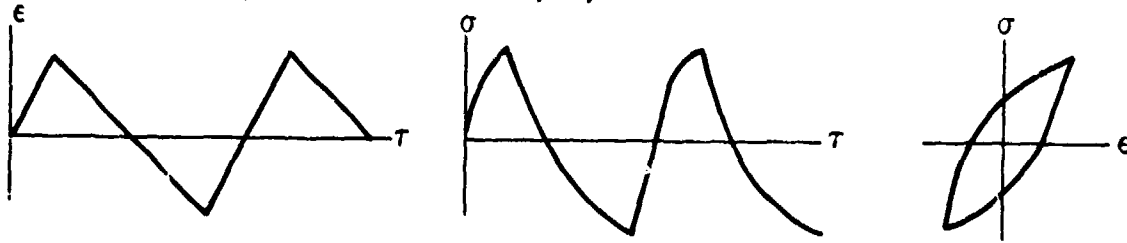
The verification tests utilized waveforms different from those for the baseline tests, which allowed examination of the ability of a model to predict these other waveforms. The waveforms used for the verification tests are shown in Fig. 6 and described in Table IV. They consisted of unbalanced strain-hold tests and dual-rate continuous-cycling tests.

The unbalanced strain-hold tests were similar to the baseline strain-hold tests except that the strain was held on the tensile side for 1 min. and on the compressive side for 10 min., or 10 min. in tension and 1 min. in compression. These tests are identified by the code 10/1 or 1/10, the first number being the tensile-hold time and the second number the compressive-hold time. In the intermediate strain-hold tests, the hold period was intermediate between the peak tensile and compressive strains rather than at the peak strain. The purpose of this test was to determine whether there was an order effect when first plastic strain and then creep strains were applied to the test specimen, followed by more plastic strain. The intermediate strain-hold tests are identified by the code II/0 or 0/II, where the I signifies an intermediate hold.

In the dual-rate continuous-cycling tests, a positive strain rate which was different from the negative strain rate was employed. When the positive strain rate was larger than the negative strain rate, the test was called a fast-slow test (F/S). When the positive rate was smaller than the negative rate, the test was called a slow-fast test (S/F). In all of the dual-rate tests, the fast strain rate was 20 cpm, and the slow strain rate was either 1 cpm or 0.05 cpm. These tests are identified by a two-digit code x-y cpm, where x is the positive strain rate and y is the negative strain rate. For example, a test having a positive strain rate of 0.05 cpm and a negative rate of 20 cpm is called a 0.05-20 cpm test.

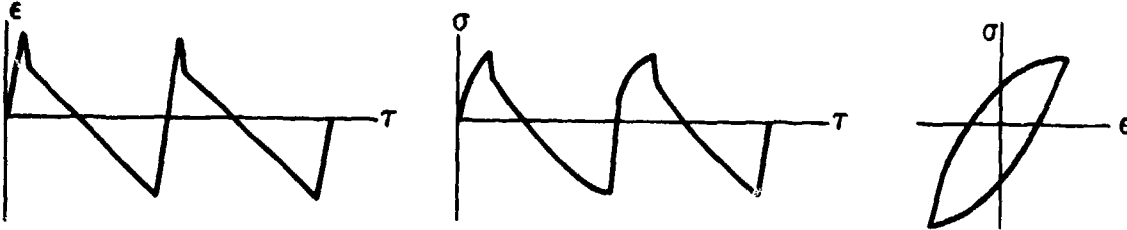
On some of the dual-rate tests, the first quarter of the strain in the slow rate was run at the fast rate, as shown in Fig. 6, in order to avoid spending a long period of time at a high tensile or compressive load which could result in creep. In these tests the strain rate was changed from

FAST/SLOW (F/S, 20 - 0.05 cpm)

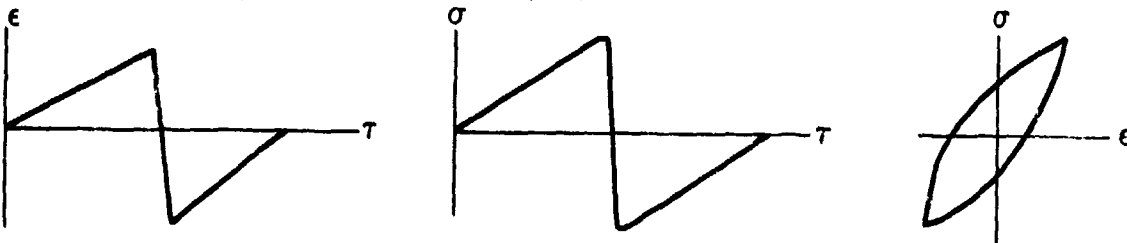


FAST/SLOW (F/S, 20 - $\frac{1}{2}$ - 0.05 cpm)

WITH RATE CHANGE HALFWAY BETWEEN MAX. AND ZERO STRAIN



SLOW/FAST (S/F, 0.05 - 20 cpm)



SLOW/FAST (S/F, 0.05 - $\frac{1}{2}$ - 20 cpm, 1 - $\frac{1}{2}$ - 20 cpm)

WITH RATE CHANGE HALFWAY BETWEEN MIN. AND ZERO STRAIN

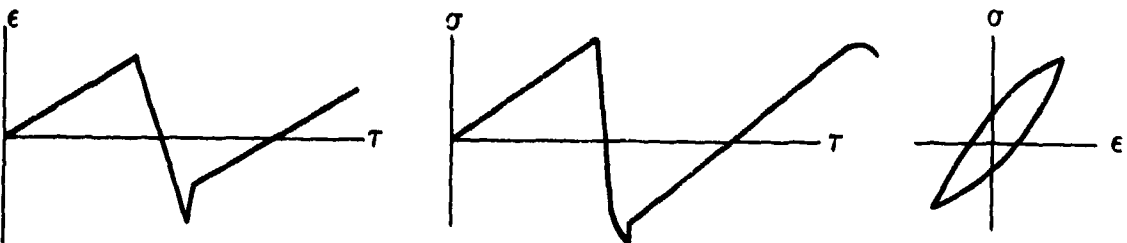
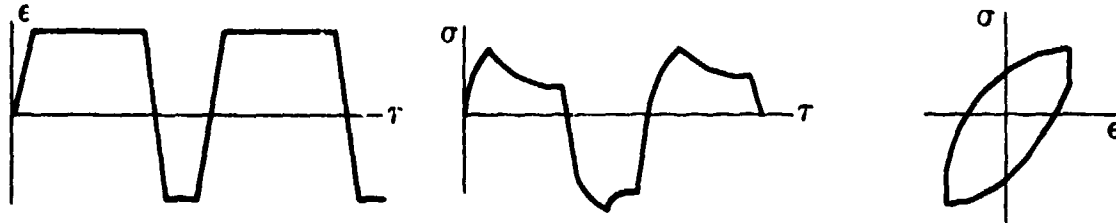
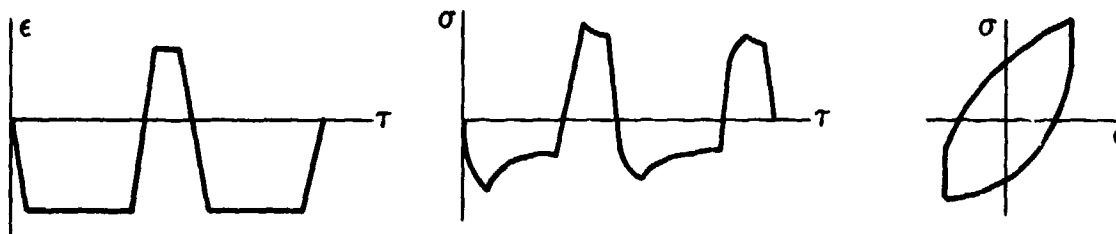


Figure 6 Waveforms and Hysteresis Loops of Verification Tests

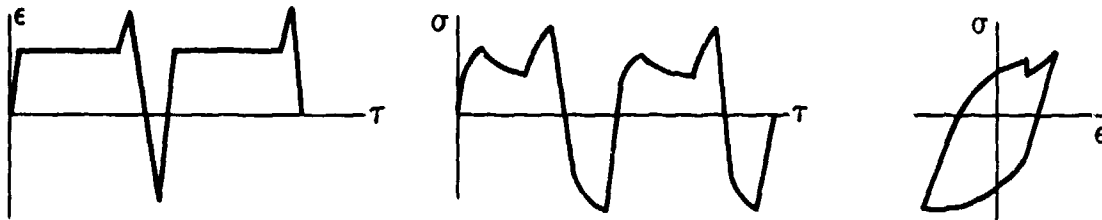
UNSYMMETRICAL STRAIN HOLD (10/1)



UNSYMMETRICAL STRAIN HOLD (1/10)



INTERMEDIATE TENSILE STRAIN HOLD (11/0)



INTERMEDIATE COMPRESSIVE STRAIN HOLD (0/11)

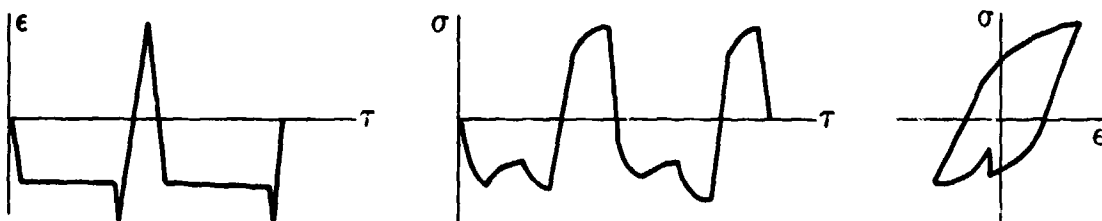


Figure 6 (continued)

TABLE IV
VERIFICATION TESTS*

Symbol	Description
20-0.05 cpm (or F/S)	Continuous cycling at two frequencies. The positive strain rate was 20-cpm and the negative strain rate was 0.05-cpm. The changes in strain rate occurred at the peak tensile and compressive strains.
20-1/2-0.05 cpm (or F/S)	As in 20-0.05-cpm, except the change from the fast to the slow strain rate occurred halfway between the peak tensile strain and zero strain.
0.05-20-cpm (or S/F)	Continuous cycling at two frequencies. The positive strain rate was 0.05-cpm and the negative strain rate was 20-cpm. The changes in strain rate occurred at the peak tensile and compressive strains.
0.05-1/2-20 cpm (or S/F)	As in 0.05-20-cpm, except the change from the fast to the slow strain rate occurred halfway between the peak compressive strain and zero strain.
1-1/2-20 cpm (or S/F)	As in 0.05-1/2-20-cpm, except the slow strain rate was 1-cpm.
I1-0	1-min. hold time before the peak tensile strain. 20-cpm ramps for the strain reversals.
0-I1	1-min. hold time before the peak compressive strain. 20-cpm ramps for the strain reversals.
10-1	10-min. hold time at the peak tensile strain and 1-min. hold time at the peak compressive strain. 20-cpm ramps for the strain reversals.
1-10	1-min. hold time at the peak tensile strain and 10-min. hold time at the peak compressive strain. 20-cpm ramps for the strain reversals.

*These tests were conducted at 1200°F (650°C), with an A ratio on total strain of infinity. All of the specimens tested were of the hourglass configuration.

the fast to the slow strain rate halfway between the peak tensile or compressive strain and the zero-strain level. These tests are identified by means of a "1/2" between the strain rates, i.e., 0.05-1/2-20 cpm.

PARAMETERS USED FOR EVALUATION OF THE MODELS

The predictive ability of a model was assessed using four different criteria concerning the ability of the model to: 1) correlate the baseline data; 2) predict the verification data; 3) avoid consistently overpredicting or underpredicting any test waveforms, and 4) conceptually predict the test results.

The ability of the models to correlate the baseline data was determined in two different ways. First, the scatter band of the predicted-vs.-observed life was determined. The scatter band was defined as the data point having the largest ratio of predicted to observed life or the reciprocal of this ratio if the ratio was less than one.

$$\text{scatter band} = \max_{\text{over data}} \begin{cases} \frac{N_p}{N_f} & \text{if } N_p > N_f \\ \frac{N_f}{N_p} & \text{if } N_p \leq N_f \end{cases}$$

where N_p is the predicted life and N_f the observed life. This is the conventional evaluation technique for models of creep-fatigue interaction. Second, the standard deviation between the predicted and the observed life was determined. The standard deviation is defined as

$$\text{standard deviation} = \left[\frac{\sum (\log N_f - \log N_p)^2}{n-1} \right]^{1/2}$$

where n is the number of data points.

This evaluation procedure is a measure of two aspects of the predictive ability of a model, the scatter band indicating how far away from the mean value the data points fall, and the standard deviation indicating how well the data points group about the mean value. A model which minimizes both of these quantities would be the preferred model.

The lives of the verification tests were predicted using constants in the model which were determined from the baseline tests. If the predicted life was within a factor of two of the observed life, then the model was considered to have been verified. If the prediction was greater than two, then the model was considered to be limited in applicability because of its inability to generalize to other waveforms not used in generating the constants of the model.

The life predictions of each model for the baseline tests were examined to determine whether any test waveforms were consistently overpredicted or underpredicted. This phenomenon was termed segregation because the data were segregated to one side or the other of the best-fit line. Segregation occurred because the model was not correctly taking into account the material behavior.

The formulation of the model implied that the material will behave in certain ways. For example, models that contain frequency terms predict that the fatigue life will be reduced as the frequency becomes slower. Each model was examined to determine whether the material behavior during the baseline and verification tests was as the model predicted.

No attempt was made to assess the applicability of the models on the basis of creep or environmental mechanisms controlling the fatigue life. Studies of the effect of environment as a function of creep on the fatigue life of René 95 at 1200°F (650°C) are planned. Also, fracture surfaces and metallographic sections from some of the fatigue specimens have been examined. No definite conclusions concerning intergranular-vs.-transgranular cracking or the damage from environment or creep mechanisms have been reached.

Section III

EXPERIMENTAL RESULTS

The baseline data are presented in Table V and the verification data in Table VI. Stress and strain values were measured from the strip-chart recordings at one-half the specimen life. In most of the tests, the inelastic component of strain was small as compared to the elastic component.

As previously discussed in the section on Material, the stress-strain behavior of René 95 at 1200°F (650°C) is rather insensitive to strain rate. The 20-cpm and 0.05-cpm fatigue tests showed very similar stress-strain behavior. The half-life stress ranges and total strainranges for these tests are shown in Fig. 7.

The most noticeable effect of the strain-hold waveforms upon the stress-strain behavior was shifts in the mean stress. Figure 8 is a plot of the mean stress as a function of the total strainrange for all baseline and verification tests. It should be noted that in the 20-cpm tests, a small compressive mean stress existed which became larger with decrease in strainrange. During the tensile strain-hold tests, compressive mean stresses developed, while in the compressive strain-hold tests tensile mean stresses developed. The mean stresses became greater as the strainrange was decreased and as the hold time was increased. Some of these mean stresses became large-- +23 and -41 ksi. The unbalanced strain-hold tests had a mean stress similar to that of the tensile or compressive strain-hold tests. The 10/1 tests had compressive mean stresses, and the 1/10 tests had tensile mean stresses. These mean stresses were not so large as those in the tensile and compressive strain-hold tests. The balanced strain-hold tests did not develop large mean stresses but had small compressive mean stresses similar to those in the 20-cpm tests.

TABLE V

BASELINE DATA

René 95 - 1200°F (650°C)

A-Ratio - Infinity

SPEC. NO.	TYPE OF TEST	TOTAL STRAIN-RANGE (%)	CYCLES TO FAILURE	INEL. STRAIN-RANGE (%)	MAX. TENSILE STRESS (KSI)	MAX. COMPR. STRESS (KSI)	RELAXED TENSILE STRESS (KSI)	RELAXED COMPR. STRESS (KSI)	TIME TO FAILURE (HOURS)
17	20CPH	2.00	234	.53000	179.0	195.0	0.00	0.00	.20
18	20CPM	1.80	307	.40800	175.0	166.0	0.00	0.00	.26
224	20CPM	1.60	415	.25000	168.0	176.0	0.00	0.00	.35
22	20CPM	1.60	461	.31100	168.0	173.0	0.00	0.00	.38
240	20CPM	1.60	463	.28500	161.1	173.5	0.00	0.00	.39
26	20CPM	1.40	784	.21670	156.0	164.0	0.00	0.00	.65
27	20CPM	1.20	1629	.10400	140.0	146.0	0.00	0.00	1.36
255	20CPM	1.10	5332	.02370	128.0	151.0	0.00	0.00	4.44
29	20CPM	1.00	5158	.01770	116.0	133.0	0.00	0.00	4.30
30	20CPM	.90	16215	.01160	107.0	125.0	0.00	0.00	13.50
234	20CPM	.90	19160	.01300	99.0	133.8	0.00	0.00	15.97
235	20CPM	.90	22364	.00850	99.2	129.2	0.00	0.00	18.64
239	20CPM	.89	28697	.01300	106.7	120.4	0.00	0.00	23.91
23	.05CPM	1.80	110	.45000	161.0	181.0	0.00	0.00	36.17
24	.05CPM	1.70	159	.35000	168.0	188.0	0.00	0.00	52.48
20	.05CPM	1.60	301	.25000	161.0	179.0	0.00	0.00	101.29
25	.05CPM	1.50	282	.18000	145.0	182.0	0.00	0.00	94.00
34	.05CPM	1.30	526	.12000	137.0	165.0	0.00	0.00	175.33
19	.05CPM	1.20	1138	.10000	117.0	156.0	0.00	0.00	360.94

TABLE V (Continued)

BASELINE DATA

René 95 - 1200°F (650°C)

A-Ratio - Infinity

SPEC. NO.	TYPE OF TEST	TOTAL STRAIN RANGE (%)	CYCLES TO FAILURE	IMEL. STRAIN RANGE (%)	MAX. TENSILE STRESS (KSI)	MAX. COMPR. STRESS (KSI)	RELAXED TENSILE STRESS (KSI)	RELAXED COMPR. STRESS (KSI)	TIME TO FAILURE (HOURS)
245	1-0	2.00	171	.65700	171.0	194.0	30.46	0.00	2.99
5	1-0	1.80	255	.52200	161.0	187.0	19.10	0.00	4.47
10	1-0	1.60	257	.29700	160.0	191.0	8.90	0.00	4.51
7	1-0	1.40	748	.20600	138.0	178.0	8.00	0.00	13.09
12	1-0	1.20	1289	.08930	129.0	166.0	1.60	0.00	23.02
39	1-0	1.10	1781	.08900	108.0	154.0	4.80	0.00	31.17
38	1-0	1.00	5013	.04900	101.0	148.0	1.50	0.00	87.72
233	1-0	1.00	6519	.06050	89.3	158.4	1.90	0.00	114.08
33	1-0	1.00	9609	.03800	82.8	159.0	.51	0.00	168.15
237	1-0	.90	16418	.04590	70.3	151.9	1.20	0.00	287.31
228	10-0	1.40	481	.18500	130.0	191.0	7.56	0.00	80.57
40	10-0	1.20	1705	.12600	108.0	178.0	6.20	0.00	285.58
6	0-1	1.80	207	.42900	178.0	181.0	0.00	15.00	3.50
11	0-1	1.60	209	.46800	162.0	161.0	0.00	15.90	3.66
14	0-1	1.60	219	.32400	177.0	174.0	0.00	10.70	3.83
8	0-1	1.40	413	.19200	165.0	158.0	0.00	6.20	7.30
13	0-1	1.20	846	.09790	156.0	140.0	0.00	2.30	14.80
241	0-1	1.10	1940	.04900	141.0	129.8	0.00	1.40	33.95
16	0-1	1.00	3093	.01030	124.0	123.0	0.00	.40	54.12
238	0-1	.90	4619	.02800	127.4	101.4	0.00	1.40	80.83

TABLE V (Continued)

BASELINE DATA

René 95 - 1200°F (650°C)

A-Ratio - Infinity

SPEC. NO.	TYPE OF TEST	TOTAL STRAIN RANGE (%)	CYCLES TO FAILURE	INEL. STRAIN RANGE (%)	MAX. TENSILE STRESS (KSI)	MAX. COMPR. STRESS (KSI)	RELAXED TENSILE STRESS (KSI)	RELAXED COMPR. STRESS (KSI)	TIME TO FAILURE (HOURS)
222	0-10	1.40	224	.13590	176.0	155.0	0.00	5.05	37.52
41	0-10	1.20	283	.18500	164.0	117.0	0.00	14.00	47.40
253	0-10	1.00	1397	.03053	141.0	110.0	0.00	.69	234.00
1	1-1	1.80	156	.55000	181.0	196.0	28.60	21.60	5.29
2	1-1	1.60	238	.34900	170.0	184.0	18.60	14.00	8.07
32	1-1	1.40	358	.20100	150.0	172.0	9.70	7.10	12.13
9	1-1	1.20	959	.12200	135.0	154.0	7.50	8.80	32.48
4	1-1	1.00	1215	.11600	120.0	134.0	10.80	6.70	41.52
15	1-1	1.00	1288	.07800	117.0	136.0	6.20	5.10	43.65
229	1-1	.90	5277	.02450	95.2	128.0	0.00	0.00	179.42
28	10-10	1.80	115	.70100	179.0	193.0	54.60	47.70	36.41
31	10-10	1.40	199	.49700	158.0	171.0	49.00	43.10	65.85
230	10-10	1.20	331	.15720	142.0	160.0	18.70	15.20	110.55

TABLE VI
VERIFICATION DATA
René 95 - 1200°F (650°C)

A-Ratio - Infinity

SPEC. NO.	TYPE OF TEST	TOTAL STRAIN -RANGE (%)	CYCLES TO FAILURE	INEL. STRAIN -RANGE (%)	MAX. TENSILE STRESS (KSI)	MAX. COMPR. STRESS (KSI)	RELAXED TENSILE STRESS (KSI)	RELAXED COMPR. STRESS (KSI)	RELAXED STRESS PERIOD (KSI)	STRESS* AT HOLD PERIOD (KSI)	STRAIN* AT HOLD PERIOD (%)	TIME TO FAILURE (HOURS)
251	20-0-05 cpm	1.40	636	.09850	161.0	177.0	0.00	0.00	0.00	161.0	.70	114.64
262	20-1/2-0.05 cpm	1.20	1086	.04700	144.0	147.0	0.00	0.00	0.00	67.5	.29	181.45
261	1-1/2-20 cpm	1.40	499	.11000	157.0	169.0	0.00	0.00	0.00	-77.5	-.34	8.52
256	0.05-1/2-20 cpm	1.80	60	.26200	181.0	197.0	0.00	0.00	0.00	-197.0	-.90	10.27
252	0.05-20 cpm	1.40	194	.06640	166.0	175.0	0.00	0.00	0.00	-175.0	-.70	32.23
260	0.05-1/2-20 cpm	1.40	646	.10000	153.0	174.0	0.00	0.00	0.00	-71.0	-.30	107.94
253	0.05-1/2-20 cpm	1.20	1731	.07200	126.0	162.0	0.00	0.00	0.00	-89.0	-.30	289.22
242	I1-0	1.80	472	.42220	163.0	166.0	13.00	0.00	0.00	155.0	.80	8.28
246	I1-0	1.80	253	.41200	170.0	190.0	16.50	0.00	0.00	144.0	.70	4.43
244	I1-0	1.60	447	.26640	154.0	181.0	10.00	0.00	0.00	144.0	.70	7.81
247	0-I1	1.80	263	.35590	172.0	186.0	0.00	0.00	14.70	156.0	-.70	4.60
227	10-1	1.40	455	.29210	144.0	176.0	23.60	13.20	13.20			63.80
223	10-1	1.20	945	.15850	118.0	164.0	11.60	5.30	5.30			174.03
226	1-10	1.40	349	.22100	165.0	161.0	15.90	13.70	13.70			64.27
225	1-10	1.20	464	.16170	150.0	140.0	12.20	10.60	10.60			85.45

*For Tests 251 through 259, the stress and strain at hold period are the stress and strain when the strain rate changed from the fast to the slow rate.

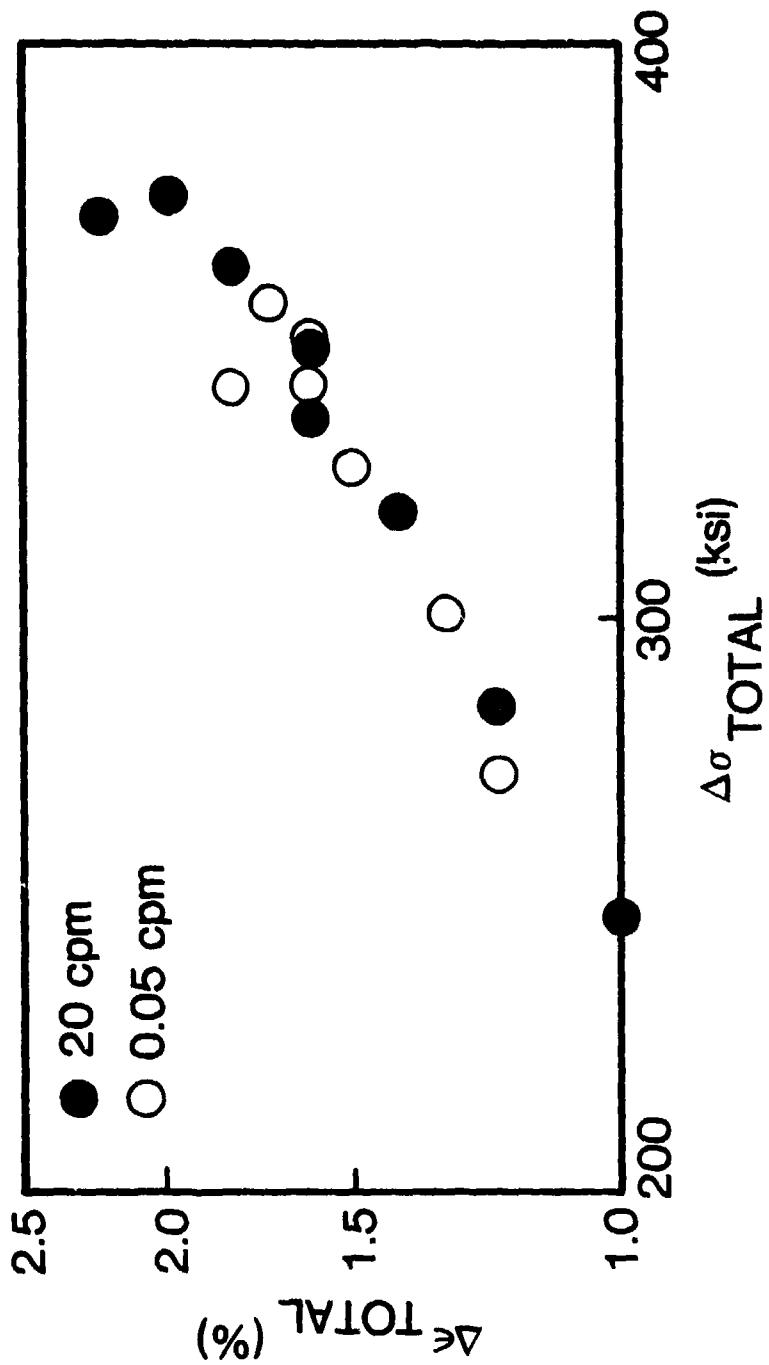


Figure 7 Stress Range as Function of Total Strainrange for 20-cpm and 0.05-cpm Continuously Cycling Tests

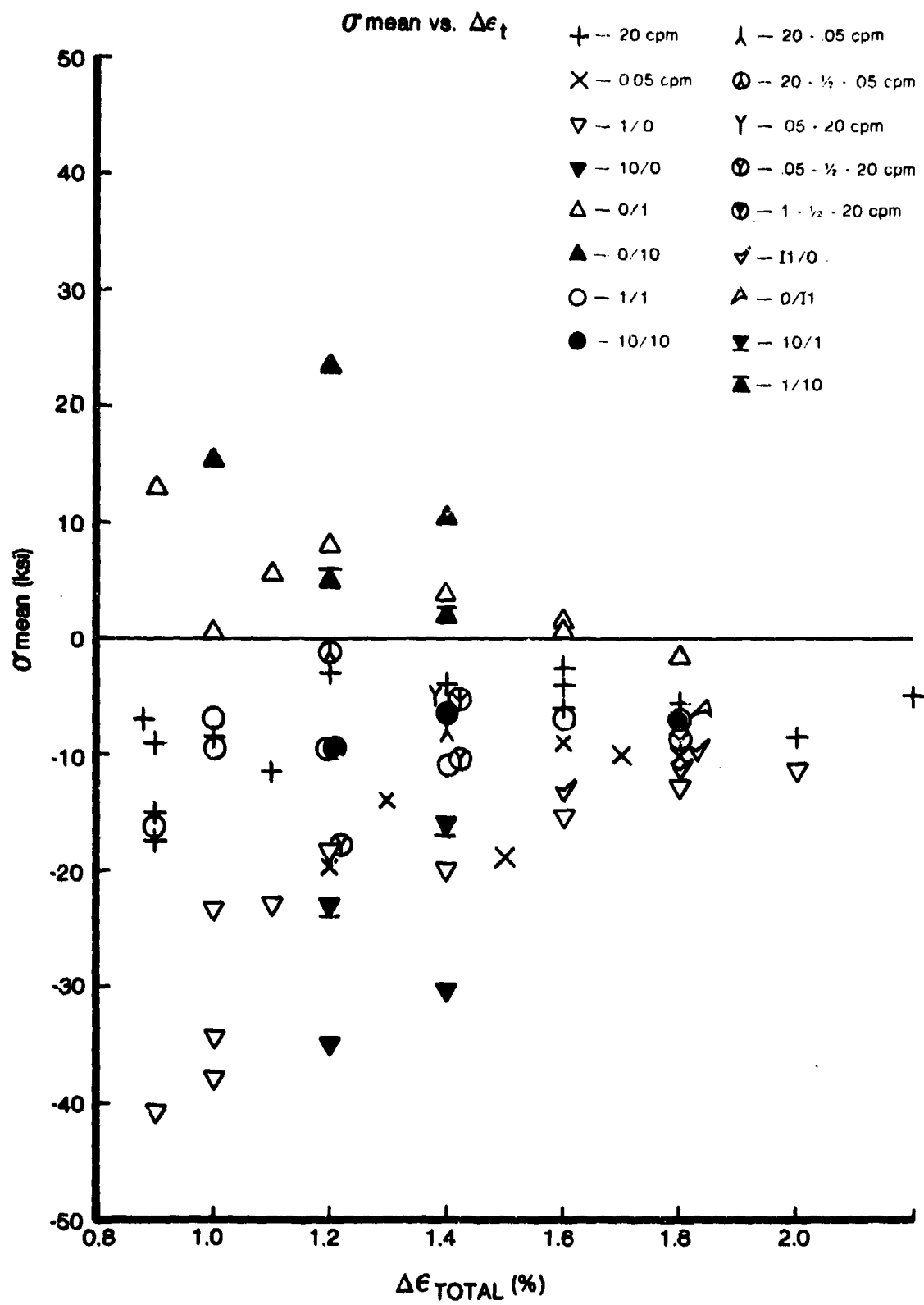


Figure 8 Mean Stress as Function of Total Strainrange

The excellent creep resistance of René 95 at 1200°F (650°C) was observed in the stress-relaxation behavior of the strain-hold tests. Except at the higher strainranges, only a small amount of stress relaxation occurred; at the lower strainranges virtually none was observed. Generally, a significant amount of stress relaxation occurred during the first 10 sec. of the hold period, with additional stress relaxation taking place during the remaining 50 or 590 sec. One example of the stress-relaxation behavior is given in Fig. 9 for a balanced strain-hold test.

The dual-rate tests exhibited time-dependent behavior when the strain rate was changed from the fast to the slow rate. As shown in Fig. 10, when the rate change occurred between the peak compressive or tensile strain and the zero strain level, a process similar to strain recovery occurred. In this process the stress remained almost constant although the total strain was decreased. When the rate change occurred at the peak tensile or compressive strain, stress relaxation took place, as shown in Fig. 11.

The lives of the fatigue tests were longer than the transition fatigue life, which is approximately 72 cycles. The transition fatigue life is defined as the number of cycles where the elastic-strain-vs-life line and the inelastic-strain-vs-life line intersect for the 20-cpm tests, as shown in Fig. 12. Some of the fatigue test lives were over two decades longer than the transition life.

The lives of the baseline fatigue tests plotted as a function of the total strainrange are shown in Fig. 13. Based on the total strainrange, the most damaging baseline waveforms were the compressive strain-hold tests and the balanced strain-hold tests. The life reduction became greater as the hold time became longer. The least damaging baseline waveforms were those for the 20-cpm and the tensile strain-hold tests.

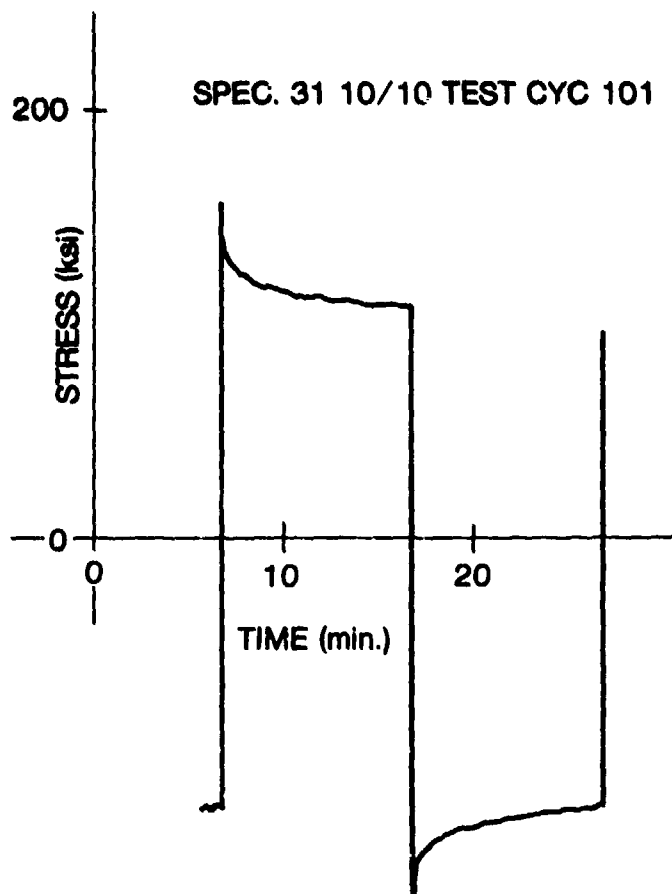


Figure 9 Typical Stress-Relaxation Behavior

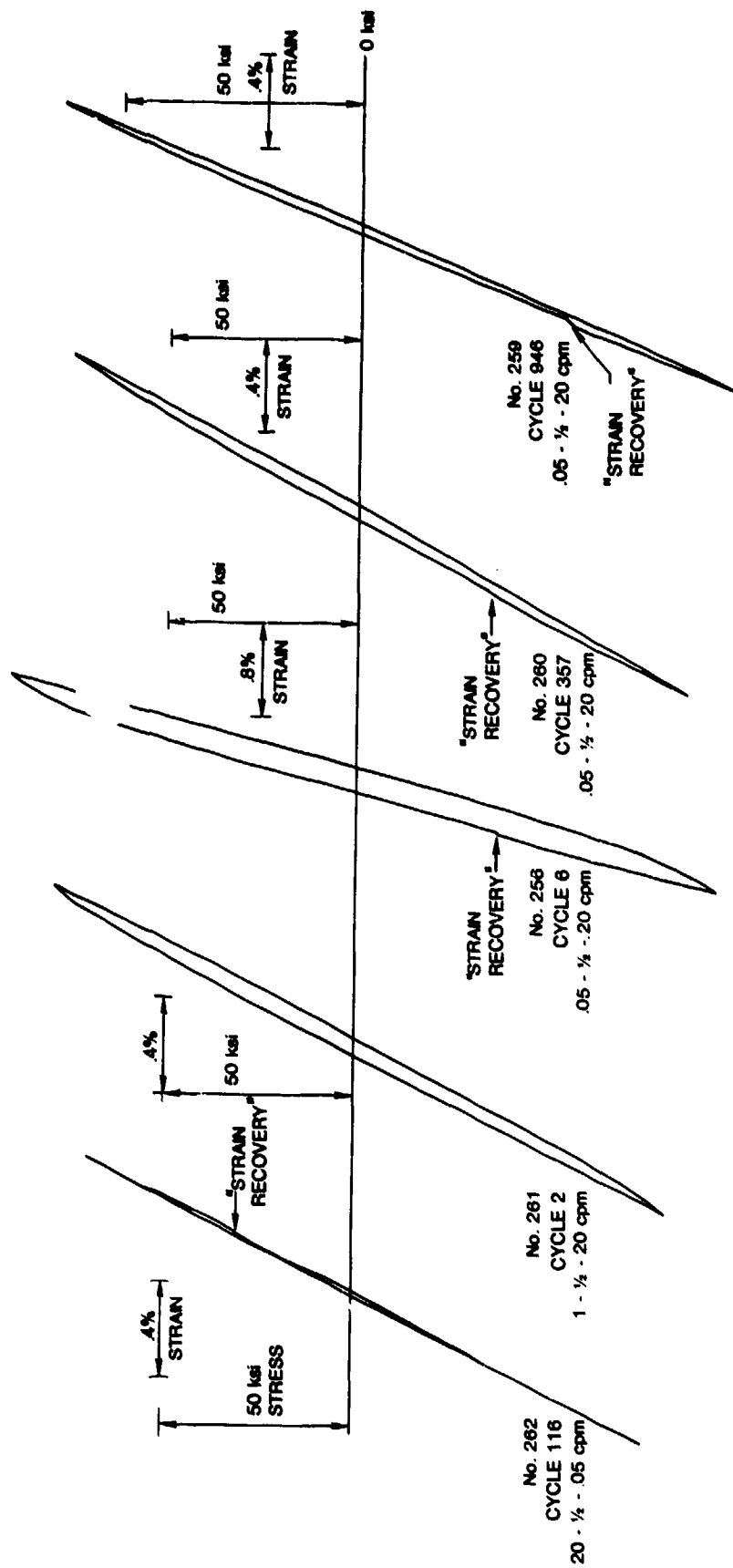


Figure 10 Hysteresis Loops of 20-1/2-0.05 cpm, 1-1/2-20 cpm, and 0-05-1/2-20 cpm Tests Indicating Type of Strain-Recovery Process

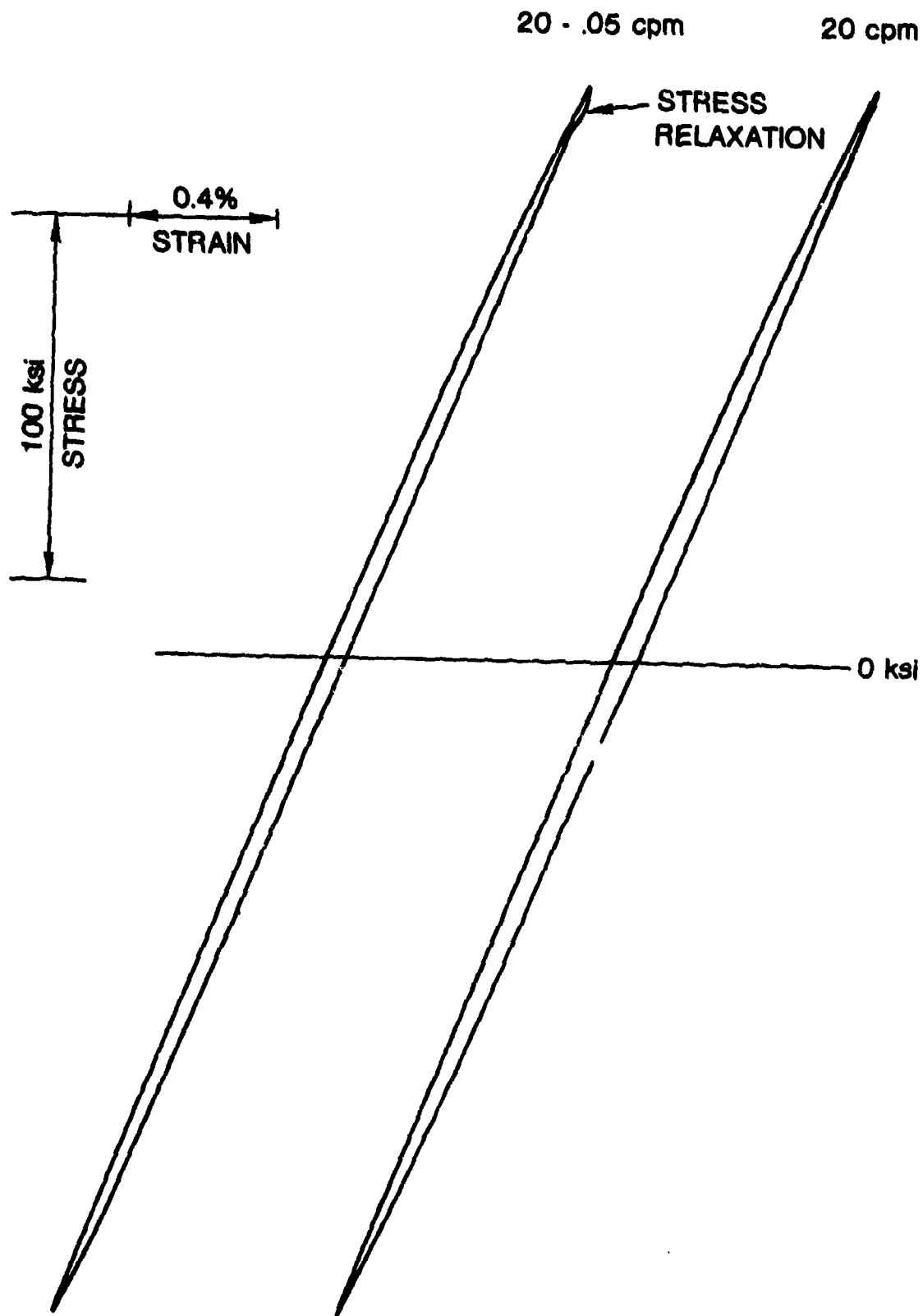


Figure 11 Hysteresis Loops of 20-0.05 cpm and 0.05-20 cpm Tests With Their Companion Specimens Indicating Stress Relaxation

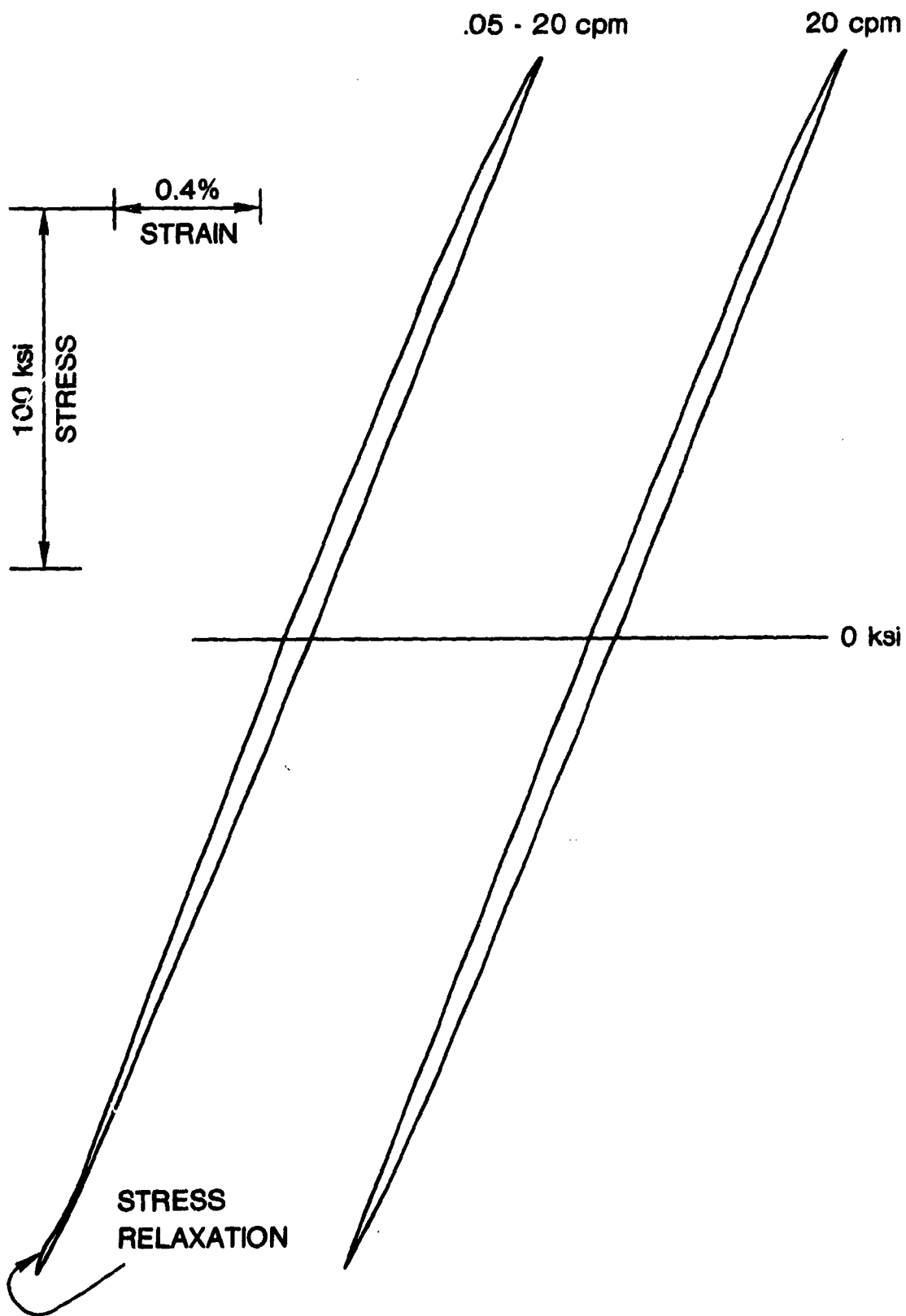


Figure 11 (Continued)

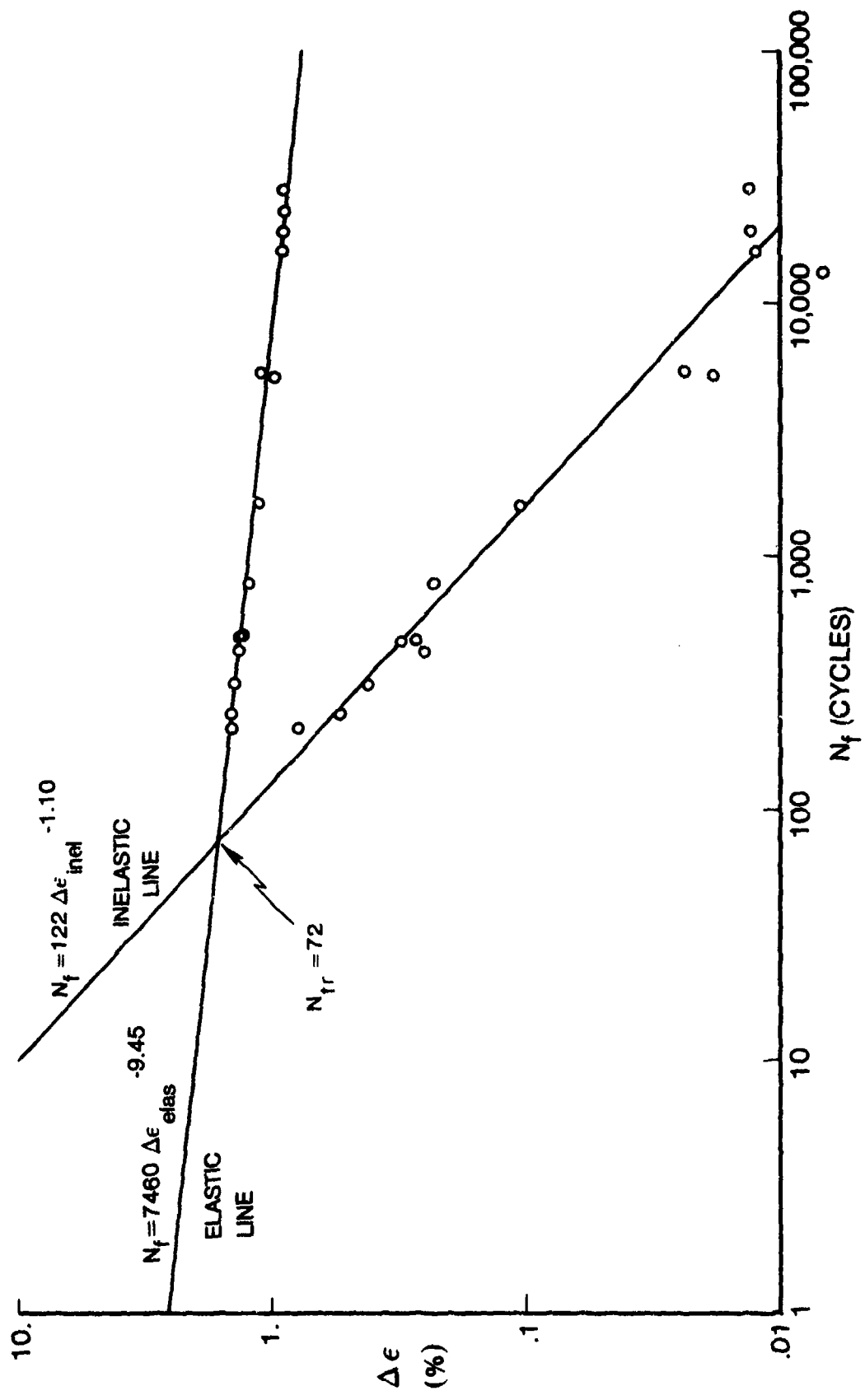


Figure 12 Elastic and Inelastic Strain as Function of Life for 20-cpm Tests

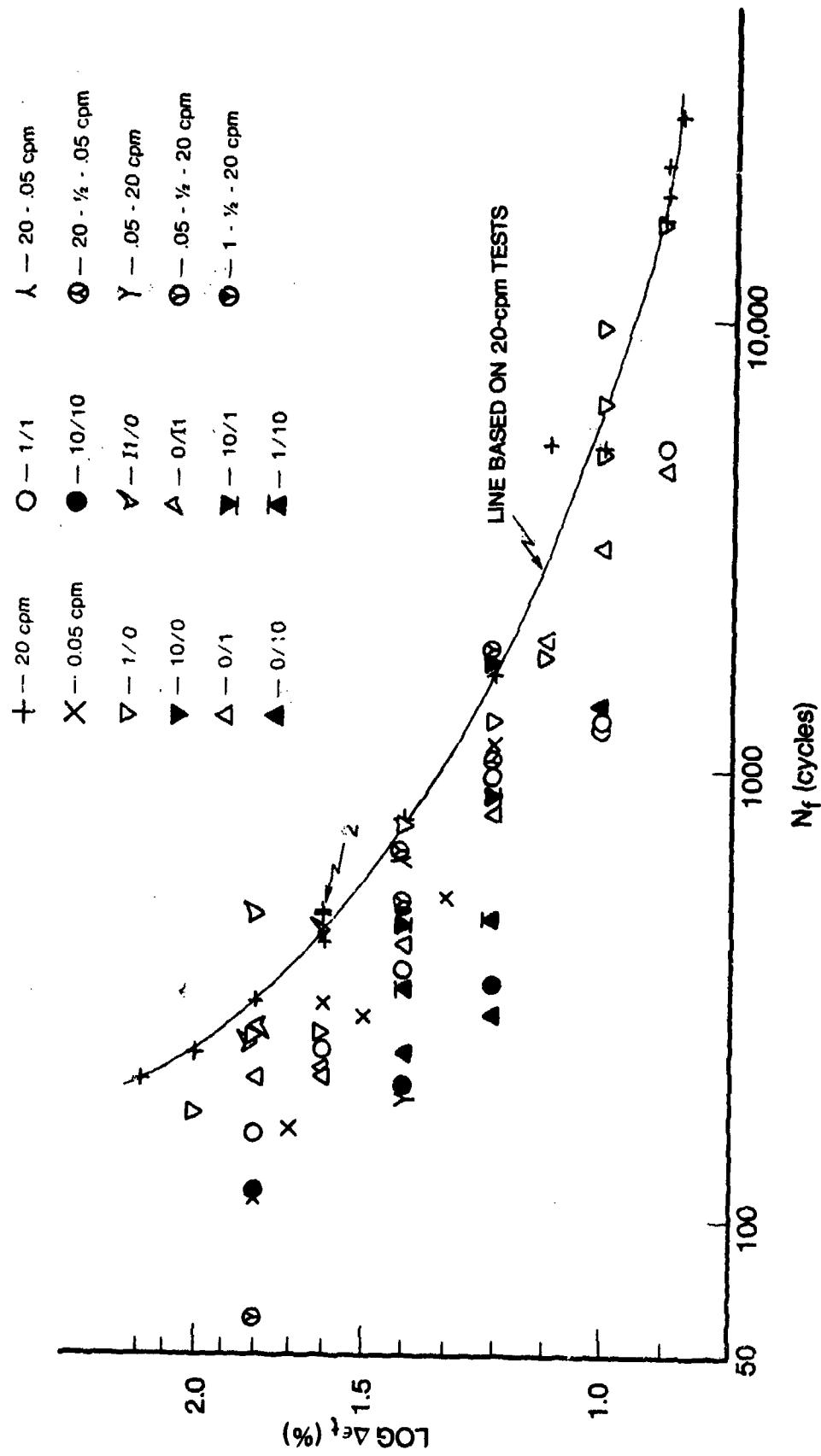


Figure 13 Total Strainrange as Function of Cycles to Failure

The lives of the baseline fatigue tests plotted as a function of the inelastic strainrange are shown in Fig. 14. Based upon the inelastic strain, the most damaging baseline waveforms were the compressive hold tests and the 0.05-cpm tests. The balanced hold tests were not as damaging at the lower strainranges. The least damaging baseline tests were the tensile hold tests--especially at lower strainranges--and the 20-cpm tests.

As shown in Figs. 13 and 14, the fatigue life was sensitive to frequency, although the stress-strain behavior was not. The 0.05-cpm tests had shorter lives than the 20-cpm tests for similar strainranges, but they did not have smaller stress ranges, as shown in Figs. 3 and 7.

The validation data are also plotted in Figs. 13 and 14, along with the baseline data. Based upon either the inelastic or total strainrange, the intermediate strain-hold tests had longer lives than the tension or compression strain-hold tests. Based upon these same strainranges, the unbalanced strain-hold tests had lives between those of the tension and compression strain-hold tests. Holding the strain only at the peak tensile or peak compressive stress produced the most severe effects on test life.

The lives of two of the dual-rate tests plotted as a function of the total or inelastic strainrange were irregular. When compared to the other dual-rate tests, these tests had very short lives. Specimen 262--a 0.05-1/2-20 cpm test at 1.8% total strainrange--and Specimen 252--a 0.05-20 cpm test at 1.4% total strainrange--had very short lives of 60 and 194 cycles, respectively. These very short life tests are felt to be valid. The test specimens had multiple crack-initiation sites which indicates that the short life was not due to an inclusion or void contained in the specimen.

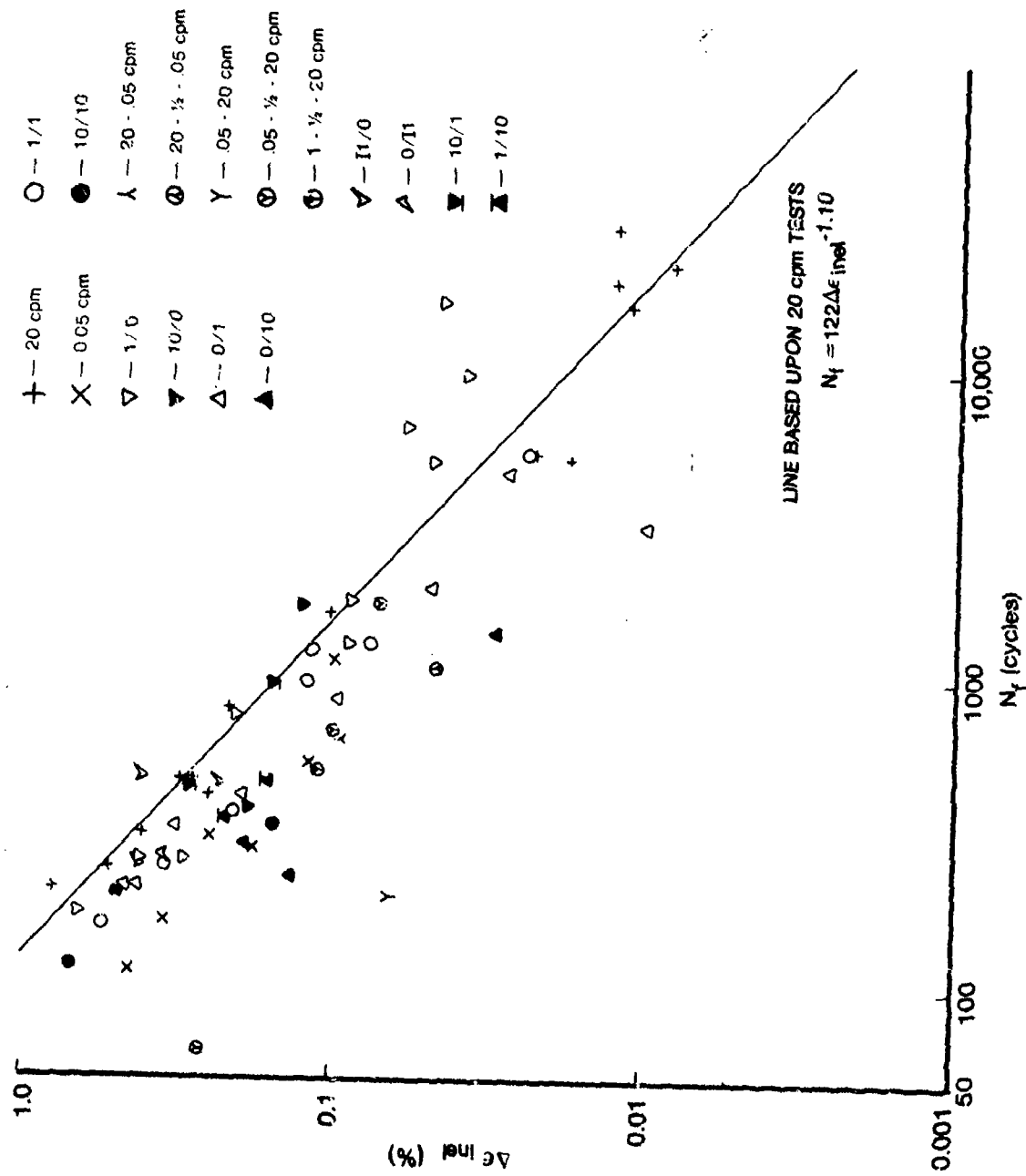


Figure 14 Inelastic Strainrange as Function of Cycles to Failure

Except for Specimens 262 and 252, the lives of the other dual-rate tests were not much shorter than those of the 20-cpm tests when compared on the basis of total strainrange but were much shorter when compared on the basis of inelastic strainrange.

An attempt was made to assess the experimental scatter inherent in the material. The following test conditions were replicated: three 20-cpm tests at 1.6% and 0.9% total strainrange each; three 1/0 tests at 1.0% total strainrange; two 0/1 tests at 1.6% total strainrange; and two 1/1 tests at 1.0% total strainrange. The results are given in Table V. The scatter in test lives was 12%, 38%, 92%, 5%, and 6%, respectively.* The 92% scatter for the 1/0 tests should be viewed with caution because the mean stress for these tests varied from -23.5 ksi (-162 MPa) for the shortest life to -38.1 ksi (-263 MPa) for the longest life. Thus, the scatter in life may have been due to the various mean stresses, which is a scatter in the stress-strain-time behavior rather than in the life behavior.[†]

Based upon these replication tests, the scatter in the material was at most $\pm 92\%$, or about a factor of two. If the $\pm 92\%$ scatter were to be rejected due to mean stress variation, then the next highest scatter would be $\pm 38\%$, or about a factor of 1.4. It should be pointed out that this limited number of replication tests probably does not provide a statistically meaningful measure of the scatter in the material. The scatter may be higher than $\pm 38\%$. Based upon the author's experience with this particular program, the scatter did not appear to be greater than $\pm 100\%$, or a factor of 2.

* Scatter in test lives = $[(\text{longest life} - \text{shortest life}) / \text{shortest life}] \times 100$.

[†] Scatter in the stress-strain-time behavior means that the stress and inelastic strain are not the same for different specimens cycled under the same waveform. Scatter in the life behavior means that the life is not the same for different specimens having the same stresses and strains. If specimens cycled under the same waveform develop the same stresses and strains, i.e., no scatter in the stress-strain-time behavior, then differences in the life can be attributed to scatter in the life behavior. However, if the stresses and strains are different, then the lives would be expected to be different, and it would not be possible to determine the scatter in the life behavior.

Section IV

MODELS

STRAINRANGE PARTITIONING MODEL

The Strainrange Partitioning (SRP) Model^{1,2,3} extends the Manson-Coffin Law^{19,20} which is valid at room temperature, to high temperature by considering the interaction of time-dependent inelastic strains and time-independent inelastic strains. The time-dependent inelastic strain is identified as creep strain, and the time-independent inelastic strain is identified as plastic strain or plasticity. At room temperature, all inelastic strain caused by tensile loading is plastic strain, and it is reversed by plastic strain caused by compressive loading. At high temperature, both creep and plastic strains can occur during tensile loading, and these inelastic strains are reversed by a combination of creep and plastic strains during compressive loading. The manner in which these different types of inelastic strains are postulated to reverse themselves is the basis of the SRP model.

A typical high-temperature hysteresis loop is shown in Fig. 15. From Point 1 to Point 2, the load is rapidly applied; therefore, only plastic strain can occur. At Point 2 the load is held constant, and the material is allowed to creep to Point 3. When Point 3 is reached, the load is reversed and the material is loaded to Point 4. The loading from Points 3 to 4 is done rapidly enough that only plastic strain occurs. When Point 4 is reached, the load is held constant and the material creeps to Point 1. When Point 1 is reached, the cycle repeats itself. The inelastic strain due to tensile loading is composed of plastic strain from Point 1 to 2 and creep strain from Point 2 to 3. The amount of plastic strain is represented by line segment AC, and the amount of creep strain is line segment CD. This tensile inelastic strain is reversed by the inelastic strain caused by compressive loading. This compressive inelastic strain is composed of plasticity from Point 3 to Point 4 and creep from Point 4 to 1. The amount of plasticity is line segment DB, and the amount of creep is line segment BA.

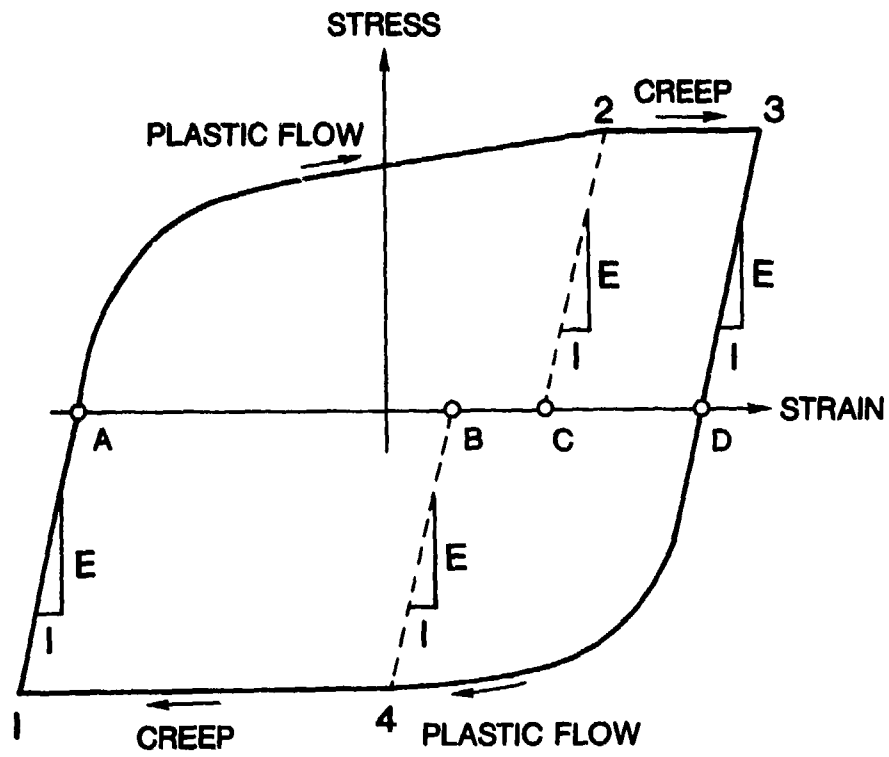


Figure 15 Typical High-Temperature Hysteresis Loop to Explain Strainrange Partitioning

The SRP model postulates that the compressive plastic strain reverses the tensile plastic strain and that the compressive creep strain reverses the tensile creep strain. This process of the compressive plastic strain reversing the tensile plastic strain is designated the strainrange $\Delta\epsilon_{pp}$,* and the compressive creep strain reversing tensile creep strain is the strainrange $\Delta\epsilon_{cc}$. If there is insufficient compressive plastic strain to reverse all of the tensile plastic strain, then the extra tensile plastic strain is reversed by compressive creep strain. This tensile plastic strain reversed by compressive creep strain is the strainrange $\Delta\epsilon_{pc}$. If there is insufficient compressive creep strain to reverse all of the tensile creep strain, then the extra tensile creep strain is reversed by compressive plastic strain. This tensile creep strain reversed by compressive plastic strain is the strainrange $\Delta\epsilon_{cp}$. $\Delta\epsilon_{pc}$ and $\Delta\epsilon_{cp}$ cannot occur in the same hysteresis loop because there can only be a deficiency in compressive plastic strain or compressive creep strain, but not both.

For the hysteresis loop in Fig. 15, the tensile plastic strain of AC is reversed by the compressive plastic strain of DB. Since DB is less than AC, there is insufficient compressive plastic strain available to reverse all of the tensile plastic strain. Some of the compressive creep strain must be used to reverse the remaining tensile plastic strain of AC-DB. The tensile creep strain of CD is entirely reversed by the compressive creep strain AC. Thus, in Fig. 15, the values of the partitioned strainranges are as follows:

$$\Delta\epsilon_{pp} = DB$$

$$\Delta\epsilon_{cp} = 0$$

$$\Delta\epsilon_{pc} = AC-DB$$

$$\Delta\epsilon_{cc} = CD$$

* The first subscript is the type of inelastic strain in tension, and the second subscript is the type of inelastic strain in compression that reverses the tensile inelastic strain.

The general rules for partitioning the inelastic strain can be given with reference to Fig. 15

$$\Delta\epsilon_{pp} = \begin{cases} \text{lesser of AC or DB if AC} \neq 0 \text{ or DB} \neq 0 \\ 0 \text{ if AC} = 0 \text{ or DB} = 0 \end{cases}$$

$$\Delta\epsilon_{cp} = \begin{cases} \text{CD-BA if CD} > \text{BA} \\ 0 \text{ if CD} \leq \text{BA} \end{cases}$$

$$\Delta\epsilon_{pc} = \begin{cases} \text{AC-DB if AC} > \text{DB} \\ 0 \text{ if AC} \leq \text{DB} \end{cases}$$

$$\Delta\epsilon_{cc} = \begin{cases} \text{lesser of CD or BA if CD} \neq 0 \text{ or BA} \neq 0 \\ 0 \text{ if CD} = 0 \text{ or BA} = 0 \end{cases}$$

According to the SRP model, the Manson-Coffin Law

$$N_f = C \Delta\epsilon_{inel}^\beta \quad (1)$$

is valid only when no creep strain occurs. For this case the inelastic strain is all tensile plasticity reversed by compressive plasticity or $\Delta\epsilon_{pp}$. Thus, according to the SRP model, the Manson-Coffin Law could be rewritten in terms of $\Delta\epsilon_{pp}$

$$N_{pp} = C_{pp} \Delta\epsilon_{inel}^{\beta_{pp}} \quad (2)$$

where N_{pp} is the cycles to failure if $\Delta\epsilon_{inel}$ is totally made up of pp strain, and C_{pp} and β_{pp} are constants. It is conceivable that tests could be run where the entire inelastic strain in the hysteresis loop would be cp, pc, or cc strain. For each of these tests, a different number of cycles to failure would be expected. Thus, the SRP model proposes a relation between each of these types of strain and the life which is similar to the one written for pp

$$N_{cp} = C_{cp} \Delta \epsilon_{inel}^{\beta_{cp}} \quad (3)$$

$$N_{pc} = C_{pc} \Delta \epsilon_{inel}^{\beta_{pc}} \quad (4)$$

$$N_{cc} = C_{cc} \Delta \epsilon_{inel}^{\beta_{cc}} \quad (5)$$

where N_{cp} , N_{pc} , and N_{cc} = cycles to failure if $\Delta \epsilon_{inel}$ is all cp, pc, or cc strain; and C_{cp} , C_{pc} , C_{cc} , β_{cp} , β_{pc} , and β_{cc} are constants.

When the inelastic strain is not of one type, as in Fig. 15, some method is required for combining the four strainranges in order to predict the cycles to failure. The SRP model makes use of the interaction damage rule² to accomplish this combination and life prediction.*

$$\frac{1}{N_f} = \frac{f_{pp}}{N_{pp}} + \frac{f_{cp}}{N_{cp}} + \frac{f_{pc}}{N_{pc}} + \frac{f_{cc}}{N_{cc}} \quad (6)$$

where $f_{pp} = \Delta \epsilon_{pp} / \Delta \epsilon_{inel}$; $f_{cp} = \Delta \epsilon_{cp} / \Delta \epsilon_{inel}$; $f_{pc} = \Delta \epsilon_{pc} / \Delta \epsilon_{inel}$; and $f_{cc} = \Delta \epsilon_{cc} / \Delta \epsilon_{inel}$. [N_{pp} , N_{cp} , N_{pc} , and N_{cc} are given in Eqs. (2)-(5).] The interaction damage rule states that the amount of damage done by each type of strain is its fraction of the inelastic strain times the inverse of the cycles to failure if all the inelastic strain in the hysteresis loop was of that type of strain. When the sum of these damages is taken, the cycles to failure of the test is the inverse of this sum.

In practice, it is not possible to achieve hysteresis loops that are entirely cp, pc, or cc. In order to achieve pure cp, pc, or cc strains, all inelastic strain due to plasticity must be avoided in the same half of the hysteresis loop in which the creep strain occurs. The only way to avoid inelastic strains due to plasticity is to keep the stresses below the proportional limit, here the material creeps at a slow rate. Thus, a long time is required to achieve a measureable amount of creep strain. For René 95, these times are on the order of hours. A test which lasts 2,000 cycles and one cycle is complete in 4 hr. would require about one year to run. This is both impractical and uneconomical.

* Originally the linear damage rule¹ was used to predict the life.

It was impossible to run a test that was purely cp, pc, or cc; therefore, in the tests run to determine the constants in Eqs. (3)-(5), pp strain as well as the strain of interest was present. It was necessary to use the interaction damage rule to separate the pp damage from the damage of interest in these tests. In order to perform this separation, the constants for the pp strainrange in Eq. (2) were first determined. These constants were found by using the continuous-cycling tests at 20 cpm, which was sufficiently rapid that all the inelastic strain was $\Delta\epsilon_{pp}$. Using the constants in Eq. (2), the value of N_{pp} in the interaction damage rule for each of these tests was found. The interaction damage rule was then solved for the value of N_{cp} or N_{pc}

$$N_{cp} = \frac{f_{cp}}{\frac{1}{N_f} - \frac{f_{pp}}{N_{pp}}} \quad N_{pc} = \frac{f_{pc}}{\frac{1}{N_f} - \frac{f_{pp}}{N_{pp}}}$$

The value of the constants in Eqs. (3) and (4) was then determined since the value of N_{cp} or N_{pc} and $\Delta\epsilon_{inel}$ for each of the tests was known. For the tests having cc and pp strain, some cp or pc strain occurred as well. The amount of damage done by the cp and pc strain was determined in the same manner as the damage done by the pp strain. After solving for N_{pp} , N_{cp} , and N_{pc} , the interaction damage rule was rewritten to solve for N_{cc}

$$N_{cc} = \frac{f_{cc}}{\frac{1}{N_f} - \frac{f_{pp}}{N_{pp}} - \frac{f_{cp}}{N_{cp}} - \frac{f_{pc}}{N_{pc}}}$$

Having the values of N_{cc} and $\Delta\epsilon_{inel}$ for each test, the constants in Eq. (5) were determined.

A least-squares routine was used to determine the constants in Eqs. (2)-(5). The logarithm of each side of the equation was taken in order to linearize the equation. The inelastic strain was considered to be the independent variable; and N_{pp} , N_{cp} , N_{pc} , or N_{cc} was considered to be the dependent variable.

The values of the plastic and creep strains could not be determined from hysteresis loops because these loops were not always available. Instead, these values were determined from the strip-chart recordings of the inelastic strain and the applied force since these recordings were made throughout the test. The values of the strains and forces at one-half the specimen life, $N_f/2$, were used because the values at this point are commonly accepted as being representative of the test. An example of the strip charts for a cp test is shown in Fig. 16. A stress-relaxation period has been used between Points 2 and 3 to produce creep strain; this period was used rather than a period where the load is held constant. The value of $\Delta \epsilon_{inel}$ was determined by measuring the vertical distance between Points 1 and 3 on the inelastic-strain strip chart. On this same strip chart, the vertical distance between Points 2 and 3 was taken to be the amount of tensile creep strain. However, the location of Point 2 could not be determined accurately because the line from 1 to 2 is written over the line from 3' to 1. The point where the curve from 2 to 3 departs from the line 3' to 1 is determined from the width of the ink lines and lies somewhere in the band on Fig. 16. In order to overcome this difficulty, the amount of force that was relaxed during the strain-hold period was used to calculate the amount of creep strain

$$\epsilon_{tc} = \frac{F_r}{E \cdot A}$$

where ϵ_{tc} is the tensile creep strain, F_r is the relaxed force, E the modulus of elasticity, and A the area of the specimen. The amount of relaxed force is represented by the vertical distance between Points 2 and 3 on the force strip chart.

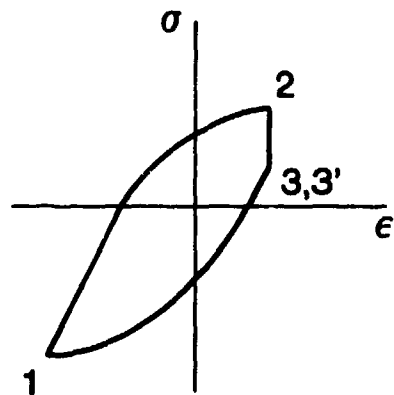
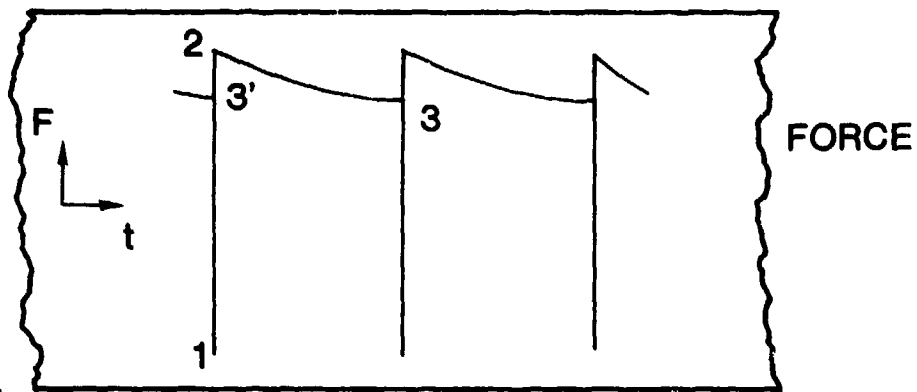
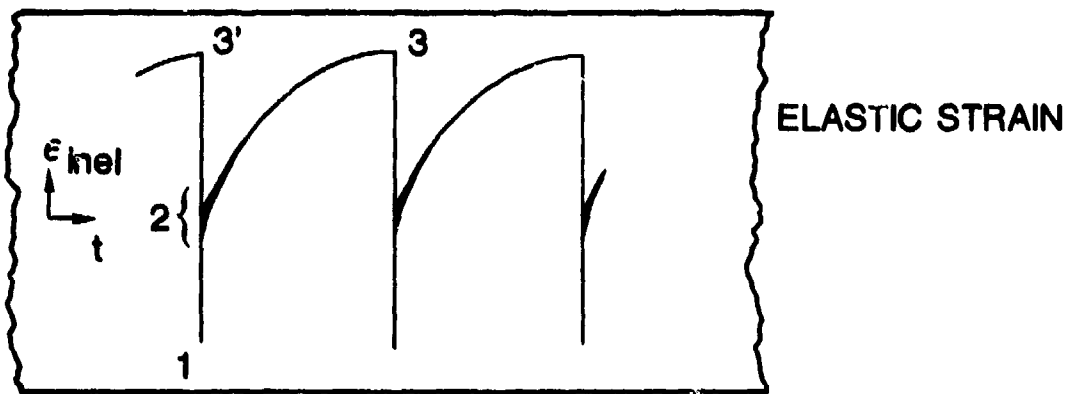


Figure 16 Inelastic Strain and Force Strip Charts and Hysteresis Loop for a cp Test

Using the procedure outlined above, the equations for the partitioned strainranges were determined

$$\begin{aligned}
 N_{pp} &= 0.777 \Delta \epsilon_{inel}^{-1.10} \\
 N_{cp} &= 1.40 \Delta \epsilon_{inel}^{-0.882} \\
 N_{pc} &= 0.429 \Delta \epsilon_{inel}^{-0.870} \\
 N_{cc} &= 0.130 \Delta \epsilon_{inel}^{-1.20}
 \end{aligned}
 \tag{7}$$

These equations and the data used to generate them are presented in Figs. 17 (a-e), and the data are given in Table VII. The constants in the above equations are not identical to those given in the previous analysis¹⁴ because a slightly larger data base was used in the present analysis. The constants for the two analyses produce nearly identical lines through the data.

Specimen Nos. 4 and 16 were not used to determine the constants in Eqs. (4) and (5) because the percent cc damage* of No. 4 was less than 10% and No. 16 could not be accurately partitioned. Also, the 0.05-cpm tests were not used to determine the constants in Eq. (5). These tests could not be directly partitioned from the individual test results.

All of the cp tests with lives greater than 5000 cycles had negative values for N_{cp} because these tests lasted longer than pp tests having the same inelastic strainrange. According to the interaction damage rule

$$\text{if } N_f > \frac{N_{pp}}{f_{pp}}, \text{ then } N_{cp} < 0.$$

A negative value of N_{cp} indicates that the cp strain exerts a healing effect to increase the specimen life. It should be noted that all the cp tests having negative values of N_{cp} also had large compressive mean stresses.

* Percent cc damage = $\frac{f_{cc}}{N_f} \times N_f \times 100$. It is the percentage of life that can be attributed to cc damage.

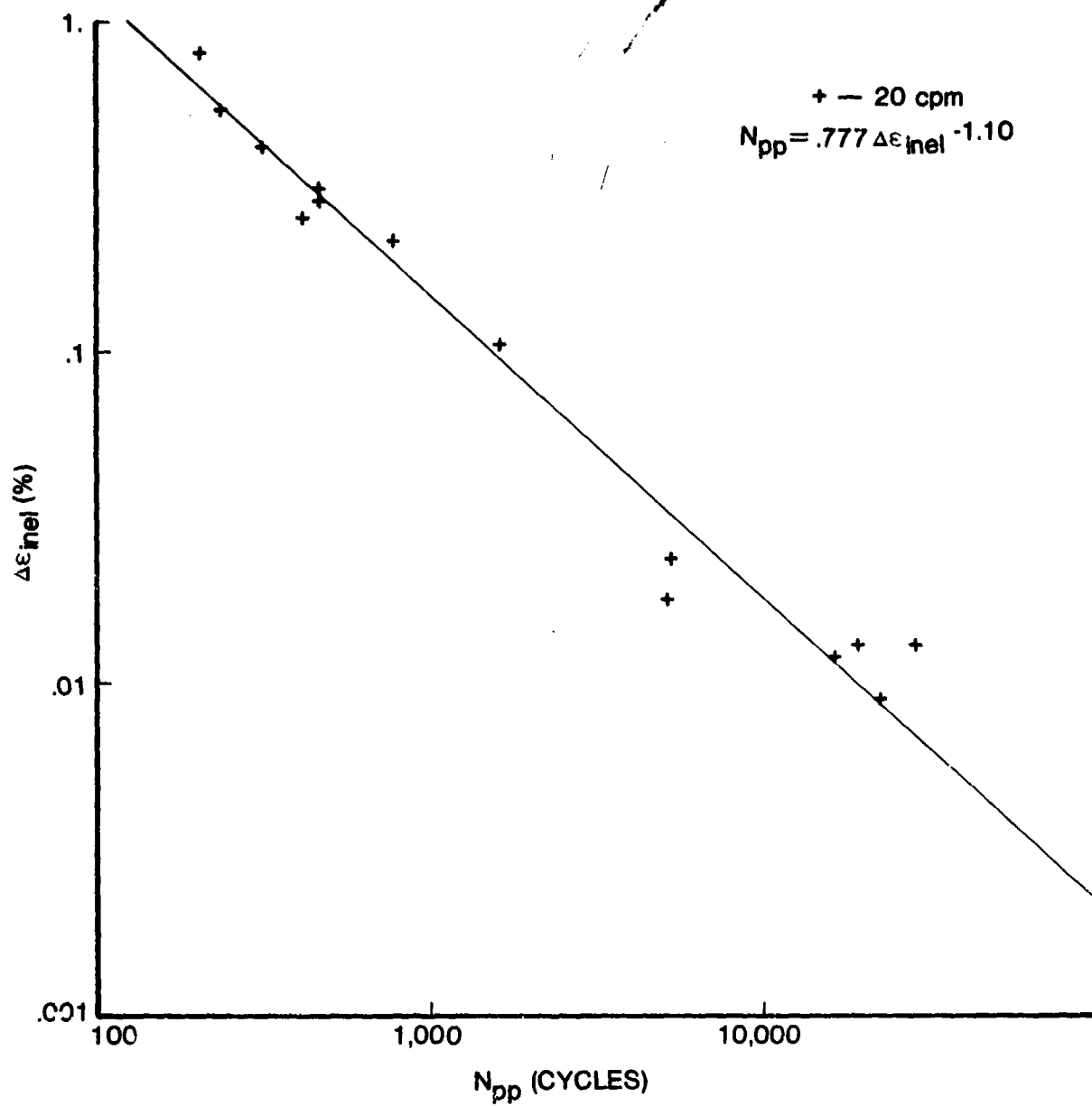


Figure 17a Inelastic Strainrange as Function of N_{pp}

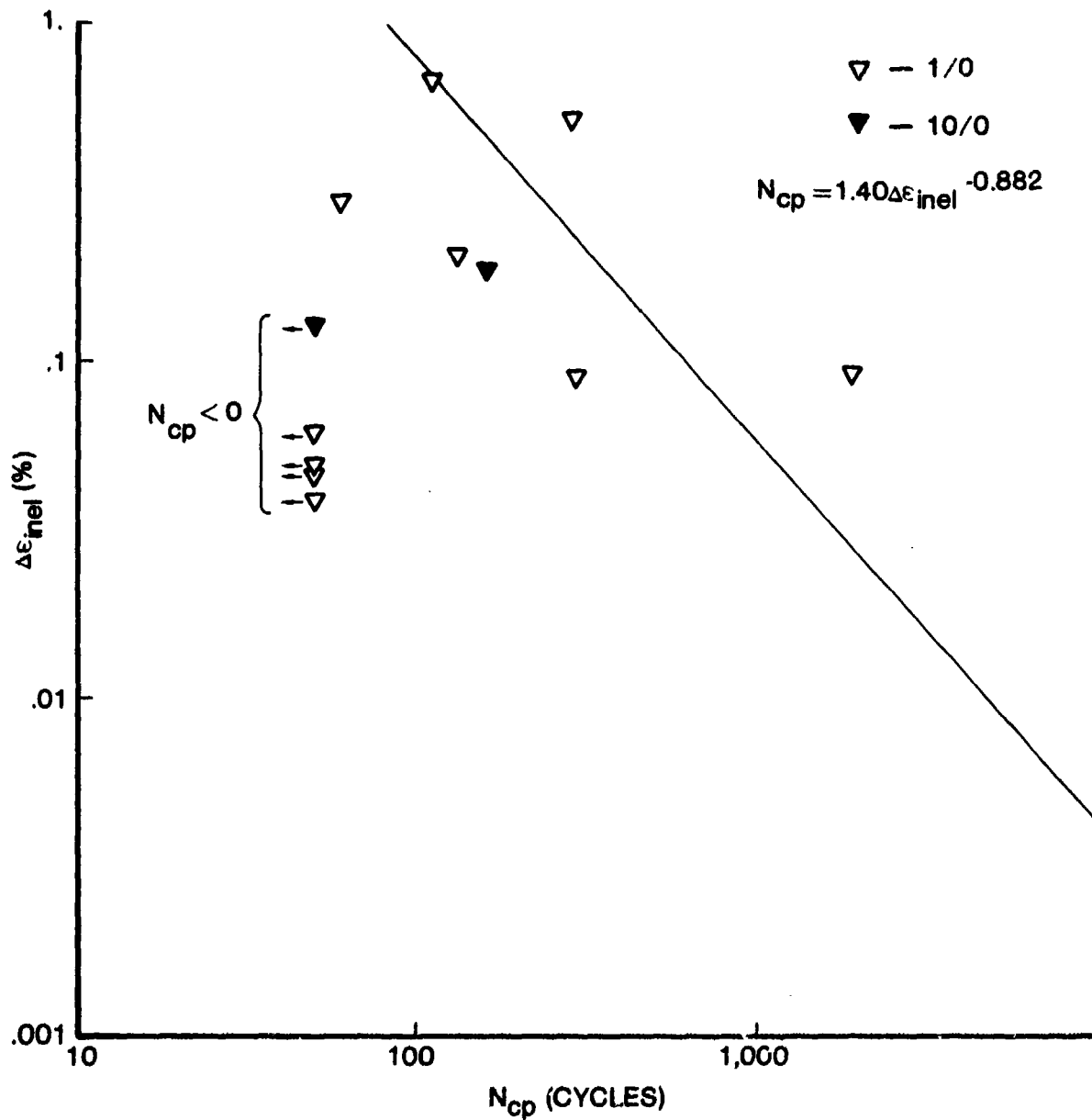


Figure 17b Inelastic Strainrange as Function of N_{cp}

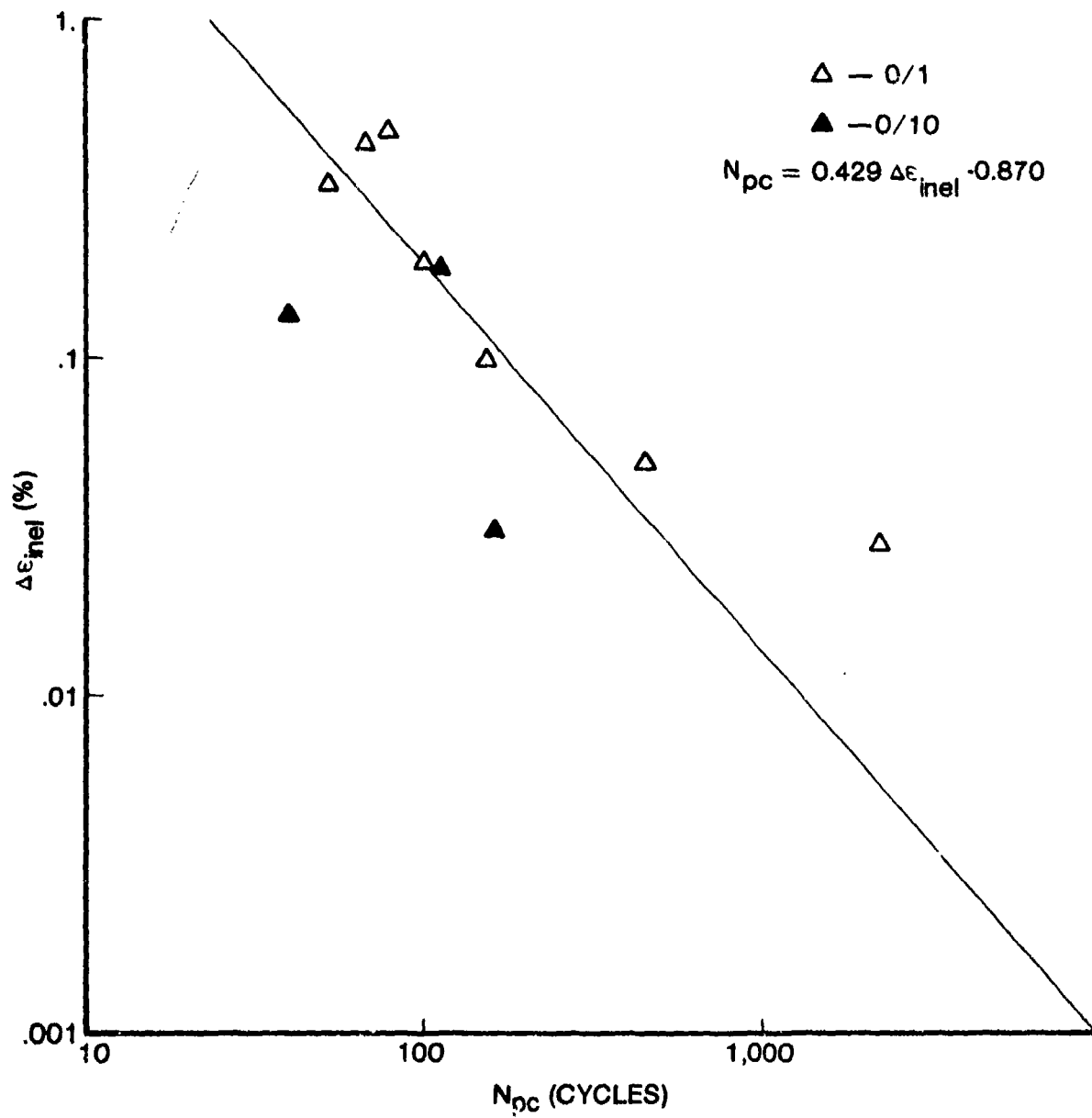


Figure 17c Inelastic Strainrange as Function of N_{pc}

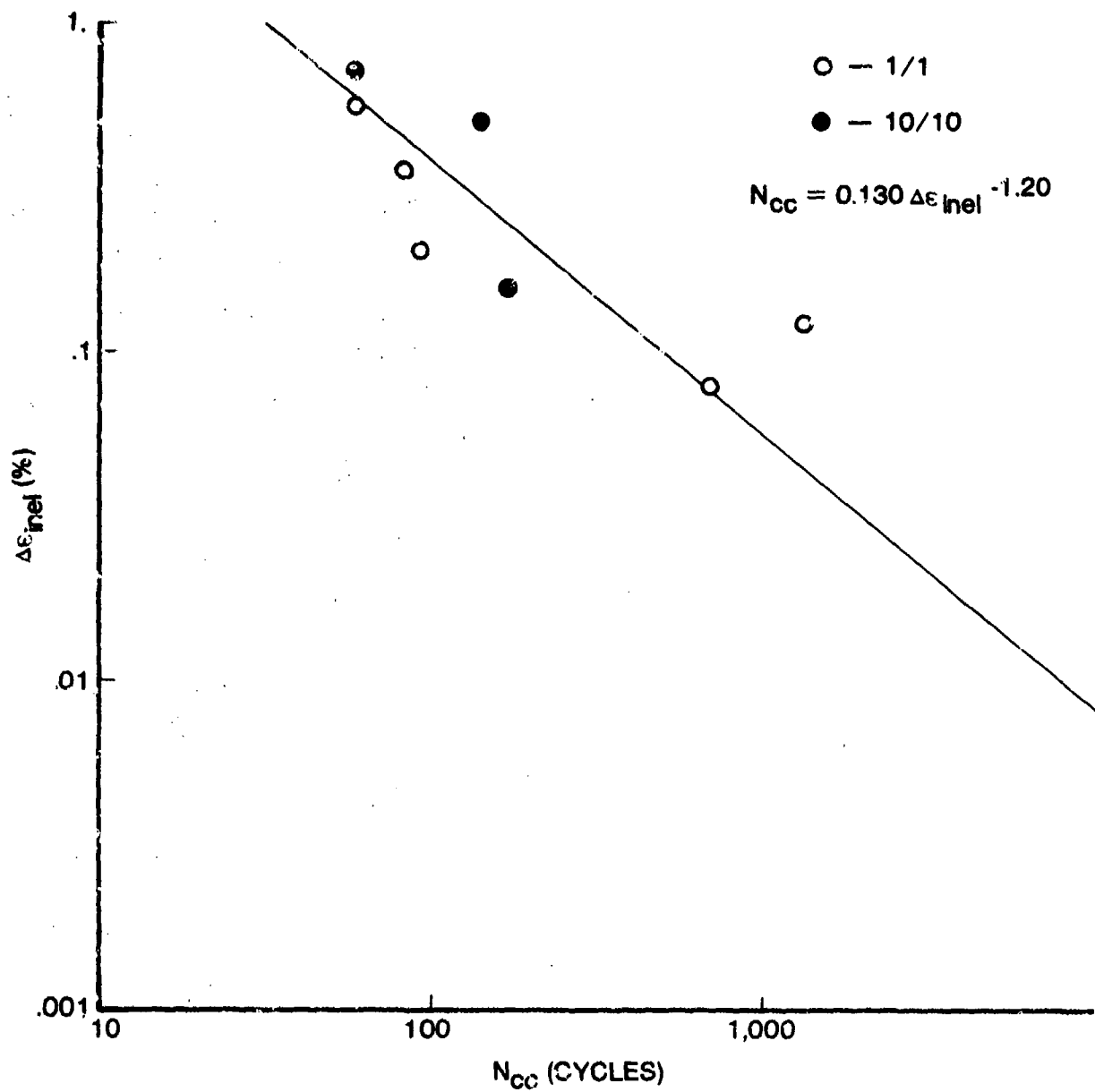


Figure 17d Inelastic Strainrange as Function of N_{cc}

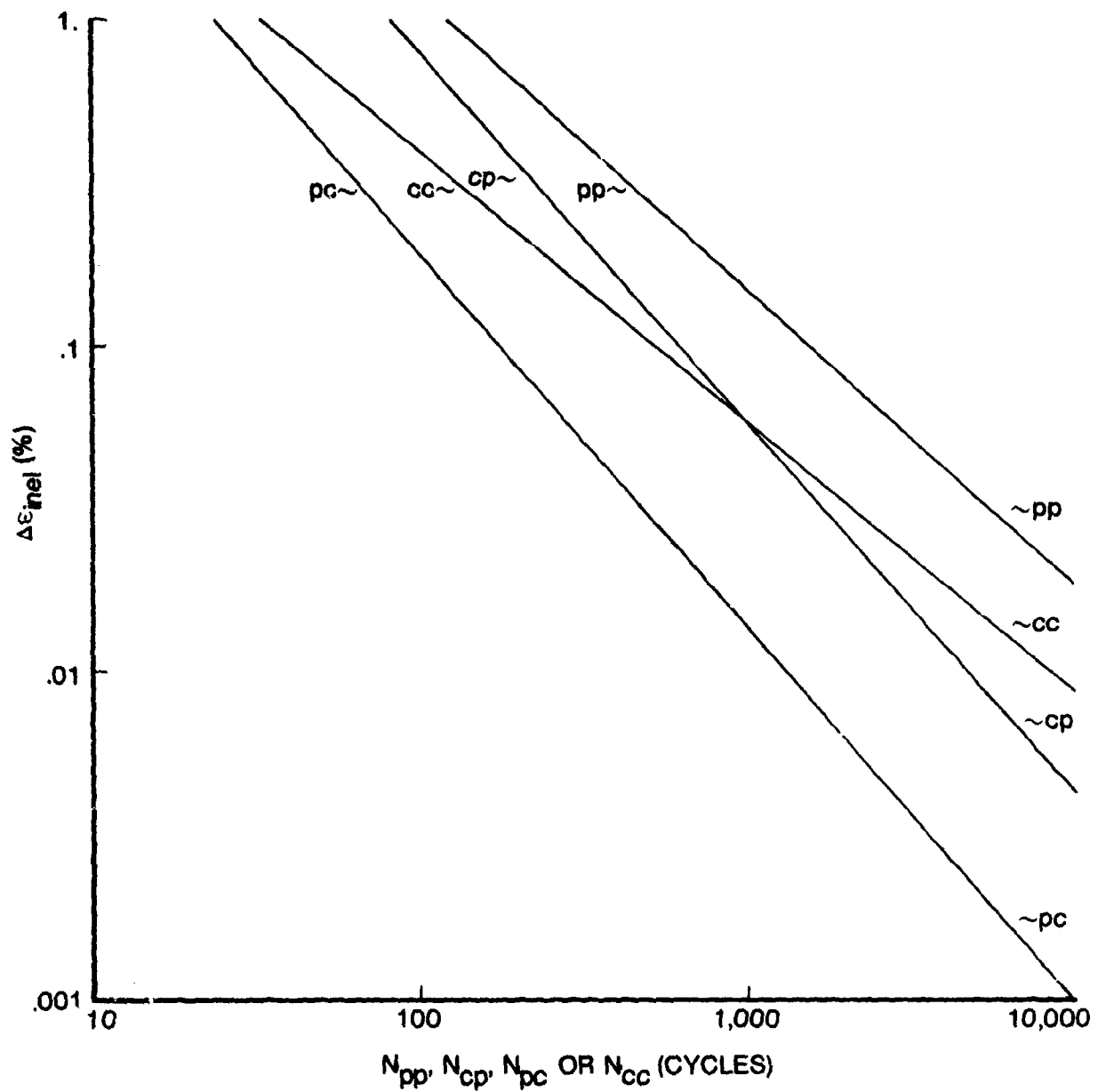


Figure 17e Strainrange-Partitioning Lines

TABLE VII
PARTITIONED STRAINRANGES
René 95 - 1200°F (650°C)
(Values are in %)

SPEC. NO.	TYPE OF TEST	E _{PP}	E _{CP}	E _{PC}	E _{CC}
17	20CPM	.5300	.0000	.0000	.0000
18	20CPM	.4080	.0000	.0000	.0000
224	20CPM	.2500	.0000	.0000	.0000
22	20CPM	.3110	.0000	.0000	.0000
240	20CPM	.2850	.0000	.0000	.0000
26	20CPM	.2167	.0000	.0000	.0000
27	20CPM	.1040	.0000	.0000	.0000
255	20CPM	.0237	.0000	.0000	.0000
29	20CPM	.0177	.0000	.0000	.0000
30	20CPM	.0116	.0000	.0000	.0000
234	20CPM	.0130	.0000	.0000	.0000
235	20CPM	.0085	.0000	.0000	.0000
239	20CPM	.0130	.0000	.0000	.0000
23	.05CPM	.4320	.0000	.0000	.0180
24	.05CPM	.3360*	.0000	.0000	*.0140
20	.05CPM	.2400*	.0000	.0000	*.0100
25	.05CPM	.1728*	.0000	.0000	*.0072
34	.05CPM	.1200	.0000	.0000	.0000
19	.05CPM	.1000	.0000	.0000	.0000

*Values estimated by assuming that f_{pp} and f_{cc} of Specimens 24, 20 and 25 were equal to those of Specimen 23. This is a conservative assumption.

TABLE VII (Continued)

PARTITIONED STRAINRANGES

René 95 - 1200°F (650°C)

(Values are in %)

SPEC. NO.	TYPE OF TEST	EPP	ECP	EPC	ECC
245	1-0	.5371	.1199	.0000	.0000
5	1-0	.4468	.0752	.0000	.0000
10	1-0	.2620	.0350	.0000	.0000
7	1-0	.1745	.0315	.0000	.0000
12	1-0	.0830	.0063	.0000	.0000
39	1-0	.0701	.0189	.0000	.0000
38	1-0	.0431	.0059	.0000	.0000
233	1-0	.0530	.0075	.0000	.0000
33	1-0	.0360	.0020	.0000	.0000
237	1-0	.0412	.0047	.0000	.0000
228	10-0	.1552	.0298	.0000	.0000
40	10-0	.1016	.0244	.0000	.0000
6	0-1	.3699	.0000	.0591	.0000
11	0-1	.4058	.0000	.0622	.0000
14	0-1	.2819	.0000	.0421	.0000
8	0-1	.1676	.0000	.0244	.0000
13	0-1	.0888	.0000	.0091	.0000
241	0-1	.0435	.0000	.0055	.0000
16	0-1	^a	^a	^a	^a
238	0-1	.0225	.0000	.0055	.0000
222	0-10	.1160	.0000	.0199	.0000
41	0-10	.1299	.0000	.0551	.0000
253	0-10	.0278	.0000	.0027	.0000
1	1-1	.4374	.0276	.0000	.0850
2	1-1	.2758	.0181	.0000	.0551
32	1-1	.1628	.0102	.0000	.0280
9	1-1	.0874	.0000	.0051	.0295
4	1-1	.0735	.0161	.0000	.0264
15	1-1	.0536	.0043	.0000	.0201
229	1-1	.0245	.0000	.0000	.0000
28	10-10	.4860	.0272	.0000	.1878
31	10-10	.3041	.0232	.0000	.1697
230	10-10	.0836	.0138	.0000	.0598

^aCould not accurately partition.

TABLE VII (Continued)

PARTITIONED STRAINRANGES

René 95 - 1200°F (650°C)

(Values are in %)

SPEC. NO.	TYPE OF TEST	EPP	ECP	EPC	ECC
251	20-0.05 cpm	0.0867	0.0118	0.0000	0.0000
262	20-1/2-0.05 cpm	a	a	a	a
261	1-1/2-20 cpm	a	a	a	a
256	0.05-1/2-20 cpm	a	a	a	a
252	0.05-20 cpm	0.0584	0.0000	0.0080	0.0000
260	0.05-1/2-20 cpm	a	a	a	a
259	0.05-1/2-20 cpm	a	a	a	a
242	I1-0	.3710	.0512	.0000	.0000
246	I1-0	.3470	.0650	.0000	.0000
244	I1-0	.2270	.0394	.0000	.0000
247	0-I1	.2980	.0000	.0579	.0000
227	10-1	.1984	.0417	.0000	.0520
223	10-1	.1128	.0248	.0000	.0209
226	1-10	.1584	.0087	.0000	.0539
225	1-10	.1137	.0063	.0000	.0417

^aCould not partition. See text for reasons.

These mean stresses might be responsible for prolonging the life of the cp tests over the pp tests and thus causing the negative values of N_{cp} . Since a negative number cannot be used in the power-law relation between N_{cp} and $\Delta\epsilon_{cp}$, Eq. (3), these tests were not used in determining the cp line.

The SRP life predictions of the baseline data are given in Table VIII and are shown in Fig. 18a. The scatter band was 5.4, and the standard deviation was 0.23. The 0.05-cpm, 0/10, and long-life 1/0 tests were not well predicted. The predicted lives for these tests were either greater than two and one-half times the observed life or less than one-fifth the observed life.

The 0.05-cpm tests were partitioned by the companion-specimen method.²¹ A companion specimen was cycled at the same strainrange as the test specimen at 20 cpm until the stresses stabilized, and then it was cycled under the same stresses at 0.05 cpm until the strains stabilized. The difference between the stabilized inelastic strainranges of the 20-cpm and 0.05-cpm hysteresis loops was attributed to creep strain and taken to be the $\Delta\epsilon_{cc}$ strainrange. The inelastic strain of the test specimen was partitioned by assuming that the value of f_{cc} and f_{pp} for the test specimen was the same as that for the companion specimen. For those test specimens that had no companion specimen, a conservative assumption was made that their f_{cc} and f_{pp} values were the same as for the companion specimen having the next largest strainrange.

The SRP predictions of the verification tests are shown in Fig. 19a and listed in Table IX. Except for the dual-rate tests, the verification tests were well predicted. The dual-rate tests presented special problems in partitioning the strains. The hysteresis loops of these tests are shown in Figs. 10 and 11. In all these tests, anomalous behavior occurred when the strain rate switched from fast to slow. This behavior was similar to either stress relaxation or strain recovery.

TABLE VIII
LIFE PREDICTIONS OF BASELINE TESTS

Specimen	Type of Test	Total Strain-Range (%)	Observed Life (Cycles)	+ $\frac{\text{Observed Life}}{\text{Predicted Life}}$ or - $\frac{\text{Predicted Life}}{\text{Observed Life}}$		Damage-Rate Model
				Strainrange-Partitioning Model	Frequency-Separation Model	
21	20 cpm	2.2	203	-1.28	-1.32	-1.18
17	20 cpm	2.0	234	1.05	1.02	1.10
18	20 cpm	1.8	307	1.07	1.04	1.10
224	20 cpm	1.6	415	1.35	1.33	1.37
22	20 cpm	1.6	461	-1.04	-1.06	-1.01
240	20 cpm	1.6	463	1.05	1.03	1.12
26	20 cpm	1.4	784	-1.19	-1.21	-1.12
27	20 cpm	1.2	1,629	-1.11	-1.11	-1.02
255	20 cpm	1.1	5,332	1.40	1.42	1.38
29	20 cpm	1.0	5,158	2.00	2.02	2.09
30	20 cpm	0.9	16,215	1.01	1.03	1.08
234	20 cpm	0.9	19,160	-1.33	-1.30	-1.13
235	20 cpm	0.9	22,364	1.03	1.05	1.15
239	20 cpm	0.88	28,697	-1.99	-1.95	-1.82
23	0.05 cpm	1.8	110	2.44	1.26	1.34
24	0.05 cpm	1.7	159	2.23	1.15	1.13
20	0.05 cpm	1.6	301	1.71	-1.13	-1.16
25	0.05 cpm	1.5	282	2.63	1.36	1.41
34	0.05 cpm	1.3	526	2.39	1.15	1.19
19	0.05 cpm	1.2	1,138	1.35	-1.54	-1.31

TABLE VIII (Continued)
LIFE PREDICTIONS OF BASELINE TESTS

Specimen	Type of Test	Total Strain-Range (%)	Observed Life (Cycles)	+ $\frac{\text{Observed Life}}{\text{Predicted Life}}$ or - $\frac{\text{Predicted Life}}{\text{Observed Life}}$		Damage-Rate Model	
				Strainrange-Partitioning Model	Frequency-Separation Model		Ostergren Model
222	0-10	1.4	224	2.39	1.62	2.12	3.99
41	0-10	1.2	283	-1.08	-1.10	1.33	1.94
253	0-10	1.0	1,397	2.10	1.37	1.81	3.38
1	1-1	1.8	156	1.06	-1.06	-1.06	1.23
2	1-1	1.6	238	1.15	1.02	1.02	1.33
32	1-1	1.4	358	1.47	1.25	1.32	1.68
9	1-1	1.2	959	-1.40	-1.23	-1.13	-1.02
4	1-1	1.0	1,215	-1.53	-1.47	-1.21	-1.17
15	1-1	1.0	1,288	1.00	-1.00	1.17	1.17
229	1-1	0.9	5,277	1.37	-1.14	1.08	1.38
28	10-10	1.8	115	-1.10	-1.35	-1.34	1.06
31	10-10	1.4	199	-1.42	-1.60	-1.47	-1.06
230	10-10	1.2	331	1.48	1.35	1.40	1.79

TABLE VIII (Continued)
LIFE PREDICTIONS OF BASELINE TESTS

Specimen	Type of Test	Total Strain-Range (%)	Observed Life (Cycles)	+ $\frac{\text{Observed Life}}{\text{Predicted Life}}$ or - $\frac{\text{Predicted Life}}{\text{Observed Life}}$		Damage-Rate Model
				Strainrange-Partitioning Model	Frequency-Separation Model	
245	1-0	2.	171	1.02	1.39	1.08
5	1-0	1.8	255	-1.13	1.20	-1.07
10	1-0	1.6	257	1.62	2.23	1.73
7	1-0	1.4	748	-1.26	1.15	-1.13
12	1-0	1.2	1,289	1.22	1.69	1.31
39	1-0	1.1	1,781	-1.36	1.23	-1.10
38	1-0	1.0	5,013	-1.82	-1.18	-1.57
233	1-0	1.0	6,519	-2.98	-1.95	-2.60
33	1-0	1.0	9,609	-2.39	-1.71	-2.24
237	1-0	0.9	16,418	-5.44	-3.61	-4.84
228	10-0	1.4	481	1.37	2.32	1.47
40	10-0	1.2	1,705	-1.80	1.00	-1.61
6	0-1	1.8	207	-1.15	-1.35	1.31
11	0-1	1.6	209	-1.25	-1.50	1.19
14	0-1	1.6	219	1.11	-1.04	1.72
8	0-1	1.4	413	-1.00	-1.10	1.62
13	0-1	1.2	846	1.09	-1.07	1.70
241	0-1	1.1	1,940	-1.18	-1.13	1.55
16	0-1	1.0	3,093	^a	3.12	5.12
238	0-1	0.9	4,619	-2.31	-1.45	1.08

^a Could not be accurately partitioned

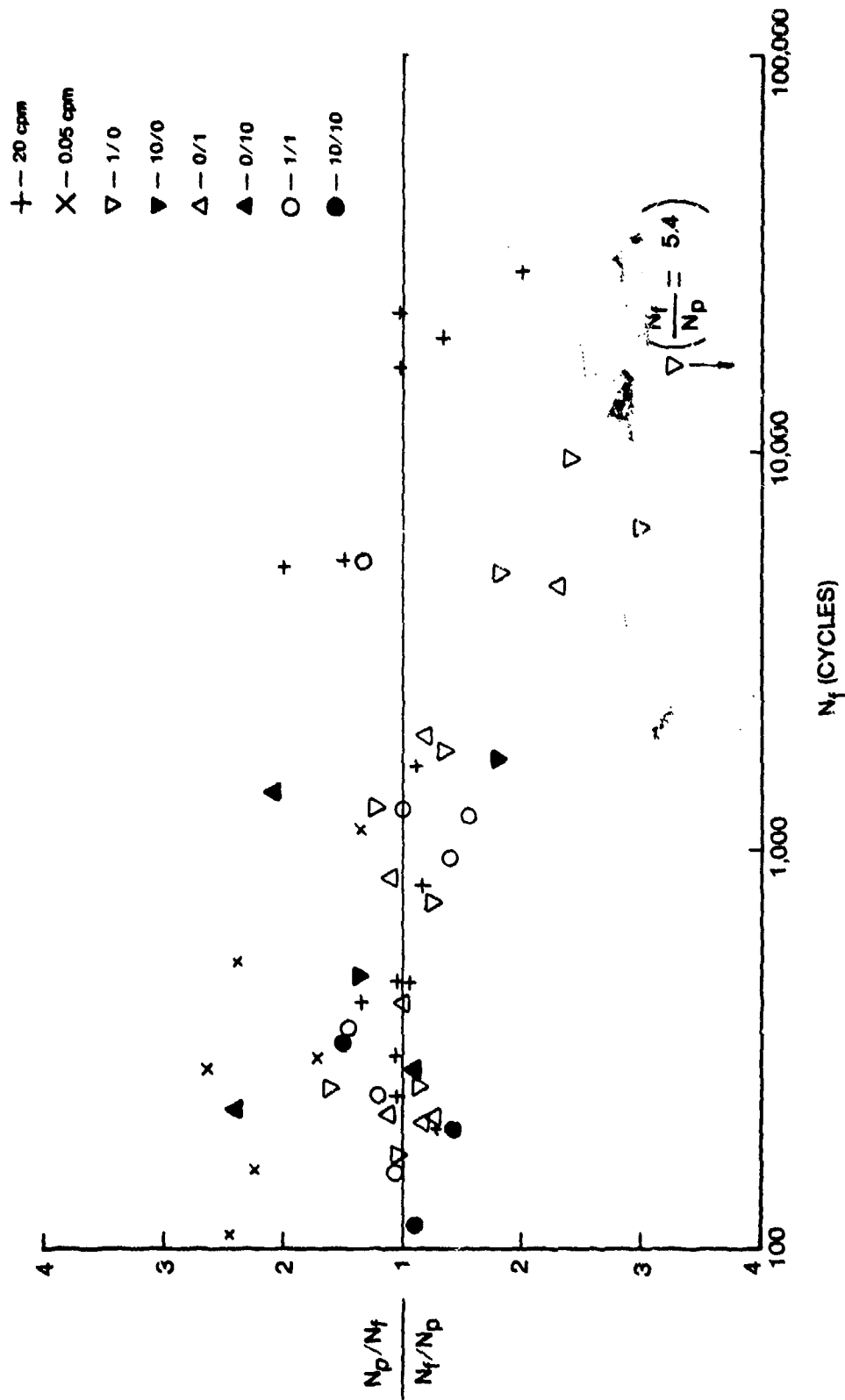


Figure 18a Life Predictions of Baseline Tests by the Strainrange-Partitioning Model

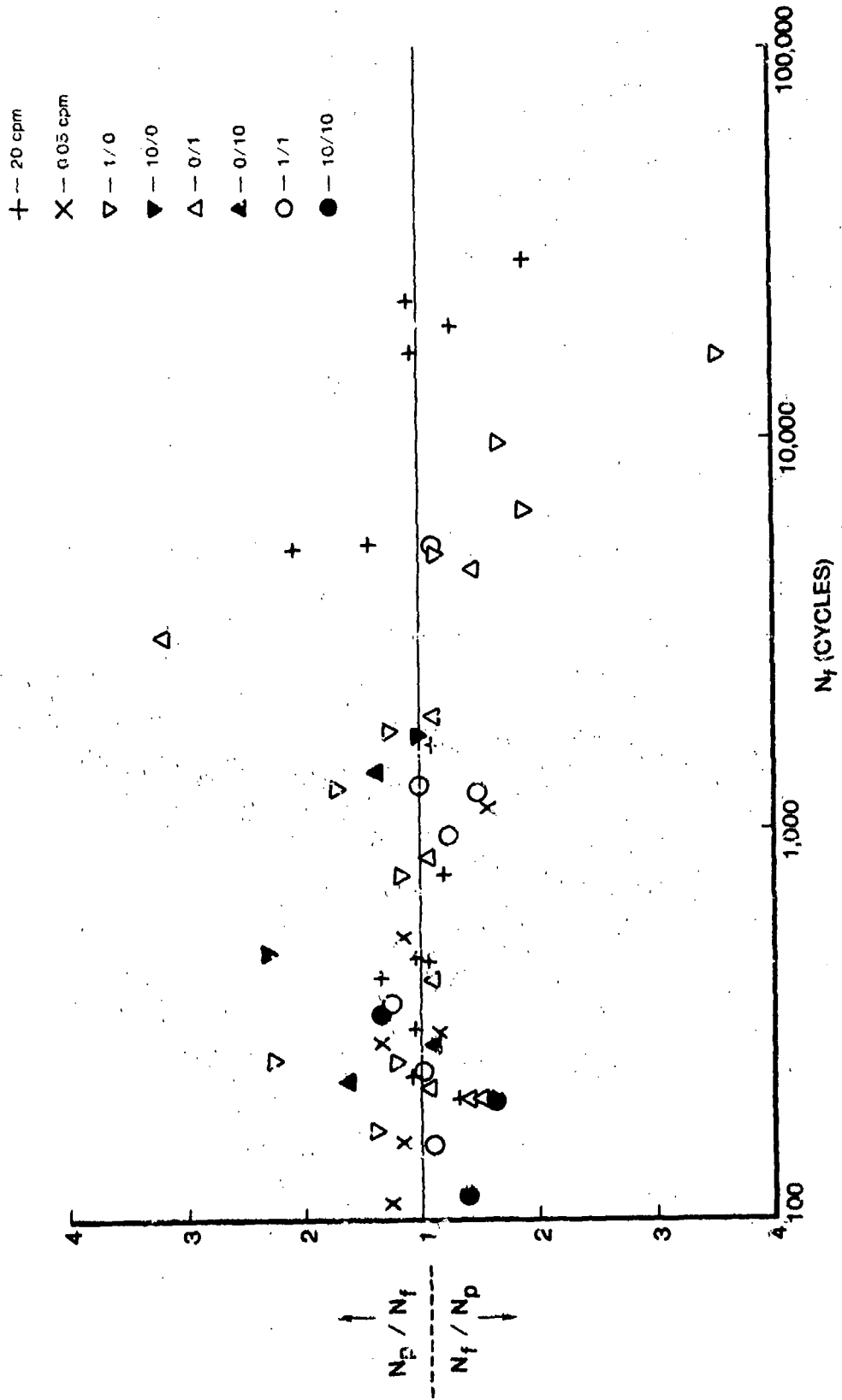


Figure 18b Life Predictions of Baseline Tests by the Frequency-Separation Model

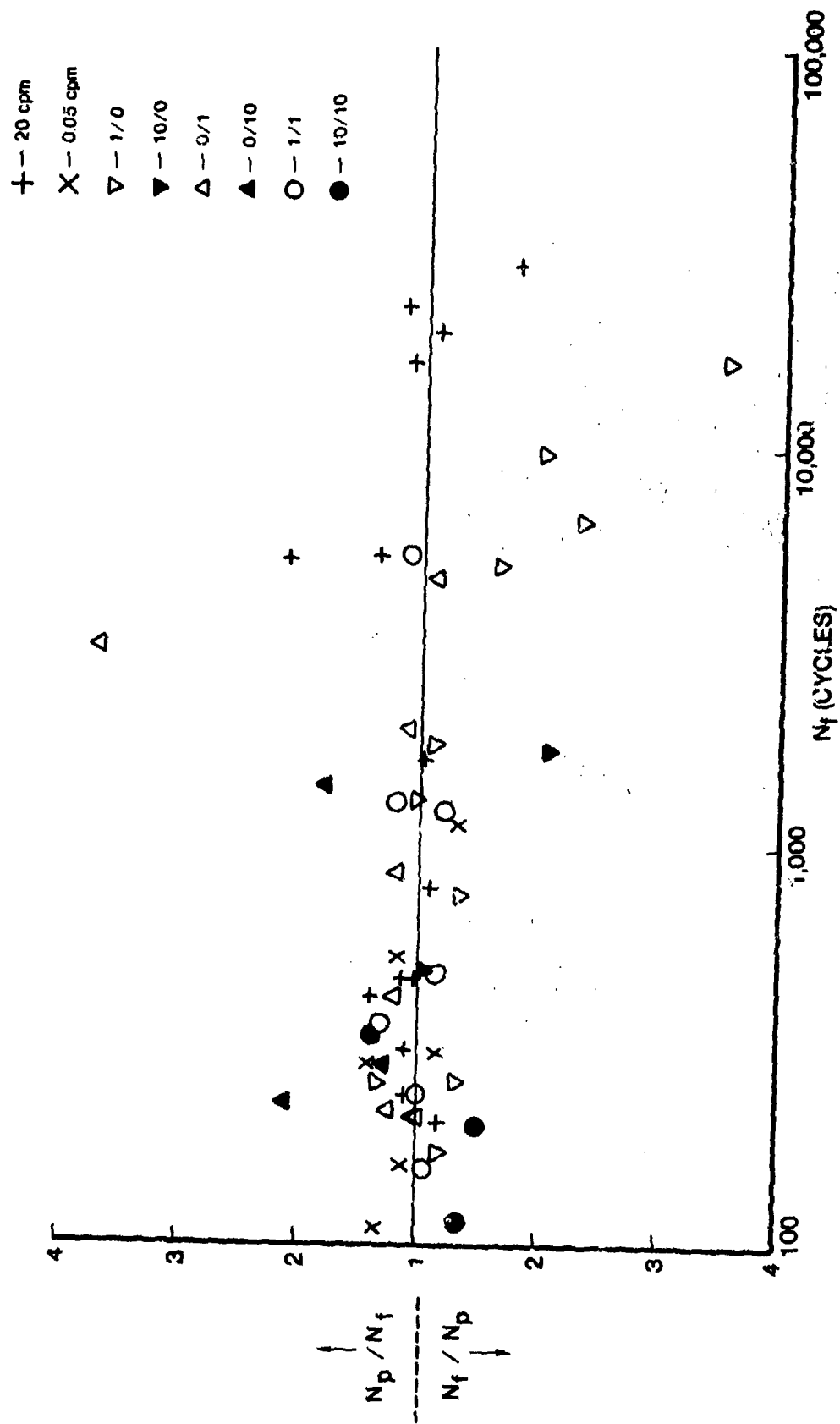


Figure 18c Life Predictions of Baseline Tests by the Ostergrer Model

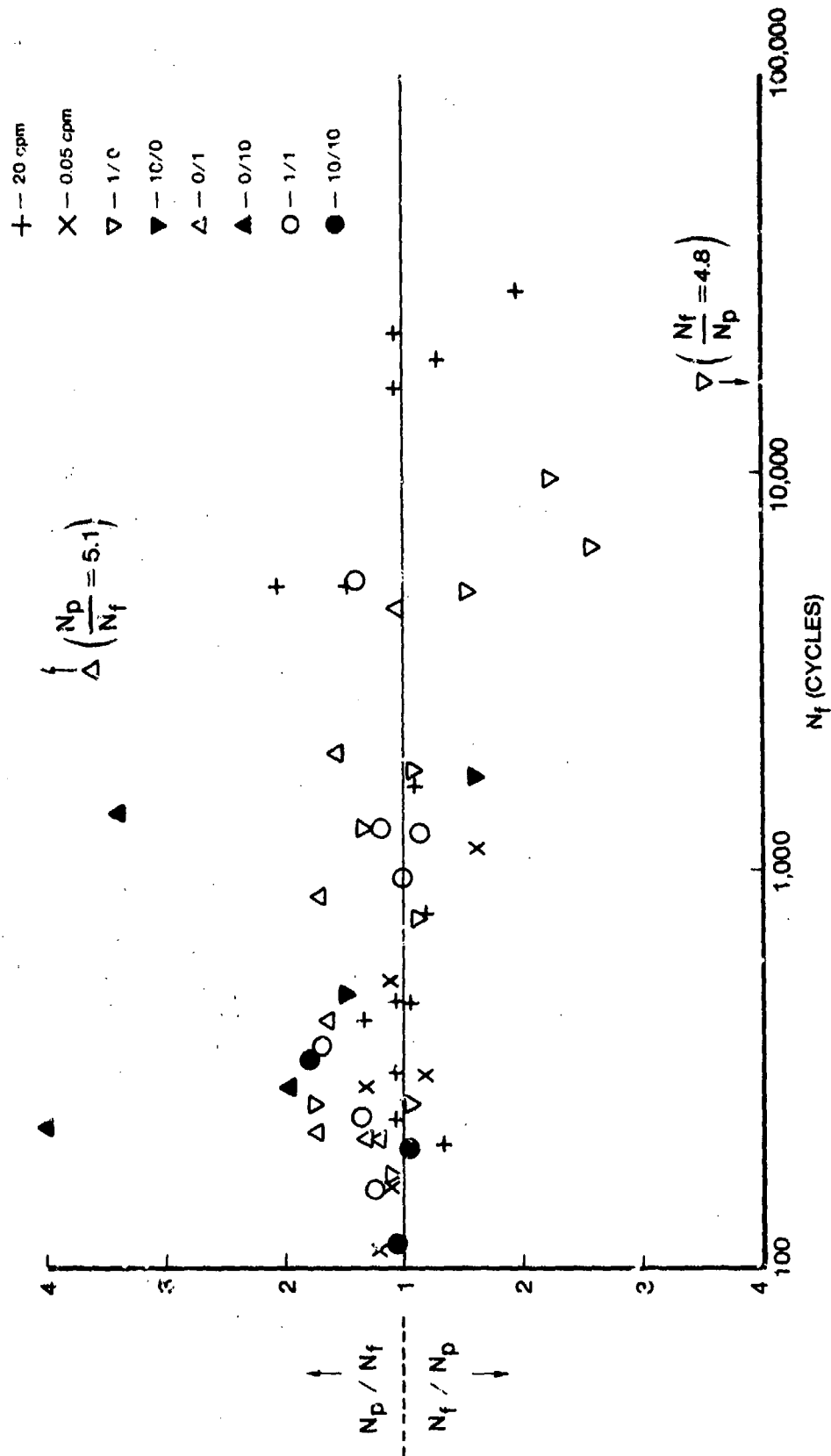


Figure 18d Life Predictions of Baseline Tests by the Damage-Rate Model

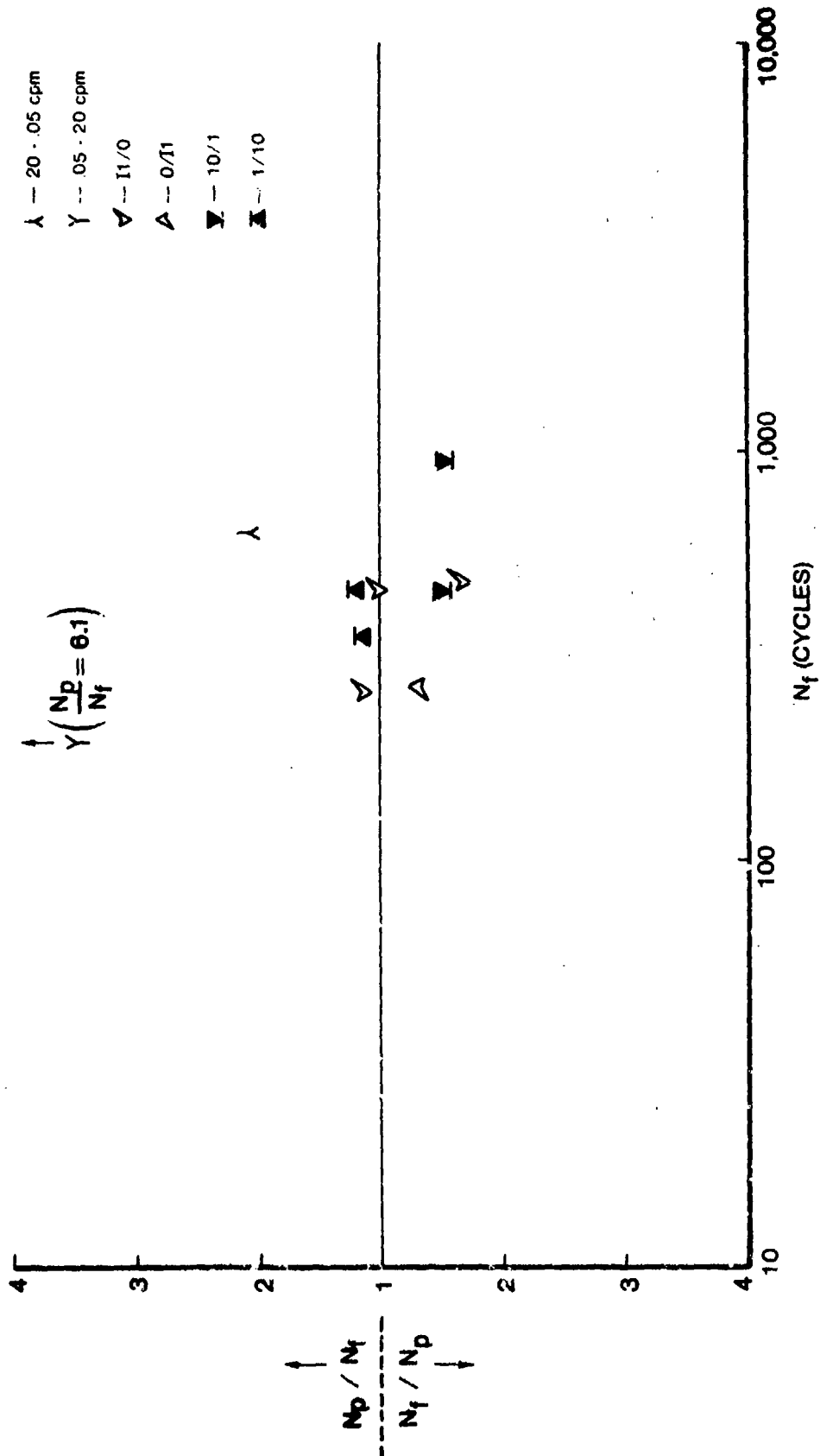


Figure 19a Life Predictions of Verification Tests by Strainrange-Partitioning Model

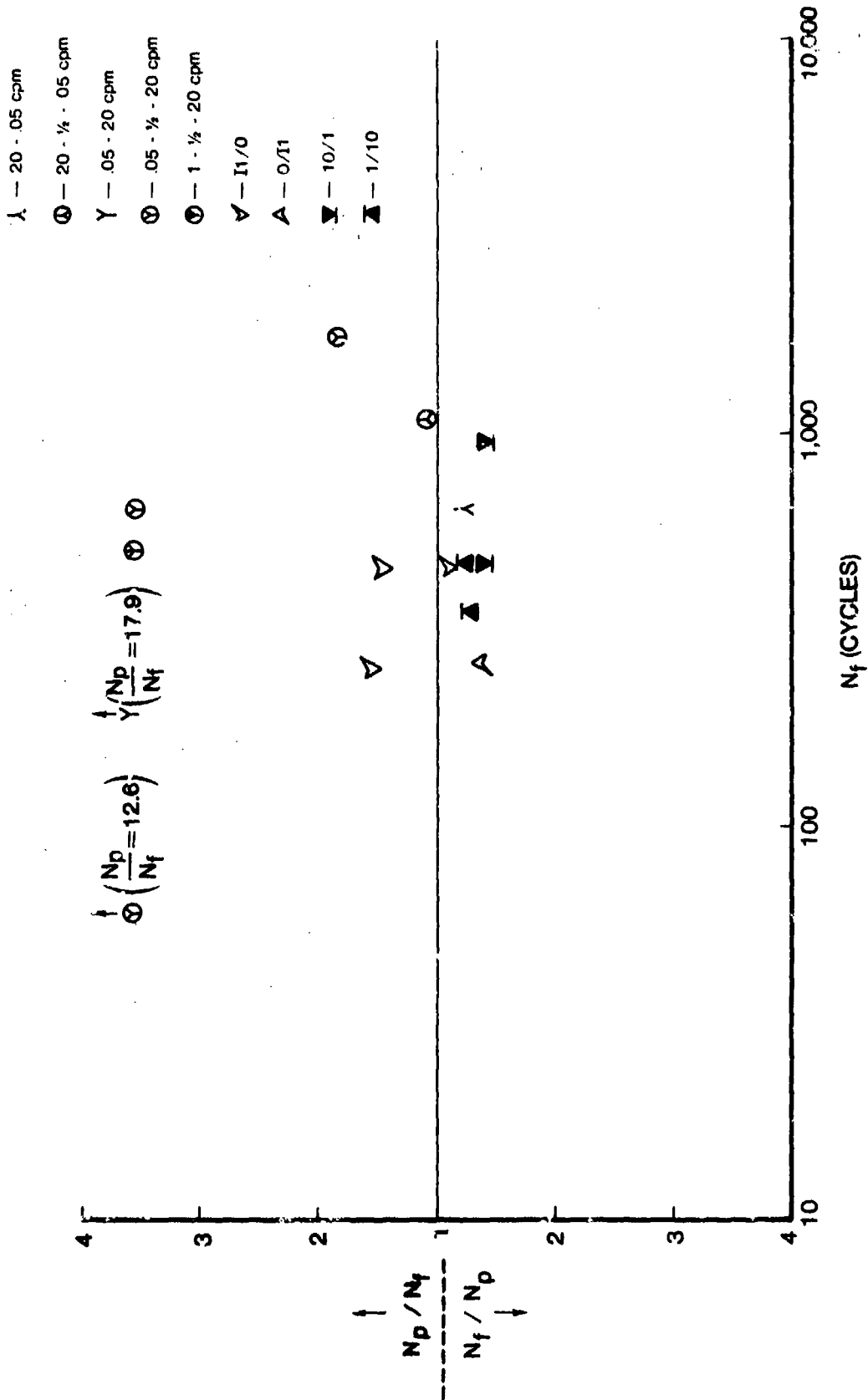


Figure 19b Life Predictions of Verification Tests by the Frequency-Separation Model

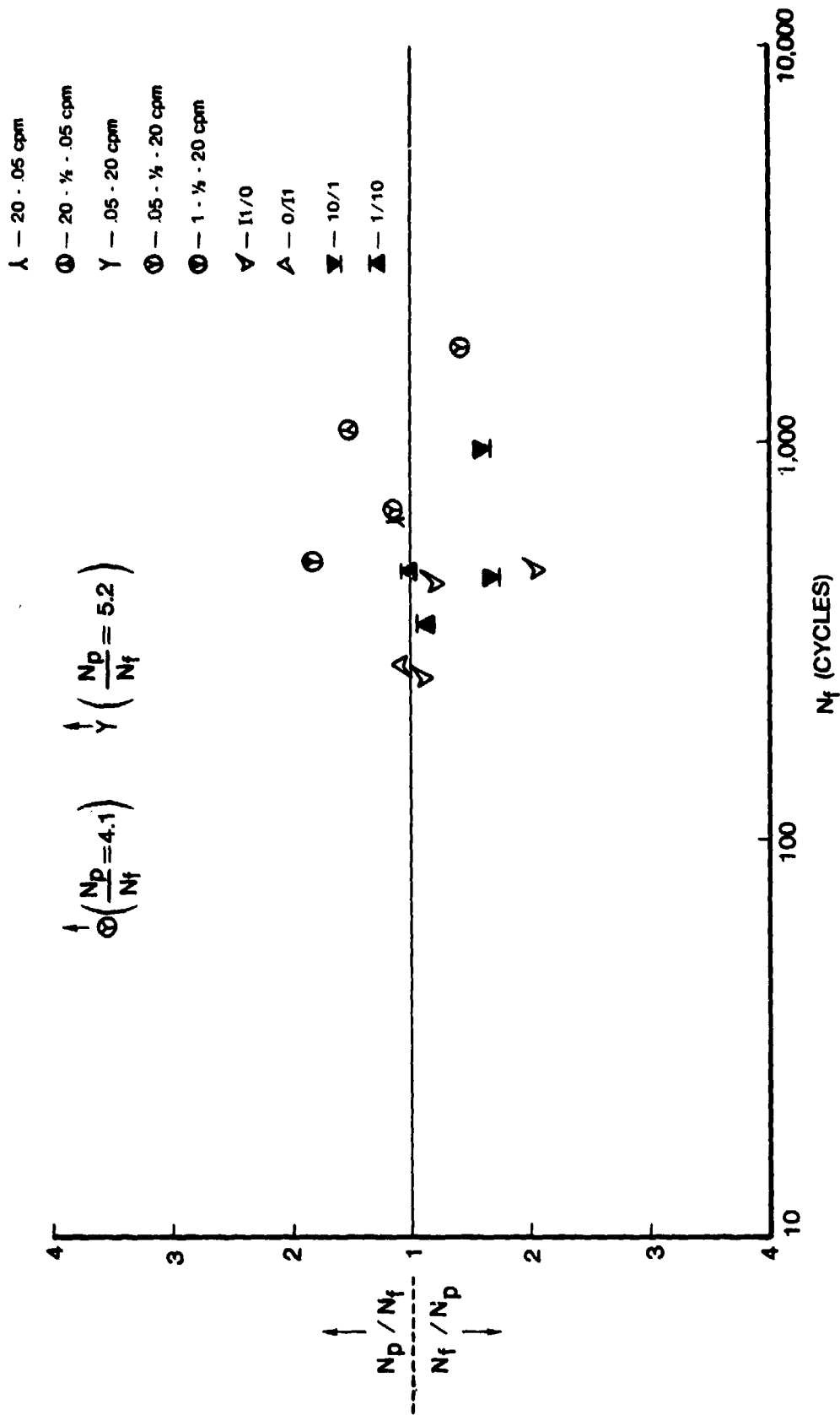


Figure 19c Life Predictions of Verification Tests by the Ostergren Model

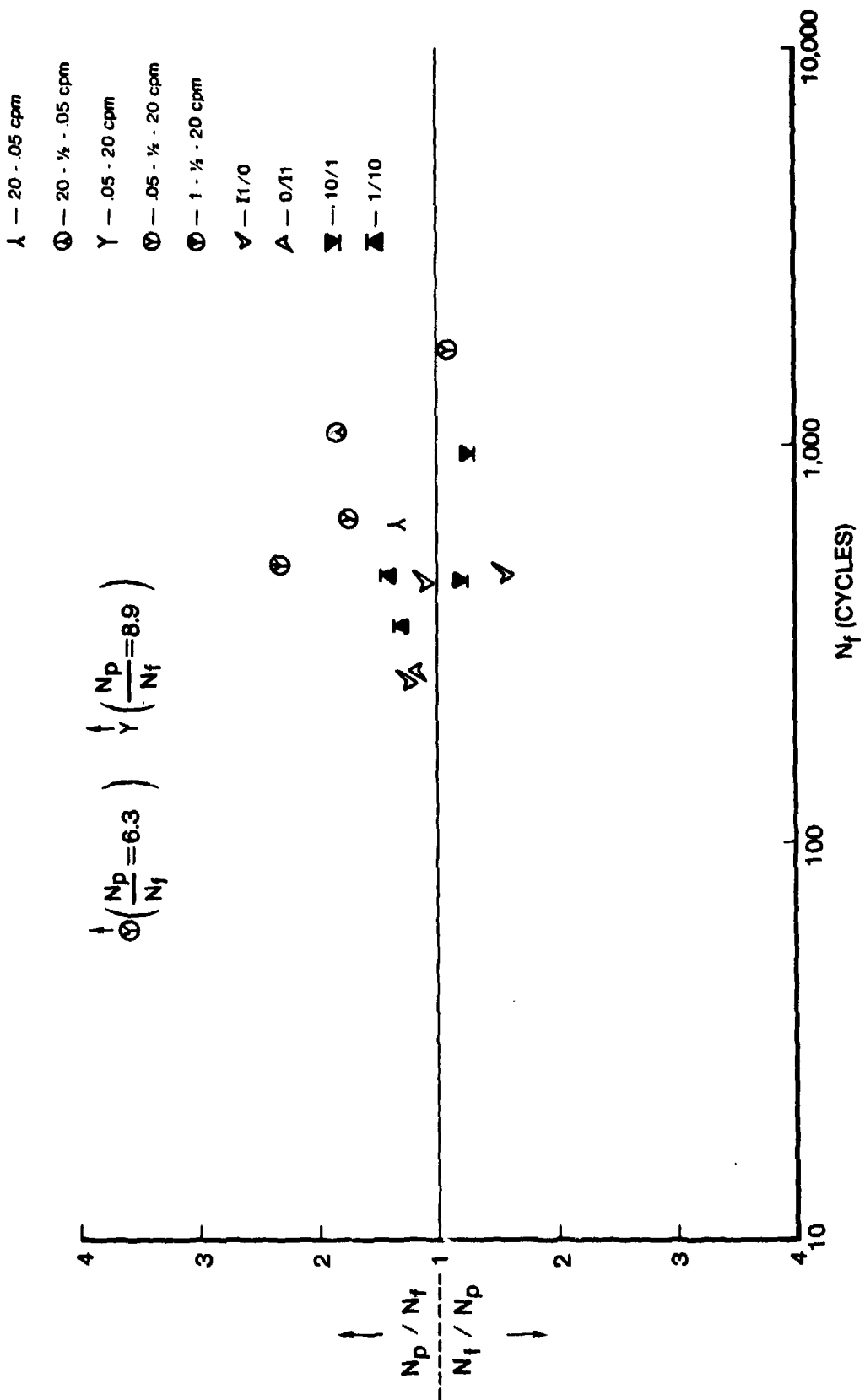


Figure 19d Life Predictions of Verification Tests by the Damage-Rate Model

Table IX

LIFE PREDICTIONS OF VERIFICATION TESTS

Specimen	Type of Test	Total Strain-Range (%)	Observed Life (Cycles)	+ $\frac{\text{Observed Life}}{\text{Predicted Life}}$ or - $\frac{\text{Predicted Life}}{\text{Observed Life}}$			
				Strainrange-Partitioning Model	Frequency-Separation Model	Ostergren Model	Damage-Rate Model
251	20-0-0.05 cpm	1.4	639	2.08	-1.23	1.12	1.37
262	20-1/2-0.05 cpm	1.2	1,086	a	1.09	1.50	1.83
261	1-1/2-20 cpm	1.40	499	a	3.45	1.79	2.29
256	0.05-1/2-20 cpm	1.8	60	a	12.60	4.07	6.28
252	0.05-20 cpm	1.4	194	6.09	17.88	5.22	8.92
260	0.05-1/2-20 cpm	1.4	646	a	3.41	1.14	1.70
259	0.05-1/2-20 cpm	1.2	1,731	a	1.83	-1.41	-1.09
242	I1-0	1.8	472	-1.64	-1.22	-2.04	-1.57
246	I1-0	1.8	253	1.13	1.57	-1.11	1.22
244	I1-0	1.6	447	1.02	1.44	-1.17	1.11
247	0-II	1.8	263	-1.32	-1.39	-1.02	1.25
227	10-1	1.4	455	-1.49	-1.34	-1.68	-1.19
223	10-1	1.2	945	-1.50	-1.41	-1.58	-1.27
226	1-10	1.4	349	1.17	-1.31	-1.12	1.31
225	1-10	1.2	464	1.23	-1.23	-1.00	1.42

^aCould not accurately partition

For the 20-0.05 cpm and 0.05-20 cpm tests, stress relaxation took place when the strain rate changed. These tests were partitioned using a companion specimen, as was the case for the 0.05-cpm tests. The hysteresis loops of the companion specimen and the test specimen are shown in Fig. 11. The amount of creep strain was 12% of the inelastic strainrange for both tests. Since the creep strain was due to stress relaxation, the 0.05-20 cpm test was assigned pp and pc strain, and the 20-0.05 cpm test was assigned pp and cp strain. It should be noted that this strain assignment is opposite that which these tests are supposed to produce.²² As seen in Fig. 11, the only creep strain was due to stress relaxation.

In the 20-1/2-0.05 cpm and 0.05-1/2-20 cpm tests where the strain rate was switched halfway between the peak and zero strain, a process similar to strain recovery took place. Hysteresis loops for these tests are shown in Fig. 10. Although recovery is a time-dependent process, it is not clear whether it is a creep process and should be considered a cp or pc type of strain. Therefore, it was decided to attempt neither to partition these tests nor to predict their lives by the SRP method. The 1-1/2-20 cpm test was not predicted because a companion specimen was not available.

The SRP model segregated three test types--the 0.05-cpm, 0/10, and long life cp tests. The 0.05-cpm and 0/10 tests were consistently overpredicted, sometimes by factors greater than two and one-half. All of the cp tests having lives greater than 1700 cycles were underpredicted. One of these underpredictions was by five and one-half.

The consistent overprediction of the life for the 0.05-cpm tests indicates that the model is unable to predict accurately the life of a material in a regime where the stress-strain behavior is frequency independent but the life is frequency dependent. The flow behavior of René 95 at 1200°F (650°C) is nearly the same at 0.05 cpm as at 20 cpm. However, the life is reduced by one-half at 0.05 cpm as compared to the life at 20 cpm. SRP accounts for life reduction in these tests by the detrimental effects of creep expressed through the cc strainrange. Since little creep was present in

these tests the cc strainrange was unable to account for the damaging effect of the slow frequency. The SRP model treated the 0.05-cpm tests as if they were 20-cpm tests, because the inelastic strain in the 0.05-cpm tests was predominantly $\Delta\epsilon_{pp}$.

This same difficulty occurred for the dual-rate tests. The value of $\Delta\epsilon_{cp}$ or $\Delta\epsilon_{pc}$ was 12% of $\Delta\epsilon_{inel}$ and could not account for the damaging effects of these waveforms.

The 0/10 tests and the long-life cp tests were also segregated. These tests all had large mean stresses. The 0/10 tests that were overpredicted had large tensile mean stresses which may have decreased the life. The long-life cp tests which were underpredicted had large compressive mean stresses which may have increased the life. However, some 0/10 and 10/0 tests having large mean stresses were well predicted by the SRP model. Thus, what effect mean stresses have upon the predictive ability of the SRP model is not clear.

The SRP Model was able to predict the majority of the baseline tests to within a factor of two. It overpredicted the long-life cp tests by as much as five and one-half times the observed life and underpredicted the 0.05-cpm tests by over two and one-half times the observed life. All the verification tests were well predicted except for the 0.05-20 cpm test. This test was underpredicted by ten times the observed life. Not all of the data were predicted because the special tests necessary to partition them were not conducted or the means of partitioning them was not clear.

FREQUENCY-SEPARATION MODEL

The Frequency Separation (FS) Model^{4,5} postulates that the basic parameters necessary to predict the creep-fatigue life are the inelastic strainrange, the tension-going frequency, and the loop-time unbalance. Each of these

parameters measures a different aspect of the life. The inelastic strainrange is the basic measure of damage in low-cycle fatigue. In the absence of time-dependent effects and mean stresses, the inelastic strainrange is sufficient for predicting the low-cycle-fatigue life.

The tension-going frequency* is a measure of the time period during which cracks are assumed to be growing. The FS Model assumes that low-cycle fatigue is primarily a process of crack propagation. Propagation is assumed to occur only when the crack is opening because this opening causes the intense local strains which advance the crack tip by local fracture. Thus, the conditions of temperature, frequency, and environment contribute to crack growth when the crack is opening. It is assumed that the crack is opening when the inelastic strain rate is positive. Thus, the tension-going frequency (the reciprocal of the tension-going time) is a measure of the time during which fatigue damage by crack propagation is occurring.

The loop-time unbalance is the ratio of tension-going to compression-going time, which can be expressed in terms of the tension-going and compression-going frequencies

$$\text{loop-time unbalance} = \frac{\tau_t}{\tau_c} = \frac{\frac{1}{\tau_c}}{\frac{1}{\tau_t}} = \frac{\nu_c}{\nu_t}$$

where τ_t = tension-going time, τ_c = compression-going time, ν_t = tension-going frequency, and ν_c = compression-going frequency. The model assumes crack growth to be dependent upon the loop-time unbalance. The crack-growth rate is assumed to be higher if the tension-going time is longer or shorter than the compression-going time, depending upon the particular material.

*The tension-and compression-going frequencies are defined as the reciprocal of the time period over which the inelastic strain rate is positive or negative, respectively. Their use in the literature also includes the time period over which the inelastic strain rate is zero, which occurs for elastic unloading. The time spent in elastic unloading is included in the tension-going frequency if the total strain rate is positive or in the compression-going frequency if the total strain rate is negative. Determination of these frequencies is illustrated in Fig. 20.

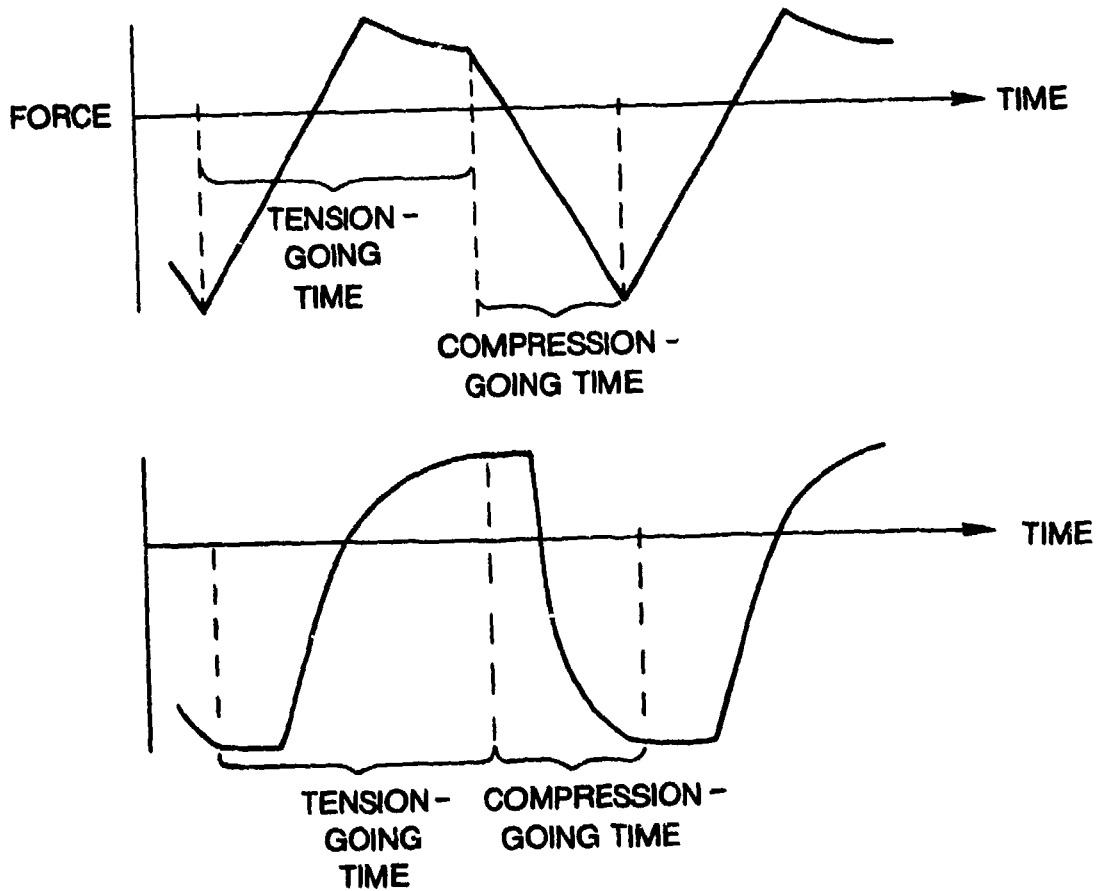
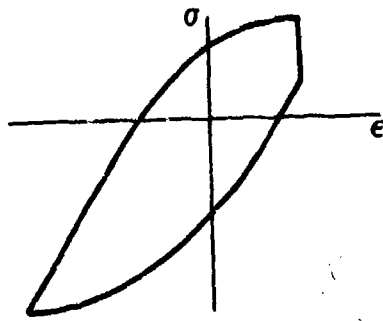


Figure 20 Illustration of Tension-Going and Compression-Going Time

These three parameters-- $\Delta\epsilon_{inel}$, ν_t , and ν_c/ν_t --are combined in a power-law relationship to predict the cycles to failure

$$N_f = C \Delta\epsilon_{inel}^\beta \nu_t^m \left(\frac{\nu_c}{\nu_t}\right)^k \quad (8)$$

where C, β , m, and k are constants. Thus, the FS Model extends the Coffin-Manson Law by the addition of two frequency terms.

The constants in Eq. (8) were determined by a least-squares fit. The logarithm of each side of the equation was first taken in order to linearize it. In the least-squares fit, the dependent variable was the cycles to failure, and the independent variables were the inelastic strainrange and the frequency terms. The value of the inelastic strainrange was determined from the inelastic-strain strip chart as explained in the description of the Strainrange Partitioning Model. The values of the frequencies were controlled during the test. Table X is a list of the values of the frequency terms for the different types of tests.

The values of the constants in Eq. (8) that yielded the best fit to the baseline data were: $C = 0.456$, $\beta = -1.11$, $m = 0.121$, and $k = 0.183$. The predicted and observed lives of the baseline data are shown in Fig. 18b, and given in Table VIII. The scatter band was 3.6 and the standard deviation 0.18. Of the baseline tests, only the cp tests were segregated. The trend of the predictions was inconsistent with the results of the cp tests. For observed lives of less than 1800 cycles, the lifetimes were consistently overpredicted; for lives greater than 1800 cycles, the lifetimes were all underpredicted, some of these underpredictions being three and one-half times lower than the observed life.

The constants obtained for Eq. (8) show that ν_t has a smaller effect upon fatigue life than ν_c . ν_t is raised to the m minus k power, which is -0.06, while ν_c is raised to the 0.18 power. Also, ν_t is raised to a negative power which indicates that the fatigue life should become longer as the

TABLE X

VALUES OF THE FREQUENCY TERMS USED IN THE
FREQUENCY-SEPARATION MODEL

Type of Test	v_c/v_t	v_t
20 cpm	1.	40. cpm
0.05 cpm	1.	0.1
1/0	41.	1.0
10/0	410.	0.1
0/1	0.024	40.
0/10	0.0024	40.
1/1	1.	1.
10/10	1.	0.1
20-0.05 cpm	0.0024	40.
20-1/2-0.05 cpm	0.0024	40.
0.05-20 cpm	410.	0.1
0.05-1/2-20 cpm	410.	0.1
1-1/2-20 cpm	41.	1.
11/0	41.	1.0
0/11	0.024	40.
10/1	10.	0.1
1/10	0.1	1.0

time spent in tension becomes longer. This small effect of v_t and the beneficial effect of slower v_t are contrary to the basic postulate of the model that v_t is a major parameter which affects fatigue life.

The FS Model was able to predict all of the verification tests to within a factor of two except the slow-fast tests. The predicted and observed lives are shown in Fig. 19b and given in Table IX. All of the slow-fast tests were overpredicted, some by factors greater than ten. The reason for this waveform being so poorly predicted may be that for the baseline data, the model predicted the effect of the tension-going time to be negligible. Thus, the long tension-going time of the slow-fast waveform was ignored by the model, and the waveform was treated as a 20-cpm test which would account for the consistent overprediction of this waveform.

The FS Model considered the following sets of waveforms to have identical lives for a given inelastic strainrange: 20-0.05 cpm, 20-1/2-0.05 cpm, and 0/10; 0.05-20 cpm, 0.05-1/2-20 cpm and 10/0; 0.05 cpm and 10/10; 1/0 and 11/0; and 0/1 and 0/11. From the test results, the waveforms within each set appeared to have identical behavior, the only exceptions being the 0.05-20 cpm, 0.05-1/2-20 cpm and 10/0 waveforms. The 0.05-20 cpm and 0.05-1/2-20 cpm tests were more damaging than the 10/0 tests. The one 0.05-20 cpm test was much more damaging than the 0.05-1/2-20 cpm tests.

Furthermore, three groups of waveforms had the same value for tension-going frequency. Within each of these groups the lives should be ordered such that those waveforms having the largest values for the loop-time unbalance would have the longest lives. These three groups of waveforms are: 20 cpm, 0/1, 0/11, 20-0.05 cpm, 20-1/2-0.05 cpm, and 0/10; 1/0, 11/0, 1-1/2-20 cpm, 1/1, and 1/10; and 0.05-20 cpm, 0.05-1/2-20 cpm, 10/0, 10/1, 0.05 cpm, and 10/10. Within each of these groups, the tests are listed from the largest value of v_c/v_t to the smallest. All fatigue

lives followed this ordering sequence with the exception of the 0.05-20 cpm, 0.05-1/2-20 cpm, 1-1/2-20 cpm, 10/1, and 1/10 waveforms. The 0.05-20 cpm, 0.05-1/2-20 cpm and 1-1/2-20 cpm waveforms have been discussed previously. The 10/1 and 1/10 waveforms did not have shorter lives as the FS Model predicted. As shown in Fig. 21, the lives of the 1/10 tests were similar to those of the 1/1 tests, and the 10/1 tests appear to be similar to the 10/0 tests. In each of these cases, the value of v_c/v_t varies by a factor of ten.

Four of the waveforms--20 cpm, 1/1, 0.05 cpm, and 10/10--had a value of 1 for v_c/v_t . For these tests the FS Model predicts that the waveform having the highest value of v_t will have the longest life. The lives of the waveforms did follow this order.

Overall, the FS Model predicted the results of most of the baseline and verification tests well. Only the slow-fast tests, a few cp tests, and one pc test were poorly predicted; and only the cp tests were segregated. Five waveforms--10/1, 1/10, 0.05-20 cpm, 0.05-1/2-20 cpm, and 1-1/2-20 cpm--failed to follow the frequency terms. The concept that v_t controlled fatigue life did not appear to be applicable to René 95 at 1200°F (650°C).

OSTERGREN MODEL

The Ostergren Model^{6,7} is based upon the premise that low-cycle fatigue is primarily a problem of crack propagation. Accordingly, cracks nucleate very early, and the majority of the life is spent growing these cracks to a critical size. The model assumes that only the deformation which occurs when the crack is open contributes to crack propagation and, thus, to fatigue damage. The measure of deformation used by the model is the hysteretic energy absorbed by the specimen. As a first approximation, the model assumes that the crack is open only when the load on the specimen is greater than zero. Thus, the model's measure of fatigue damage is the tensile hysteretic energy absorbed by the specimen. This energy is approximated as the product of the width of the hysteresis loop, its height, and a shape factor

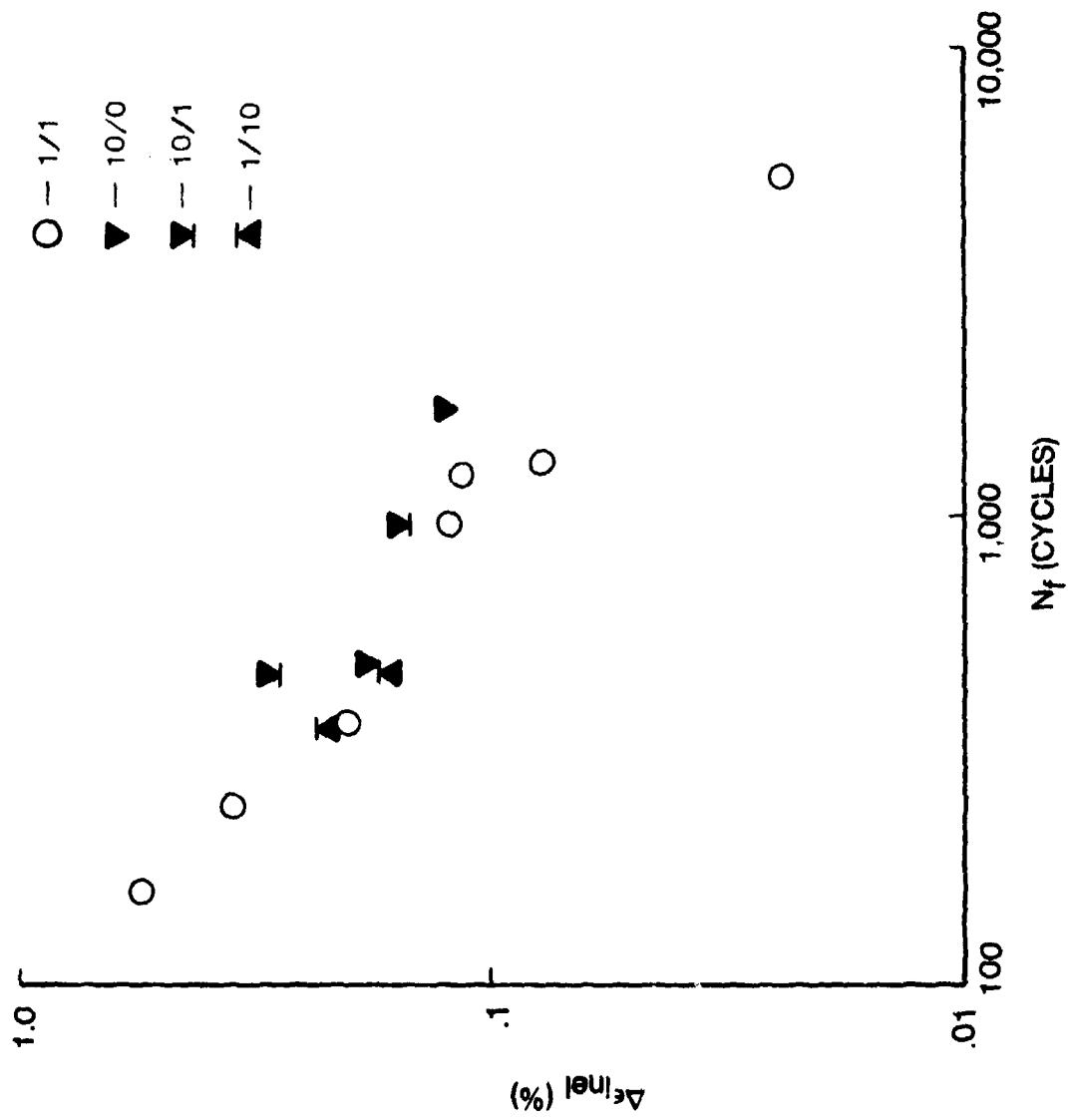


Figure 21 Inelastic Strainrange as Function of Cycles to Failure for 1/1, 10/0, 10/1, and 1/10 Tests

$$A = \alpha \cdot \Delta\epsilon_{inel} \cdot \sigma_t \quad (9)$$

where A is the area of the tensile half of the hysteresis loop, α the shape factor, $\Delta\epsilon_{inel}$ the width of the hysteresis loop and inelastic strain-range, and σ_t the height of the hysteresis loop and the peak tensile strength. The shape factor corrects the area approximated by $\Delta\epsilon_{inel} \cdot \sigma_t$ to make it equal the true area. The shape factor is assumed to remain the same for all types of isothermal tests. Thus, the measure of fatigue damage in the Ostergren Model is given by Eq. (9).

The life is predicted by postulating a power-law relationship between the measure of fatigue damage and the life

$$N_f = C(\Delta\epsilon_{inel} \cdot \sigma_t)^\beta \quad (10)$$

where C and β are constants. The shape factor, α , is included in the constant, C. In effect, what the Ostergren Model has done is to modify the Coffin-Manson Law by the addition of the tensile stress to the inelastic strainrange. It should be noted that Eq. (10), like the Coffin-Manson Law, is valid only for time-independent fatigue.

When time-dependent mechanisms are present, as in the creep-fatigue interaction, Eq. (10) is modified by a frequency term which takes into account the time dependency

$$N_f = C(\Delta\epsilon_{inel} \cdot \sigma_t)^\beta v^m \quad (11)$$

where m is a constant and v is the frequency. The frequency selected for use in Eq. (11) depends upon the material sensitivity to different waveshapes. A material is waveshape sensitive if different lives result for tensile strain-hold, compressive strain-hold, and continuous-cycling tests--although all tests have the same inelastic strainrange, tensile stress, and cyclic frequency. If the material is insensitive

to waveshape, then the proper value for frequency in Eq. (11) is the frequency of the entire cycle. If the material is waveshape sensitive, then the frequency term chosen in Eq. (11) must properly reflect this sensitivity.

The Ostergren Model was used to predict the fatigue life of AISI 304 stainless steel, whose life was degraded by waveshapes in which more time was spent under a tensile strain hold than under a compressive strain hold.⁶ To account for this sensitivity, the following frequency term was postulated:

$$v = \begin{cases} \frac{1}{\tau_o + \tau_t - \tau_c} & \text{for } \tau_t > \tau_c \\ \frac{1}{\tau_o} & \text{for } \tau_t \leq \tau_c \end{cases} \quad (12)$$

where τ_o is the time spent in cycling, τ_t the time spent in a tensile strain hold, and τ_c the time spent in a compressive strain hold. This term decreased the frequency for continuous cycling by the net time spent in a tensile hold. The approach was an empirical one designed to render the model sensitive to tensile strain holds.

René 95 was more sensitive to compressive strain holds than tensile strain holds. Since the Ostergren Model has not addressed itself to this type of sensitivity, it was necessary to alter the model slightly. The frequency term used to make the model sensitive to tensile strain holds was changed to render the model sensitive to compressive strain holds. The frequency spent in cycling was reduced by the net time spent in a compressive rather than a tensile strain hold

$$v = \begin{cases} \frac{1}{\tau_o + \tau_c - \tau_t} & \text{for } \tau_c > \tau_t \\ \frac{1}{\tau_o} & \text{for } \tau_c \leq \tau_t \end{cases} \quad (13)$$

Table XI is a summary of the different formulations of the Ostergren Model. The names of the formulations, coined by this author for future reference, refer to the postulated failure mechanism in each formulation.

The inelastic strainrange and tensile stress used to fit the model were measured from the strip charts, as discussed in the description of the SRP Model. The frequency of the tests was a controlled variable which was held constant throughout the test. The values of the frequencies used for the different types of tests and different formulations of the model are listed in Table XII. The constants in Eqs. (10) and (11) were obtained by a least-squares fit after the logarithm of each side of the equation was taken. Cycles to failure was considered to be the dependent variable; and the inelastic strainrange, tensile stress, and frequency were considered to be the independent variables.

Since it was not possible to determine beforehand which of the formulations of the model was appropriate for René 95, all of them were fitted to the baseline data. The constants in Eqs. (10) and (11) which best fit the data are given in Table XIII, along with the scatter band and standard deviation. Both the room-temperature and tensile-creep formulations predicted the data less accurately than the environmental or compressive-creep formulations. A decision was made not to use the room-temperature or the tensile-creep formulation because neither incorporated the time-dependent effects present in the fatigue tests. The room-temperature formulation has no term for these effects and is not designed for use at elevated temperatures. The frequency term of the tensile-creep formulation is raised to a very small power, 0.02, which indicates almost no dependence of life upon this term.

The compressive-creep formulation extensively segregated the data. It underpredicted the lives of most of the 20-cpm tests, and it overpredicted the lives of all cc tests. It also underpredicted the lives of the long-life cp tests. Since this extensive segregation was absent from the environmental formulation, the compressive-creep formulation was abandoned and the environmental formulation was adopted as the proper formulation of the Ostergren Model.

TABLE XI
FORMULATIONS OF THE OSTERGREN MODEL

$$N_f = C(\Delta\epsilon_{inel} \cdot \sigma_t)^\beta v^m$$

Name	Use	v
Ostergren Room Temperature	No time dependency. Use at room temperature.	Not used (or $v = 1$)
Ostergren Environmental	Time dependent. No waveshape sensitivity.	Cyclic frequency
Ostergren Tensile Creep	Time dependent. Sensitive to waveshapes with tensile holds greater than compressive holds.	$\frac{1}{\tau_o + \tau_t - \tau_c} \quad \text{if } \tau_t > \tau_c$ $\frac{1}{\tau_o} \quad \text{if } \tau_t \leq \tau_c$
Ostergren Compressive Creep	Time dependent. Sensitive to waveshapes with compressive holds greater than tensile holds.	$\frac{1}{\tau_o + \tau_c - \tau_t} \quad \text{if } \tau_c > \tau_t$ $\frac{1}{\tau_o} \quad \text{if } \tau_c \leq \tau_t$

TABLE XII

VALUES OF THE FREQUENCY TERMS USED IN THE OSTERGREN MODEL

Frequency Term For The:

<u>Type of Test</u>	<u>Environmental Formulation</u>	<u>Tensile-Creep Formulation</u>	<u>Compressive-Creep Formulation</u>
20 cpm	20. cpm	20. cpm	20. cpm
0.05 cpm	0.05	0.05	0.05
1/0	1.0	1.0	20.
10/0	0.1	0.1	20.
0/1	1.0	20.	1.0
0/10	0.1	20.	0.1
1/1	0.5	20.	20.
10/10	0.05	20.	20.
20-0.05 cpm	0.1	0.1	0.1
20-1/2-0.05 cpm	0.1	0.1	0.1
0.05-20 cpm	0.1	0.1	0.1
0.05-1/2-20 cpm	0.1	0.1	0.1
1-1/2-20 cpm	1.0	1.0	1.0
11/0	1.0	1.0	20.
0/11	1.0	20.	1.0
10/1	0.09	0.1	20.
1/10	0.09	20.	0.1

TABLE XIII

CONSTANTS, SCATTER BANDS, AND STANDARD DEVIATIONS FOR
THE VARIOUS FORMULATIONS OF THE OSTERGREN MODEL

$$N_f = C (\Delta\epsilon_{inel} \times \sigma_t)^\beta v^m$$

<u>Formulation</u>	<u>C</u>	<u>β</u>	<u>m</u>	<u>Scatter Band</u>	<u>Standard Deviation</u>
Room Temperature	147.	-1.026	-	4.2	0.22
Environmental	162.	-.976	0.137	3.6	0.18
Tensile Creep	144.	-1.024	0.016	4.2	0.22
Compressive Creep	123.	-1.003	0.138	3.1	0.17

Life predictions for the baseline tests using the environmental formulation are shown in Fig. 18c and are given in Table VIII. The scatter band was 3.6 and the standard deviation 0.18. Most of the tests were predicted to within a factor of two. One pp test, two pc tests, and three cp tests yielded predictions greater than a factor of two.

The life predictions for the verification tests are shown in Fig. 19c and are given in Table IX. All the tests except a 11/0, a 0.05-20 cpm, and a 0.05-1/2-20 cpm test were predicted to within a factor of two. The 11/0 test was predicted to 2.05, slightly above a factor of two. The 0.05-20 cpm and 0.05-1/2-20 cpm tests were underpredicted by factors of 5.2 and 4.1, respectively. The reason for the poor predictions of these slow-fast tests is not understood.

The Ostergren Model underpredicted the lives of all the cp tests having lives greater than 1700 cycles. Also, it overpredicted the lives of the three 0/10 tests and all but one of the pc tests.

The Ostergren Model predicted that the following groups of waveforms should have the same life for the same value of $\Delta\epsilon_{inel} \times \sigma_t$ since they have the same frequency: 1/0, 11/0, 0/1, 0/11 and 1-1/2-20 cpm; 20-0.05 cpm, 20-1/2-0.05 cpm, 0.05-20 cpm, 0.05-1/2-20 cpm, 10/0, and 0/10; 10/1 and 1/10; and 0.05 cpm and 10/10. The tests generally were identical as predicted by the model or the data were inconclusive. The only exceptions were the 0.05-20 cpm, 0.05-1/2-20 cpm, 10/0, and 0/10 tests. Data from these tests are plotted in Fig 22. The 0.05-20 cpm test had a much shorter life than expected. The 0.05-1/2-20 cpm and 10/0 data appeared to fall on one line; and the 20-0.05 cpm, 20-1/2-0.05 cpm, and 0/10 data appeared to fall on another line.

According to the Ostergren Model, the life of a test should decrease as the test frequency is decreased. Figure 23 is a plot of the baseline and validation tests where $\Delta\epsilon_{inel} \times \sigma_t$ is plotted as a function of life.

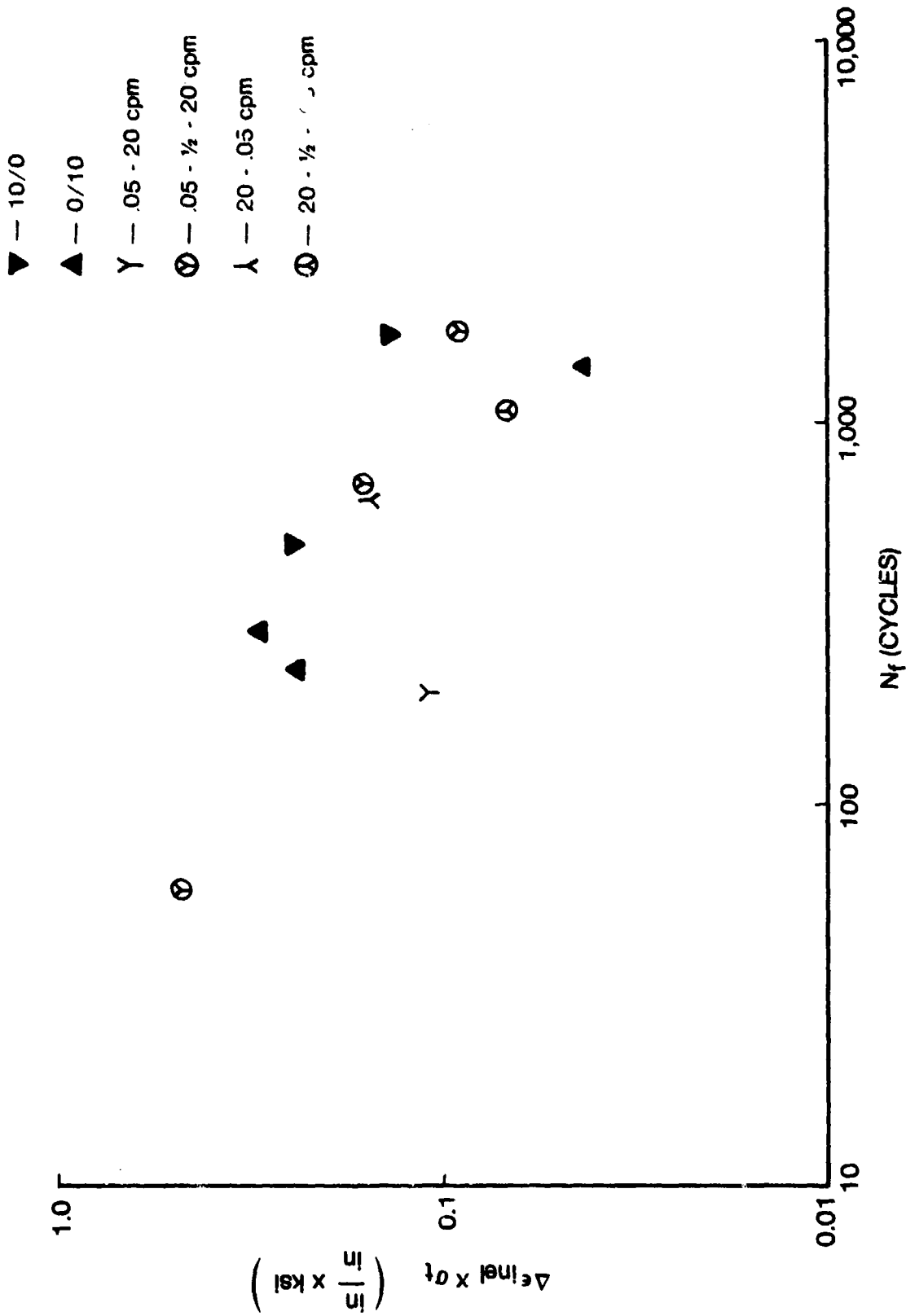


Figure 22 $\Delta \epsilon_{inel} \times \sigma_t$ for 10/0, 0/10, 0.05-20 cpm, 0.05-1/2-20 cpm, 20-0.05 cpm, and 20-1/2-0.05 cpm Tests

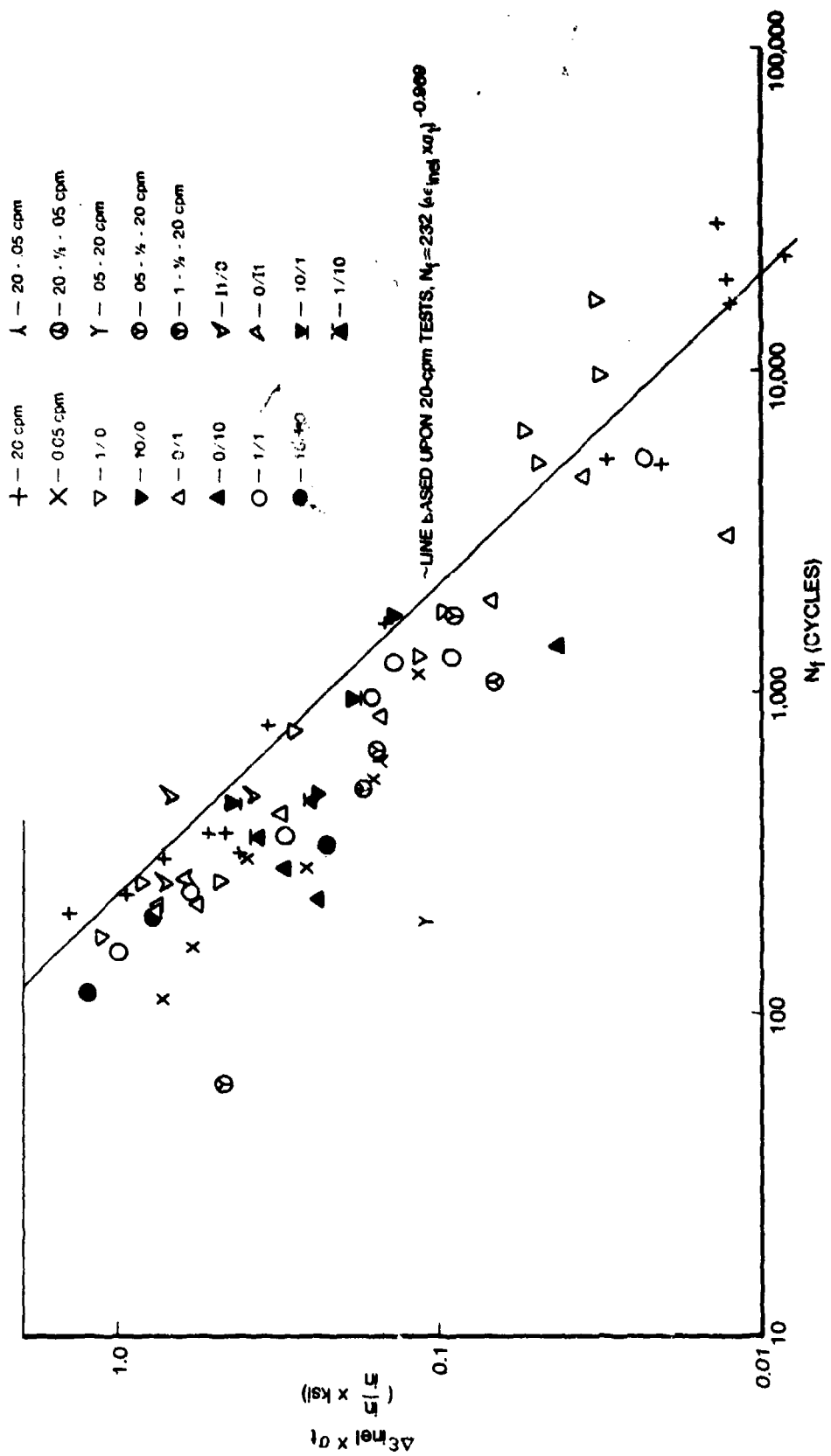


Figure 23 $\Delta \epsilon_{inel} \times \sigma_t$ as Function of N_f

It can be seen that the life does not always decrease for a decreasing frequency. The 1/0 and 11/0 tests have a lower frequency than the 20-cpm tests; yet, in some cases, the 1/0 and 11/0 tests last longer than the 20-cpm tests. Also, the 10/1 and 1/10 tests are not nearly so damaging as would be expected from their low value of frequency. On the other hand, the 0/10 tests are more damaging than their frequency terms would suggest. The 0.05-20 cpm and 0.05-1/2-20 cpm tests have the same value of frequency, but they do not have the same life with respect to $\Delta\epsilon_{inel} \times \sigma_t$. The 0.05-20 cpm test and one of the 0.05-1/2-20 cpm tests were the most damaging and could not be accounted for by the Ostergren Model.

In summary, the Ostergren Model was able to correlate most of the baseline data and to predict all the validation tests except some of the slow/fast tests. The model segregated only two parts of the data. However, the tests did not always follow the behavior expected of them by the model.

DAMAGE RATE MODEL

The Damage Rate Model (DRM)^{8,9,10} is based upon the premise that low-cycle fatigue is primarily a process of crack propagation and cavity growth. Microcracks and cavities are assumed to be originally present in the virgin material, and the majority of the low-cycle-fatigue life is spent growing these microcracks and cavities to a critical size at which time they link up and form a macrocrack. Once a macrocrack is formed, it propagates rapidly until fracture takes place.

The model postulates a growth law for the microcracks and cavities

$$\frac{da}{dt} = \begin{cases} a^T |\epsilon_{inel}|^m |\dot{\epsilon}_{inel}|^k & \begin{cases} \text{in the presence of} \\ \text{tensile stress} \end{cases} \\ a^C |\epsilon_{inel}|^m |\dot{\epsilon}_{inel}|^k & \begin{cases} \text{in the presence of} \\ \text{compressive stress} \end{cases} \end{cases} \quad (14)$$

$$\frac{dc}{dt} = \begin{cases} cG |\epsilon_{inel}|^m |\dot{\epsilon}_{inel}|^{k_c} & \text{in the presence of} \\ & \text{tensile stress} \\ c(-G) |\epsilon_{inel}|^m |\dot{\epsilon}_{inel}|^{k_c} & \text{in the presence of} \\ & \text{compressive stress} \end{cases} \quad (15)$$

where a is crack length, c is cavity length, t is time, ϵ_{inel} is the inelastic strain, $\dot{\epsilon}_{inel}$ is the inelastic strain rate, and T , C , G , m , k , and k_c are constants. The law states that microcrack and cavity growth is a function of the inelastic strain and the inelastic strain rate. The microcrack is assumed to grow at different rates under compressive and tensile stresses. The cavity is assumed to shrink under a compressive load. However, the cavity is not allowed to have a size which is less than the initial cavity size.

The growth laws of Eqs. (14) and (15) are integrated over the specimen life from the initial microcrack and cavity size to the critical crack and cavity size when a macrocrack is formed. The integration is performed over an ideal cycle* in which the peak tensile and compressive stresses are equal, the peak tensile and compressive inelastic strains are equal, and the inelastic strain rate is constant. The critical crack and cavity size which causes failure is determined from a microcrack and cavity-growth interaction equation

$$\frac{\ln a/a_0}{\ln a_f/a_0} + \frac{\ln c/c_0}{\ln c_f/c_0} = 1 \quad (16)$$

where a_0 is the initial crack size, a_f the critical crack size, c_0 the initial cavity size, and c_f the critical cavity size. When Eqs. (14) and (15) are integrated over such an ideal cycle and Eq. (16) is used, the predictive equations of the DRM result. For continuous cycling at a constant frequency or strain rate

$$N_f = \frac{m+1}{4A} \left(\frac{\Delta\epsilon_{inel}}{2} \right)^{-(m+1)} (\dot{\epsilon}_{inel})^{1-k} \quad (17)$$

where $A = [(C + T)/2]/[\ln(a_f/a_0)]$ and A is a constant. For hold times

*Strictly speaking, the integration should be performed over the actual cycle observed in the test. However, the DRM, as its authors presently propose it, makes use of the equations developed from integrating an ideal cycle. Use of the observed cycle instead of the ideal cycle would create a different model.

$$\begin{aligned}
D_a = & \frac{4A}{m+1} \left(\frac{\Delta \epsilon_{inel}}{2} \right)^{m+1} (\dot{\epsilon}_{inel})^{k-1} \\
& + |\epsilon_{inel \max}|^m \int_0^{t_t} \frac{2A}{1+C/T} |\dot{\epsilon}_{inel}|^k dt \\
& + |\epsilon_{inel \min}|^m \int_0^{t_c} \frac{2A}{1+T/C} |\dot{\epsilon}_{inel}|^k dt
\end{aligned} \tag{18}$$

$$D_c = G \int_0^{t_t} |\epsilon_{inel}|^m |\dot{\epsilon}_{inel}|^{k_c} dt - G \int_0^{t_c} |\epsilon_{inel}|^m |\dot{\epsilon}_{inel}|^{k_c} dt \tag{19}$$

$$N_f = \frac{1}{D_a + D_c} \tag{20}$$

where D_a is the damage due to crack growth, D_c is the damage due to cavity growth, t_t the time spent in a tensile hold, t_c the time spent in a compressive hold, $\epsilon_{inel \max}$ is the inelastic strain at the beginning of the tensile hold time, $\epsilon_{inel \min}$ the inelastic strain at the beginning of the compressive hold time, and C/T is a constant. In Eq. (18) the first term on the right-hand side is the damage caused by continuous cycling, the second term is the damage due to a tensile hold, and the third term is the damage caused by a compressive hold. In Eq. (19) the first term on the right-hand side is the damage caused by a tensile hold, and the second term is the healing due to a compressive hold. For F/S (fast-slow) tests

$$N_f = \frac{m+1}{4A} \left(\frac{\Delta \epsilon_{inel}}{2} \right)^{-(m+1)} \left[\frac{\dot{\epsilon}_{inel f}^{(k-1)}}{1+C/T} + \frac{\epsilon_{inel s}^{(k-1)}}{1+T/C} \right]^{-1} \tag{21}$$

where $\dot{\epsilon}_{inel f}$ is the inelastic strain rate for the fast rate and $\dot{\epsilon}_{inel s}$ the inelastic strain rate for the slow rate.

For S/F (slow-fast) tests

$$D_a = \frac{4A}{m+1} \left(\frac{\Delta \epsilon_{inel}}{2} \right)^{(m+1)} \left[\frac{\dot{\epsilon}_{inel s}^{(k-1)}}{1+C/T} + \frac{\dot{\epsilon}_{inel f}^{(k-1)}}{1+T/C} \right] \quad (22)$$

$$D_c = \frac{2G}{m+1} \left(\frac{\Delta \epsilon_{inel}}{2} \right)^{(m+1)} \left[\dot{\epsilon}_{inel s}^{(k_c-1)} - \dot{\epsilon}_{inel f}^{(k_c-1)} \right] \quad (23)$$

$$N_f = \frac{1}{D_a + D_c} \quad (24)$$

The cavity growth law of Eq. (15) can also be integrated over the life of a creep test in order to predict the time to failure.

$$t_f = C' (\dot{\epsilon}_{inel})^{-\frac{k_c + m}{1+m}} \quad (25)$$

where t_f is the time to failure and C' is a constant. In order to obtain this result, the following assumptions were made: a constant inelastic strain rate, a constant critical crack size, and that only cavity growth occurs.

The values of the constants A , m , and k were determined by fitting Eq. (17) to a data set consisting of the 20-cpm and 0.05-cpm tests. The value of k_c was found by fitting Eq. (25) to the creep data. A least-squares fit was used where the time to failure was considered to be the dependent variable. The secondary creep rate observed in the creep tests was used as the inelastic strain rate. The value of G can be determined from the slow-fast tests. However, a value of G for René 95 was not determined. The reason for this will be explained later.

The ratio of C/T used in Eqs. (18), (21), and (22) was estimated from the cp and pc tests. For tests having the same value of inelastic strainrange, the C/T ratio was set equal to the ratio of the life of the pc test to

that of the cp test. This procedure was used to estimate the relative reduction in life caused by the compressive hold period as compared to the tensile hold period.

The value used for the inelastic strain rates was the inelastic strain-range divided by the time required to traverse this strainrange

$$\dot{\epsilon}_{inel} = \frac{\Delta\epsilon_{inel}}{\text{time for 1/2 cycle}}$$

$$\dot{\epsilon}_{inel f} = \frac{\Delta\epsilon_{inel}}{\text{time for fast portion of ramp}}$$

$$\dot{\epsilon}_{inel s} = \frac{\Delta\epsilon_{inel}}{\text{time for slow portion of ramp}}$$

It has been demonstrated for stainless steels in Ref. 8 that the DRM is insensitive to the waveform which the inelastic strain follows--ramp, sine, or parabolic waveform. It was assumed that for René 95 the model was also insensitive to these different waveforms.

In order to evaluate the integrands in Eqs. (18) and (19), it was necessary to determine the inelastic strain rate as a function of time during the hold period. This function was determined by assuming that the stress-relaxation behavior during the hold period is described by

$$\sigma = \sigma_0 - B \ln(t + 1) \quad (26)$$

where σ is the stress at time t , σ_0 the stress at the beginning of the hold period, B is a constant, and t is time. When Eq. (26) was divided by the modulus of elasticity and differentiated with respect to time, the inelastic strain rate as a function of time resulted*

$$\dot{\epsilon}_{inel} = \frac{-d\sigma/dt}{E} = \frac{B}{E} \frac{1}{(t + 1)}$$

*The stress which was relaxed was assumed to be converted into inelastic strain.

The value of the constant B was found separately for each test by using the value of the stress at the end of the hold period

$$B = \frac{\sigma_o - \sigma(t_h)}{\ln(t_h + 1)}$$

where t_h is the time of the hold period and $\sigma(t_h)$ the stress at the end of the hold period.

The value of the inelastic strainrange used in the cycling term of Eq. (18) was taken to be the average of the inelastic strain generated by the tensile and compressive cycling. As shown for a cp test in Fig. 24, the inelastic strain generated by tensile cycling was different from that generated by compressive cycling. This difference also occurred in the other strain-hold tests. The inelastic strain rate used in the cycling term of Eq. (17) was this inelastic strainrange divided by the time spent in cycling.

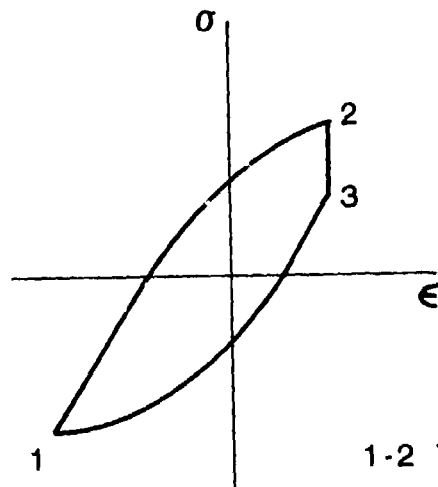
The values of $\epsilon_{inel\ max}$ and $\epsilon_{inel\ min}$ used in Eq. (18) were calculated from the peak stresses and the total strainrange

$$\epsilon_{inel\ max} = \frac{\Delta\epsilon_{tot}}{2} - \frac{\sigma_t}{E}$$

$$\epsilon_{inel\ min} = \frac{\Delta\epsilon_{tot}}{2} - \frac{\sigma_c}{E}$$

where σ_t is the stress at the start of the tensile hold period and σ_c the stress at the start of the compressive hold period. These values represent the inelastic strain at the beginning of the hold period and are given by the total strain at this point less the elastic strain. The total strain was controlled in the test. The elastic strain was the stress divided by the modulus of elasticity.

Preliminary examination of metallographic sections of cp and S/F test specimens using an SEM revealed no evidence of cavity damage.



1-2 TENSILE CYCLING
 3-1 COMPRESSIVE CYCLING
 2-3 TENSILE HOLD TIME

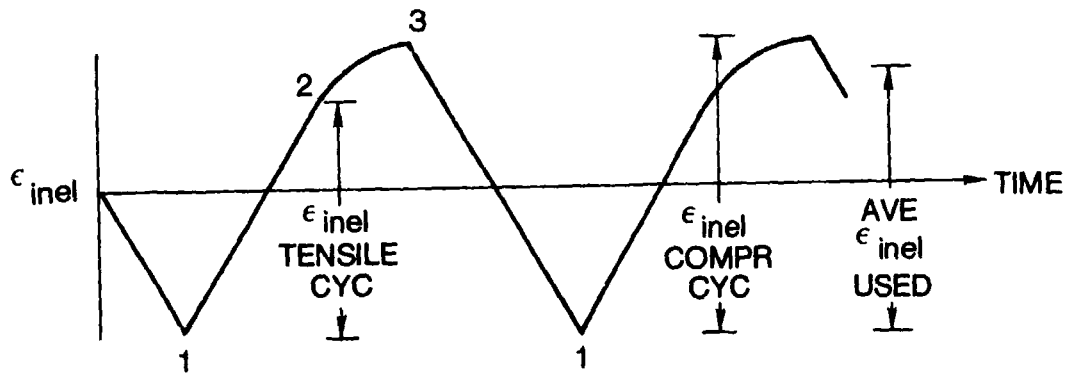


Figure 24 Illustration of Inelastic Strain Used in the Damage-Rate Model for a cp Test

Therefore, Eqs. (19) and (23) which take into account the cavity damage were not used. This assumption of no cavity damage was justified by the life predictions which will be discussed later.

It should be noted that in the use of the above procedure to fit the DRM to the data, no constants were determined in order to give the best fit for the strain-hold tests. Thus, the strain-hold tests constitute a verification of the DRM.

The constants used in the DRM were

$$\begin{aligned} m &= 0.2395 & k_c &= 0.8340 \\ k &= 0.8705 & C/T &= 2. \\ A &= 1.650 \end{aligned}$$

These constants were used in Eqs. (17), (18), (21), and (22) to predict both the baseline and verification tests. These life predictions are shown in Figs. 18d and 19d and are given in Tables VIII and IX. The scatter band for the baseline tests was 5.1, and the standard deviation was 0.24.

In order to predict the lives of the cp and the cc tests, only Eq. (18) was used. It was assumed that no cavity growth occurred. This assumption was justified because the lives of these tests were either accurately predicted or underpredicted. If cavity growth did occur, then the lives would be expected to be overpredicted because of the unaccounted for cavity growth.

The DRM was able to predict all the verification tests except three of the S/F tests, which were overpredicted by as much as 8.9 times the observed life. Equation (22) was used to predict these tests. An attempt was made to use Eq. (23) to account for cavity growth. The value of G was determined for each test by equating the predicted life and the observed life. The values of G ranged from 18.7 to -0.2. Since no value of G could be obtained which was similar for each of the S/F tests, the cavity-growth equation was assumed to be inappropriate and was not used to predict these tests.

The DRM segregated the cp and pc tests. All of the cp tests having lives greater than 1700 cycles were underpredicted. As the lives became longer, the predictions became less accurate. The lives of all the pc tests were overpredicted. These predictions became worse, as the length of the hold time was increased.

One possible reason for the cp and pc tests being segregated is that these were the only tests having large mean stresses. The DRM as used in this evaluation did not take into account mean stresses. The crack-growth law of Eq. (14) was integrated over an ideal cycle in which the mean stress was zero. If the crack-growth law were integrated over a cycle that did contain mean stresses, then better life predictions might result.

A conceptual difficulty arises in the assumed crack-growth equation, Eq. (14). The appropriate value of C/T used for René 95 was 2. This indicates that the crack growth under a compressive stress is twice as great as that under a tensile stress, contrary to what would be expected.

The DRM was able to predict the majority of the fatigue tests to within a factor of two. Some cp, pc, and S/F tests were not predicted within a factor of two. The long-life cp tests and all the pc tests were segregated.

SECTION V
COMPARISON OF THE MODELS

None of the models was able to predict the baseline tests to within the desired scatter band of two. The smallest scatter band of 3.6 was achieved by both the Frequency-Separation and Ostergren Models. The largest scatter bands were 5.1 for the Damage-Rate Model and 5.4 for the Strainrange-Partitioning Model. The standard deviation of the predictions followed this same order. This order, along with the scatter bands and standard deviations, is given in Table XIV.

Based upon the scatter band and the standard deviation, the Frequency-Separation and Ostergren Models were able to predict the baseline tests equally well and significantly better than the Damage-Rate Model and the Strainrange-Partitioning Model. Between the Damage-Rate and Strainrange-Partitioning Models, there was little difference in the scatter band and standard deviation.

None of the models was able to predict all of the verification tests to within a factor of two. No model predicted all of the slow-fast tests. The remainder of the verification tests were well predicted by all of the models. The ability of each model to predict the verification tests is also given in Table XIV.

All of the models segregated sections of the baseline data set to some extent. Table XV lists the segregation for each model. The data were segregated the least by the Frequency-Separation and Ostergren Models and most by the Damage-Rate and Strainrange-Partitioning Models. The Frequency-Separation Model had the wrong trend for the cp tests. The cp tests having short lives were overpredicted, and those having long lives were underpredicted. The Ostergren Model underpredicted the cp tests having long lives and overpredicted the 0/10 tests. The Damage-Rate Model also underpredicted the long-life cp tests but overpredicted

TABLE XIV

OVERALL ABILITY OF THE MODELS TO FIT THE DATA

<u>Model</u>	<u>Scatter Band</u>	<u>Standard Deviation</u>	<u>Ability to Predict Verification Tests</u>
Frequency Separation	3.6	0.18	All predicted except S/F
Ostergren	3.6	0.18	All predicted except S/F
Damage-Rate Model	5.1	0.24	All predicted except S/F
Strainrange Partitioning	5.4	0.23	All predicted except S/F

TABLE XV

SEGREGATION OF THE DATA BY THE MODELS

<u>Model</u>	<u>20 cpm</u>	<u>0.05 cpm</u>	<u>cp</u>	<u>pc</u>	<u>cc</u>
Frequency Separation	None	None	Underpredicts at short lives; underpredicts at long lives	None	None
Ostergren	None	None	Underpredicts at long lives	Overpredicts 10-min. holds	None
Damage-Rate Model	None	None	Underpredicts at long lives	Overpredicts at all lives	None
Strainrange Partitioning	None	Overpredicts at all lives	Underpredicts at long lives	Overpredicts 10-min. holds	None

all of the pc tests. The Strainrange-Partitioning Model underpredicted the long-life cp tests and overpredicted the 0/10 tests. It also overpredicted all of the 0.05-cpm tests. Thus, the amount of segregation of the data by the models followed the same trend as the life predictions.

In general, those tests having large mean stresses were poorly predicted by all of the models. However, some tests having large mean stresses were well predicted. Thus, the influence of mean stress could not be definitely determined. Nevertheless, the general trend seemed to be that the models had difficulty handling mean stress effects.

Each model curve fit the baseline data in order to predict its life. As the curve fitting of the data became more extensive, it became more difficult to determine whether the life predictions were due to the correct functional form and variables in the model or due to the curve-fitting routine. Of the four models, the Damage-Rate Model depended the least upon curve fitting the data and the Strainrange-Partitioning Model, the most.

The Damage-Rate Model curve fit the 20-cpm and 0.05-cpm tests to determine three constants. The fourth constant was estimated, and the other constants in the model were not used. These four constants were used to predict the hold-time tests without determining any constants to give a "best fit."

The Strainrange-Partitioning Model divided the baseline tests into four subsets* and determined the two best-fit constants for each subset. This procedure resulted in a total of eight constants.

The Frequency-Separation and Ostergren Models curve fit the entire baseline data set without dividing it into subsets. The Frequency-Separation Model used four constants, and the Ostergren Model used three.

*The 0.05-cpm tests were not used to determine the constants in the SRP Model due to problems in partitioning them. These problems are discussed in the section on the SRP Model.

Each model required a different amount and degree of effort in order to be used to predict the data. The most difficult model to use was the Strainrange-Partitioning Model. The Frequency-Separation and Ostergren models were the easiest. The Strainrange-Partitioning Model required the inelastic strain to be partitioned into creep and plastic strains. A companion specimen was required to partition the continuous-cycling tests.

The Damage-Rate Model employed four different equations to predict the tests. In these equations, the inelastic strain rate, the maximum and minimum inelastic strains, and the stress-relaxation behavior had to be calculated.

The Ostergren and Frequency-Separation Models require the frequency, inelastic strainrange, and tensile stress to be known. The frequency is usually controlled in a test, and the other two variables may be directly measured from the test record.

SECTION VI

CONCLUSIONS

None of the models was able to predict all of the baseline tests or all of the verification tests to within the desired scatter band of two. The Frequency-Separation and Ostergren Models predicted the data more accurately than the Damage Rate and Strainrange-Partitioning Models. However, the scatter band of the Frequency-Separation and Ostergren Models was 3.6 for the baseline tests. All of the models segregated the data to some extent, which indicates a deficiency in the basic formulation of the model. Thus, none of the four models studied was able to predict the fatigue behavior of René 95 at 1200°F (650°C).

REFERENCES

1. S. S. Manson, G. R. Halford, and M. H. Hirschberg, Creep-Fatigue Analysis by Strainrange Partitioning, NASA TM X-67838 (NASA-Lewis Research Center, Cleveland, OH, 1971).
2. S. S. Manson, "The Challenge to Unify Treatment of High Temperature Fatigue - A Partisan Proposal Based on Strainrange Partitioning," Fatigue at Elevated Temperatures, ASTM STP 520 (American Society for Testing and Materials, Philadelphia, PA, 1978), pp. 744-775. The interaction damage rule is postulated on pp. 751-753.
3. S. S. Manson, G. R. Halford, and M. H. Hirschberg, "Strainrange Partitioning - A Tool for Characterizing High-Temperature, Low-Cycle Fatigue," NASA TMX-71691 (NASA-Lewis Research Center, Cleveland, OH, 1975).
4. L. F. Coffin, Jr., "The Concept of Frequency Separation in Life Prediction for Time-Dependent Fatigue," in 1976 ASME-MPC Symposium on Creep-Fatigue Interaction, MPC-3 (American Society of Mechanical Engineers, NY, 1976), pp. 349-364.
5. Time-Dependent Fatigue of Structural Alloys, ORNL-5073 (Oak Ridge National Laboratory, Oak Ridge, TN, 1975), pp. 109-133.
6. W. J. Ostergren, "A Damage Function and Associated Failure Equations for Predicting Hold Time and Frequency Effects in Elevated Temperature, Low Cycle Fatigue," ASTM Standardization News 4(10), 327 (1976).
7. W. J. Ostergren, "Correlation of Hold Time Effects in Elevated Temperature Low Cycle Fatigue Using a Frequency Modified Damage Function," 1976 ASME-MPC Symposium on Creep-Fatigue Interaction, MPC-3 (American Society of Mechanical Engineers, NY, 1976), pp. 179-202.
8. S. Majumdar and P. S. Maiya, "A Unified and Mechanistic Approach to Creep Fatigue Damage," ANL-76-58 (Argonne National Laboratory, Argonne, IL, January 1976).
9. S. Majumdar and P. S. Maiya, "A Damage Equation for Creep-Fatigue Interaction," 1976 ASME-MPC Symposium on Creep-Fatigue Interaction, MPC-3 (American Society of Mechanical Engineers, NY, 1976), pp. 323-336.
10. S. Majumdar and P. S. Maiya, "Wave Shape Effects in Elevated-Temperature Low-Cycle Fatigue of Type 304 Stainless Steel," in Inelastic Behavior of Pressure Vessel and Piping Components, PVP-PB-028 (American Society of Mechanical Engineers, NY, 1978), pp. 43-54.

11. M. N. Menon, "Life Prediction Techniques for Analyzing Creep-Fatigue Interaction in Advanced Nickel-Base Superalloys," AFML-TR-76-172 (Air Force Materials Laboratory, Wright-Patterson AFB, OH, 1976).
12. L. F. Coffin Jr., "The Effect of Frequency on High-Temperature, Low-Cycle Fatigue," Proceedings of the Air Force Conference on Fatigue of Aircraft Structures and Materials, AFFDL-TR-70-144 (Air Force Flight Dynamics Laboratory, Wright-Patterson AFB, OH, 1970), pp. 301-311.
13. H. L. Bernstein, "An Evaluation of Four Models for the Creep-Fatigue Interaction in René 95 at Twelve Hundred Degrees Fahrenheit," Masters Thesis, University of Illinois, 1978.
14. J. M. Hyzak and H. L. Bernstein, "An Analysis of the Low Cycle Fatigue Behavior of the Superalloy René 95 by Strainrange Partitioning," AGARD-CP-243 (Advisory Group for Aerospace Research and Development, London, 1978), pp. 11-1 through 11-25.
15. C. E. Shamblen, R. E. Allen, and F. E. Walker, "Effect of Processing and Microstructure on René 95," Metallurgical Transactions 6A, 2073 (November 1975).
16. M. N. Menon, "Metallographic Characterization of René 95 Forgings," AFML-TR-73-180 (Air Force Materials Laboratory, Wright-Patterson AFB, OH, 1973).
17. T. Slot, R. H. Stentz, and J. T. Berling, "Controlled-Strain Testing Procedures," in Manual on Low Cycle Fatigue Testing, ASTM STP 465 (American Society for Testing and Materials, Philadelphia, PA, 1969), pp. 100-128.
18. J. B. Conway, R. H. Stentz, and J. T. Berling, Fatigue, Tensile, and Relaxation Behavior of Stainless Steels, TID-26135 (Oak Ridge National Laboratory, Oak Ridge, TN, 1975), pp. 14-31.
19. L. F. Coffin, Jr., "A Study of the Effects of Cyclic Thermal Stresses on a Ductile Metal," Transactions of the ASME 76, 923 (1954).
20. S. S. Manson, "Behavior of Materials Under Conditions of Thermal Stress," NACA-TN-2933 (NASA-Lewis Research Center, Cleveland, OH, 1953).
21. S. S. Manson, G. R. Halford, and A. J. Nachtigal, "Separation of the Strain Components for Use in Strainrange Partitioning," NASA TM X-71737 (NASA-Lewis Research Center, Cleveland, OH, 1975).
22. Time-Dependent Fatigue of Structural Alloys, ORNL-5073 (Oak Ridge National Laboratory, Oak Ridge, TN, 1975), p. 265.